EXTENDED KALMAN FILTER FOR INTEGRATING TRACKING DATA FROM GROUND-BASED RADAR AND AIRBORNE GLOBAL POSITIONING SYSTEM

by

Mark P. Green

Submitted to the

DEPARTMENT OF ELECTRICAL ENGINEERING AND COMPUTER SCIENCE

in partial fulfillment of the requirements

for the degree of

MASTER OF SCIENCE

at the

MASSACHUSETTS INSTITUTE OF TECHNOLOGY

February, 1998

© 1998 Massachusetts Institute of Technology

Author: _____
Department of Electrical Engineering and Computer Science, February, 1998

Certified by:_____
Professor George C. Verghese, Thesis Supervisor

Accepted by:_____
Arthur C. Smith, Chair, Department Committee on Graduate Students

EXTENDED KALMAN FILTER FOR INTEGRATING TRACKING DATA FROM GROUND-BASED RADAR AND AIRBORNE GLOBAL POSITIONING SYSTEM

by

Mark P. Green

Submitted to the Department of Electrical Engineering and Computer Science
on January 16, 1998 in Partial Fulfillment of the
Requirements for the Degree of Master of Science in
Electrical Engineering

ABSTRACT

An extended Kalman filter for the integration of tracking data from a ground-based radar and from an airborne GPS receiver is designed and tested. The filter utilizes the combined raw measurement data from each sensor and provides a position estimate in an earth centered, earth fixed frame. State space models are presented for the target dynamics and the GPS and radar measurements. The filter is tested with real and simulated data. The results demonstrate distinct advantages to utilizing a combined filter as opposed to employing separate position estimators based on each of the two sensors. The first is that the combined filter is capable of converging to a position solution even with partial measurements, from either or both sensors, which would result in divergence of estimators utilizing individual sensor data only. The second advantage is that, since the error variance of position estimates is dependent upon the relative target, sensor, and satellite geometry, inclusion of even partial measurements from one sensor into the filter can significantly improve the performance of the filter over an estimator using a single sensor's measurements only.

Thesis Supervisor: George C. Verghese
Title: Professor of Electrical Engineering

Table of Contents

Introduction

1. Plant Model
    1.1 Target Dynamics Model
        1.1.1 Continuous Time Target Dynamics Model
        1.1.2 Acceleration Model Parameters
        1.1.3 Discrete Time Target Dynamics Model
        1.1.4 Process Noise Covariance for Target Dynamics Model;
    1.2 GPS Receiver Clock Model
        1.2.1 Continuous Time GPS Receiver Clock Model
        1.2.2 Discrete Time GPS Receiver Clock Model
        1.2.3 Process Noise Covariance for Receiver Clock Model
    1.3 Composite Plant Model

2. GPS Measurement Model
    2.1 GPS Navigation Solution
    2.2 GPS Measurement Sensitivity Matrix
    2.3 GPS Measurement Noise
        2.3.1 GPS Measurement Error/Noise Model
        2.3.2 Differential Correction Technique
        2.3.3 GPS Measurement Noise Covariance Matrix

3. Radar Measurement Model
    3.1 Radar Position Measurements
    3.2 Radar Measurement Sensitivity Matrix
    3.3 Radar Measurement Error/Noise Model

4. Filter Description
    4.1 Matrix Definitions
    4.2 Implementation Description

5. Filter Simulation and Test
    5.1 2D Simulations
        5.1.1 2D Planar Radar-Only Filter Simulations
        5.1.2 2D Planar Radar+GPS Filter Simulations
        5.1.3 Summary of 2D Simulations
    5.2 Filter Tuning
    5.3 3D Filter Simulation and Testing
        5.3.1 3D GPS-Only Filter Tests
            5.3.1.1 Geometric Dependence of Error Covariance
            5.3.1.2 Observability Conditions (GPS-Only Filter)
        5.3.2 3D Radar-Only Filter Simulation
            5.3.2.1 Observability Conditions (Radar-Only Filter)
        5.3.3 Combined 3D Radar+GPS Filter Tests
            5.3.3.1 Full Radar and GPS Measurement Sets
            5.3.3.2 Partial Radar or GPS Measurement Set
            5.3.3.3 Partial Radar and GPS Measurements

Conclusions

References

Introduction

The tracking, or monitoring of position, of airborne targets from the ground has traditionally been accomplished through the use of ground-based sensors, such as a microwave radar system. These systems typically bounce microwave pulses off targets to determine their range and angle from the radar site. In the last decade, a satellite based navigation system called the Global Positioning System (GPS) has become fully operational. This system allows a user to determine their position accurately anywhere on or above the earth, using a small, inexpensive receiver. In a cooperative scenario, where data from a GPS receiver placed in an aircraft is transmitted down to a ground site, GPS may be used as a tracking system. Currently there is much interest in the use of GPS based tracking systems for air traffic control and military test range monitoring. In both of these applications, ground-based radar has been the primary method of position determination for a considerable time, and large infrastructures are in place utilizing radar only. In cooperative tracking scenarios such as these, it is expected that GPS may one day become the primary or even sole method for position determination. Whether or not traditional radar tracking methods continue to be used in cooperative scenarios, it would be likely that, during a transitional period, systems would incorporate both sensors. Thus, the problem of how to optimally integrate these two position sensors becomes a highly relevant issue. This thesis develops and examines one methodology for this integration based on an extended Kalman filter.

An overview of the tracking scenario which this filter addresses is shown in Figure I.1. The aircraft has a GPS receiver onboard that feeds raw satellite measurement data to a transmitter. This data is transmitted to a ground site that simultaneously receives raw measurements from a radar sensor which is also tracking the target aircraft. Both sets of measurements are input to a tracking computer which formulates a position solution for the target. Typically, either sensor alone provides enough information to fix the three dimensional position of the aircraft. However, if data from both sensors is available then we should be able to utilize all the measurements to obtain a position solution that is, perhaps, more accurate, and at least more robust to failures.
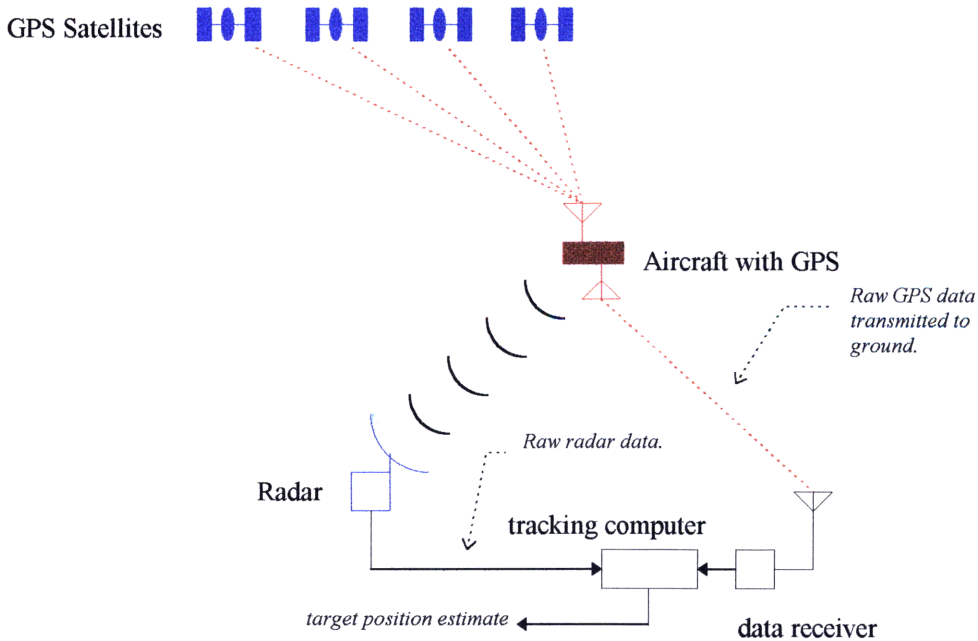

Figure I.1. Cooperative GPS and radar tracking scenario.

The data fusion method outlined above is often referred to as a "centralized" approach. In this approach, sensor data is combined in a single estimator to get a composite position estimate. In an alternate approach, each sensor derives a complete position solution separately, typically by means of a local estimator, and these estimates are then combined, in some sense optimally. This decentralized approach is, perhaps, more robust to certain types of hardware failures, if implemented properly, and has gained favor with the advent of small powerful microprocessors. However, in this thesis it is shown that combination of the raw measurement data in a centralized Kalman filter has a synergistic effect which has advantages over the local estimator approach. In situations where we may be concerned with sensor failures resulting in only partial measurement sets from any or all sensors, the local estimators would typically not converge and any position data output from them would not be usable. In the central Kalman filter estimator presented here, a position solution is possible with only partial measurements from both sensors. That is, if both the GPS and the radar sensors experience conditions which prevent them from individually obtaining a target position solution, we can often still utilize partial information from both to get an unbiased position estimate from a centralized Kalman filter. In addition, in the case of this type of partial failure in one sensor, we can also often utilize the partial measurements still available from that sensor to increase the accuracy of the position estimate over that which we would get from the other sensor only. In the case of local estimators, any partial sensor failure which would not allow convergence would result in the discarding of any remaining partial but valid information from that sensor.

It is assumed in this work that the reader is familiar with the concepts of Kalman filtering and the focus here has been to formulate the specifics required for this application. A model is presented for the process being estimated, in this case the dynamics of an airborne target, drawing primarily from the established literature. A model is developed for the GPS measurements and tested with raw data collected from several receivers. A radar measurement model is also developed, based on experience with tracking radar systems used in experimental work at Lincoln Laboratory. The filter was implemented and tested extensively in several steps. The first step involved a two dimensional theoretical formulation of the filter that used simulated measurement data. These simulations allowed significant manipulation of the target dynamics and relative sensor/target geometry and revealed the basic behavior and synergistic properties of the filter. Next, realistic full three dimensional versions of single sensor and combined sensor filters were implemented and tested. These tests were restricted to static targets since at the time of writing no actual flight tests were conducted. However, it was still possible to verify the advantageous properties of the combined filter conjectured from the two dimensional work. In summary, this is that a combined extended Kalman filter utilizing raw measurement data from both a GPS receiver and a tracking radar can provide, under many situations, more accurate and more robust position estimates than would be available from the two sensors utilized separately and simultaneously.

1. PLANT MODEL

The plant model employed in this filter can be subdivided into two parts. Primarily, we require a model for the dynamics of the aircraft or target we are trying to track, but in addition, we need a dynamic model for the behavior of the GPS receiver clock. The reason for this is explained in the Section 2.1 describing the GPS navigation solution. Both models, which are developed below, are derived from fairly standard continuous time system representations that have been proven in tracking [1][2] and GPS [3] applications.

1.1 Target Dynamics Model
1.1.1 Continuous Time Target Dynamics Model

In this application we are concerned with tracking an airborne target whose motion is unknown in advance, but can be considered predictable in the sense that it adheres to some simple physical equations of motion. We start the development with the state space representation for motion of a rigid body with a constant velocity. In a single coordinate this represention is:

$$\begin{bmatrix} \dot{x}(t) \\ \ddot{x}(t) \end{bmatrix} = \begin{bmatrix} 0 & 1 \\ 0 & 0 \end{bmatrix} \begin{bmatrix} x(t) \\ \dot{x}(t) \end{bmatrix} \tag{1}$$

This kinematic model is noiseless, and with known initial conditions we can exactly determine the state, i.e. position, of the target at any future time. In the general target tracking problem it is unlikely that we will encounter a non-accelerating target for all time. That is, it is unlikely the target will remain in a constant velocity, straight line trajectory during the entire tracking period. We therefore wish to extend the zero-acceleration model given in (1) to allow for possible changes in target velocity. A common approach to handling unknown accelerations is to model them as an input noise process. Our state space model, in one coordinate, then becomes:

$$\begin{bmatrix} \dot{x}(t) \\ \ddot{x}(t) \end{bmatrix} = \begin{bmatrix} 0 & 1 \\ 0 & 0 \end{bmatrix} \begin{bmatrix} x(t) \\ \dot{x}(t) \end{bmatrix} + \begin{bmatrix} 0 \\ 1 \end{bmatrix} a(t) \tag{2}$$

where $a(t)$ is the acceleration noise process. In this model we assume that motion in each coordinate axis is decoupled and that the acceleration noise processes are mutually independent. Thus in two dimensions the model would look like:

$$\begin{bmatrix} \dot{x}(t) \\ \ddot{x}(t) \\ \dot{y}(t) \\ \ddot{y}(t) \end{bmatrix} = \begin{bmatrix} 0 & 1 & 0 & 0 \\ 0 & 0 & 0 & 0 \\ 0 & 0 & 0 & 1 \\ 0 & 0 & 0 & 0 \end{bmatrix} \begin{bmatrix} x(t) \\ \dot{x}(t) \\ y(t) \\ \dot{y}(t) \end{bmatrix} + \begin{bmatrix} 0 & 0 \\ 1 & 0 \\ 0 & 0 \\ 0 & 1 \end{bmatrix} \begin{bmatrix} a_x(t) \\ a_y(t) \end{bmatrix} \tag{3}$$

A first approach, which limits the filter state vector to two states per coordinate, would be to model the acceleration noise as white. A simulation of the kind of dynamics modeled by (3), with $a_i(t)$ as white noise processes, is shown in Figure 1.1, which displays a typical target trajectory in two dimensions. This simulation used two independent, equal variance acceleration noise processes as inputs. Although the noise variance may be lowered to somewhat reduce the jaggedness of the trajectories, this plot serves to demonstrate that the white noise acceleration model is not, in general, a good representation for typical aircraft motion. It is, perhaps, a reasonable approximation for accelerations due to wind turbulence, however.
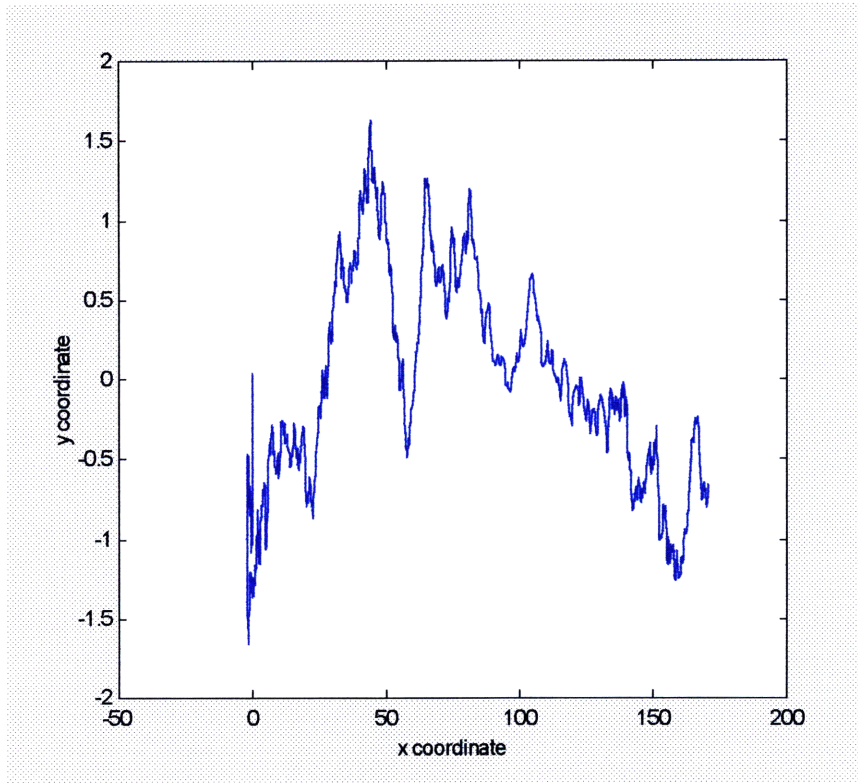
7

Figure 1.1 Simulation of white noise acceleration model for target dynamics.

It turns out, as might be expected, that the kinds of accelerations a typical maneuvering aircraft might undergo are mostly time correlated. For example, a pilot induced turn would correspond to a time correlated acceleration for the duration of the turn. Thus a more reasonable approach is to model the acceleration noise as being a first order Gauss-Markov process. The acceleration process would then be given by:

$$\dot{a}(t) = -\alpha \cdot a(t) + w(t) \tag{4}$$

where $w(t)$ is a white gaussian noise process. The notation used here follows that of ref. [1]. Taking the Laplace transform of (4) (ignoring initial conditions) we have:

$$H(s) = \frac{A(s)}{W(s)} = \frac{1}{s + \alpha} \tag{5}$$

which implies we can view (4) as the equivalent of putting white noise through a stable causal shaping filter with transfer function $H(s)$ to get our acceleration noise process $A(s)$. The power spectral density of this output process is given by:

$$S_A(s) = H(s)H(-s)S_W(s) \tag{6}$$

8

If we define our input white noise process to have variance $2\alpha\sigma_m^2$, then $S_A(s)$ becomes:

$$S_A(s) = \frac{-2\alpha\sigma_m^2}{(s-\alpha)(s+\alpha)} \tag{7}$$

Taking the inverse transform of (7) gives the autocorrelation function of our acceleration process:

$$R_a(\tau) = E[a(t)a(t+\tau)] = \sigma_m^2 e^{-\alpha|\tau|} \quad \text{for } \alpha{>}0 \tag{8}$$

This acceleration process model, therefore, represents the time correlation of acceleration inputs as positively correlated with an exponential decay.
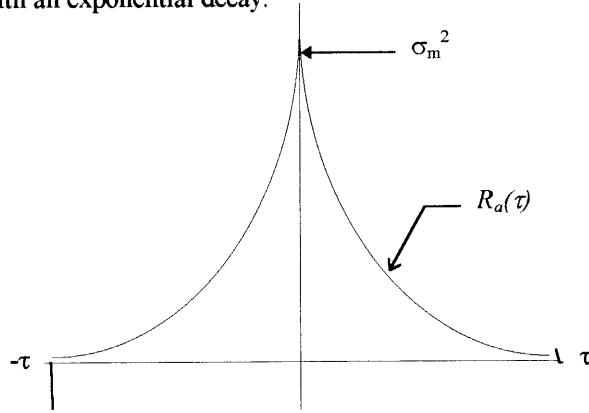

Figure 1.2. Acceleration process auto-correlation function.

A complete state space description of our target dynamics can now be obtained by augmenting the state description given in (2) with the acceleration process given in Equation (4). In one coordinate this yields:

$$\begin{bmatrix} \dot{x}(t) \\ \ddot{x}(t) \\ \dot{a}(t) \end{bmatrix} = \begin{bmatrix} 0 & 1 & 0 \\ 0 & 0 & 1 \\ 0 & 0 & -\alpha \end{bmatrix} \begin{bmatrix} x(t) \\ \dot{x}(t) \\ a(t) \end{bmatrix} + \begin{bmatrix} 0 \\ 0 \\ 1 \end{bmatrix} w_x(t) \tag{9}$$

where $w_x(t)$ is the white noise input process driving that coordinate. As we have defined it, this white noise process will have an autocorrelation function given by:

$$R_w(\tau) = 2\alpha\sigma_m^2\delta(\tau) \tag{10}$$

A simulation of the dynamics modeled, in two coordinates, by (9) is shown in Figure 1.3. This simulation used the exact same noise inputs that drove the white noise acceleration model simulation shown in Figure 1.1. Now, however, they were run through the shaping filter which essentially time correlates the acceleration of the target. Figure 1.3 displays target dynamics which we would believe to be much more realistic. The final target dynamics model in one coordinate is shown in Figure 1.4.
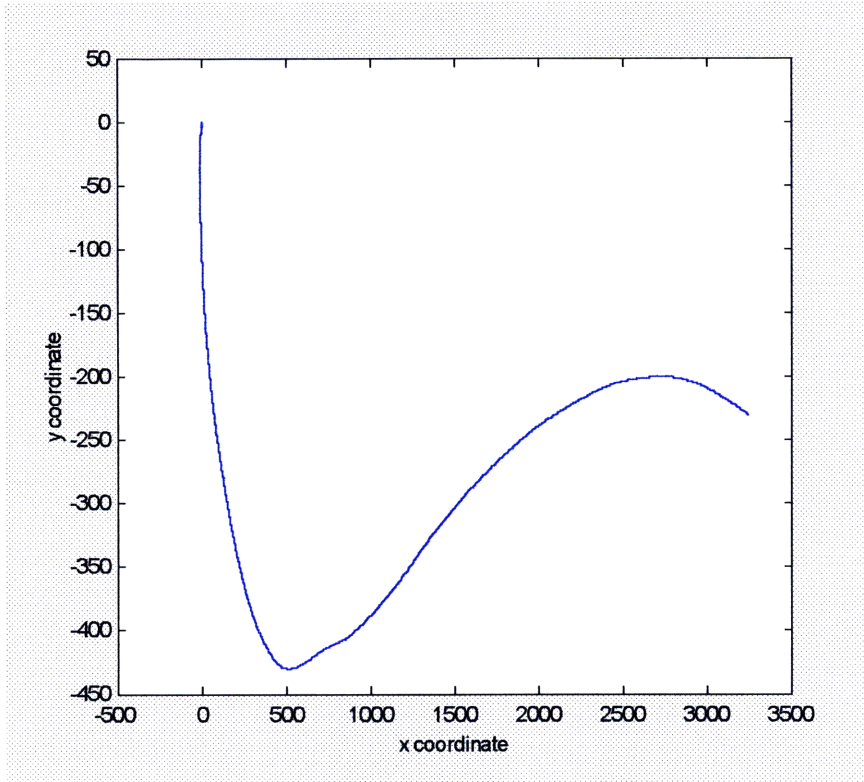
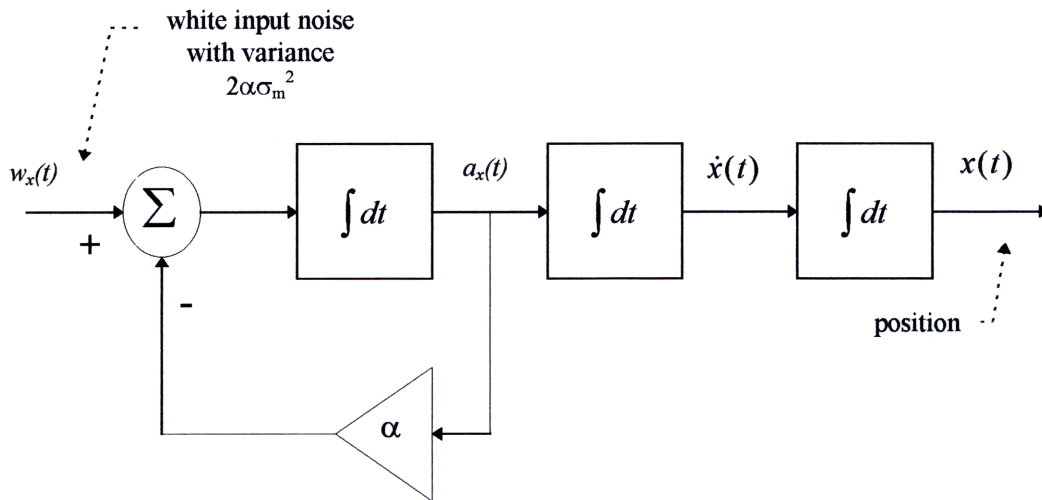Figure 1.3. Simulation of colored noise acceleration model for target dynamics.

Figure 1.4. Target dynamics model in single coordinate.

Extending the final continuous time target dynamics model to three spatial dimensions gives us the state space system:

$$
\begin{bmatrix} \dot{x}(t) \\ \ddot{x}(t) \\ \dot{a}_x(t) \\ \dot{y}(t) \\ \ddot{y}(t) \\ \dot{a}_y(t) \\ \dot{z}(t) \\ \ddot{z}(t) \\ \dot{a}_z(t) \end{bmatrix} = \begin{bmatrix} 0 & 1 & 0 & 0 & 0 & 0 & 0 & 0 & 0 \\ 0 & 0 & 1 & 0 & 0 & 0 & 0 & 0 & 0 \\ 0 & 0 & -\alpha_x & 0 & 0 & 0 & 0 & 0 & 0 \\ 0 & 0 & 0 & 0 & 1 & 0 & 0 & 0 & 0 \\ 0 & 0 & 0 & 0 & 0 & 1 & 0 & 0 & 0 \\ 0 & 0 & 0 & 0 & 0 & -\alpha_y & 0 & 0 & 0 \\ 0 & 0 & 0 & 0 & 0 & 0 & 0 & 1 & 0 \\ 0 & 0 & 0 & 0 & 0 & 0 & 0 & 0 & 1 \\ 0 & 0 & 0 & 0 & 0 & 0 & 0 & 0 & -\alpha_z \end{bmatrix} \begin{bmatrix} x(t) \\ \dot{x}(t) \\ a_x(t) \\ y(t) \\ \dot{y}(t) \\ a_y(t) \\ z(t) \\ \dot{z}(t) \\ a_z(t) \end{bmatrix} + \begin{bmatrix} 0 & 0 & 0 \\ 0 & 0 & 0 \\ 1 & 0 & 0 \\ 0 & 0 & 0 \\ 0 & 0 & 0 \\ 0 & 1 & 0 \\ 0 & 0 & 0 \\ 0 & 0 & 0 \\ 0 & 0 & 1 \end{bmatrix} \begin{bmatrix} w_x(t) \\ w_y(t) \\ w_z(t) \end{bmatrix} \quad (11)
$$

Note that in (11) the state vector consists of target position, velocity, and acceleration in each coordinate. The driving functions, $w_i(t)$, are mutually independent, gaussian white noise processes that may have different variances. Expressing (11) in more compact matrix notation we have:

$$
\dot{X}_p(t) = A_p(\alpha)X_p(t) + B_pW_p(t) \quad (12)
$$

where the p subscript is used to denote that this is the portion of the plant model that deals with the target position.

1.1.2 Acceleration Model Parameters

The correlated acceleration model presented in Section 1.1.1 introduces two parameters which determine its behavior: α, the reciprocal of the correlation time constant, and σ_m^2, the variance of the target acceleration (sometimes referred to as the maneuver variance). In designing the tracking filter we desire to choose these parameters such that our modeled dynamics will match the actual target behavior as closely as possible. This selection process can be considered the tuning of the filter, and its impact on the performance of the filter is discussed in Section 5.2. Here we suggest a basic guideline for parameter selection and give a qualitative discussion of how these parameters affect model behavior.

Recall that our acceleration process, $a(t)$, which we derived from filtering a (zero mean, wide sense stationary) white noise process, had the autocorrelation function given by (8). Thus the variance of this process is given by:

$$\sigma_a^2 = R_a(0) = \sigma_m^2 \tag{13}$$

where the subscript m is used to be consistent with the literature. Presumably in our application we have we some statistical characterization available for the class of targets we wish to track. This may be available by observation or physical modeling of the targets. In either case, a first attempt at matching the actual target dynamics to the filter's model is achieved through some knowledge of the amplitude distribution of the target accelerations. i.e. from a probability density function of target acceleration amplitudes in each coordinate. Ref.[2] presents the rough guideline that the equivalent discrete process noise variance (derived in Section 1.1.3) should be of the order of the maximum acceleration expected from the target. For example:

$$\frac{a_{\max}}{2} \le 2\alpha\sigma_m^2 \le a_{\max} \tag{14}$$

A model for a typical target acceleration distribution, shown in Figure 1.5, is given in Ref.[1]. In this model, the target is assumed to undergo no accelerations, or accelerations at a maximum value, with some discrete probability. All other values of acceleration are assumed to occur with some uniform distribution. The variance of this distribution is given by:

$$\sigma_m^2 = (a_{\max})^2 \frac{(1+4P_m - P_0)}{3} \tag{15}$$

where P_0 and P_m are the probabilities of the target undergoing zero acceleration or a maximum acceleration, respectively, at any given time.
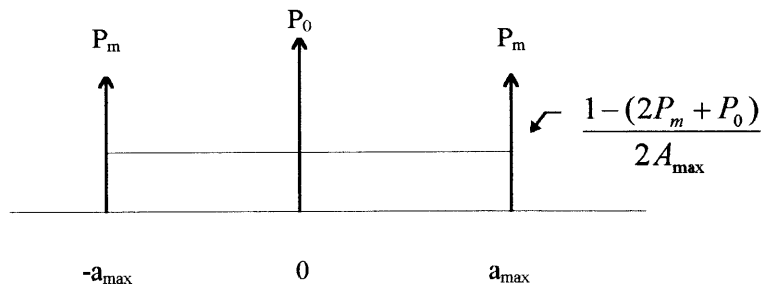

Figure 1.5. Sample target acceleration probability distribution.

Whatever method is used to select σ_m^2, the effect of this parameter can be qualitatively understood by examining Figure 1.6. This figure shows a set of trajectories generated by a discretized version of the model given in (11), limited to two dimensions. (The maneuver variance and time constants were assumed to be equal in each axis.) Independent, unit variance, white noise driving sequences were generated for the x and y coordinates, and scaled with several different values of σ_m^2. The effect of increasing the maneuver variance, while holding all other factors equal, is essentially to increase the magnitude of the maneuver. i.e. for the same acceleration noise, the shape of the maneuver remains the same, but the target undergoes a larger acceleration and moves over a longer trajectory, thus traveling faster. We can see that selecting σ_m^2 for the class of targets we want to track involves matching the range of accelerations that are possible or reasonable for those targets.
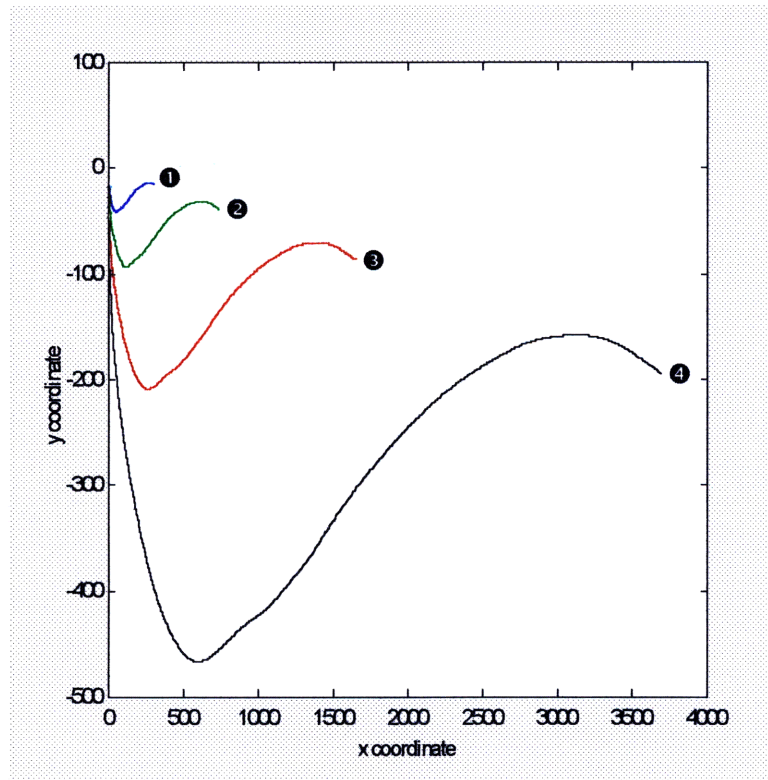

Figure 1.6. Sample trajectories showing dependence on maneuver variance.
[$\alpha_{x,y}$=1/25, T=0.1,1024 points, σ_m^2= 0.1(❶), 0.5(❷), 2.5(❸), 12.5(❹)]

The second adjustable parameter in the acceleration model is the maneuver correlation time constant, $1/\alpha$. As mentioned, it would not be reasonable to expect that target accelerations are time uncorrelated. That is, if a target is undergoing a positive acceleration, in a particular coordinate, at time t, it is likely that for some range of Δt, we would expect that the target is still accelerating in the same direction at $t+\Delta t$. We are modeling this affect as being exponentially tapered, and thus the range of effect of this correlation is determined by the decay time constant. Referring to Equation (8) and Figure 1.2 we see that a larger value of $1/\alpha$ means that the decay rate is slower and maneuvers are correlated longer. Here again a set of trajectories was generated for a range of values of α and the results are shown in Figure 1.7. The same white noise driving functions were used here as were used to generate Figure 1.6. The effect of a longer time constant is essentially to result in smoother, wider turns. A shorter time constant (larger α) results in sharper (more jagged) turns. Once again, the objective here would be to match the model to the type of dynamics expected from the target behavior. For example, if we expect a lot of evasive maneuvers we would expect to choose a shorter time constant (larger α).
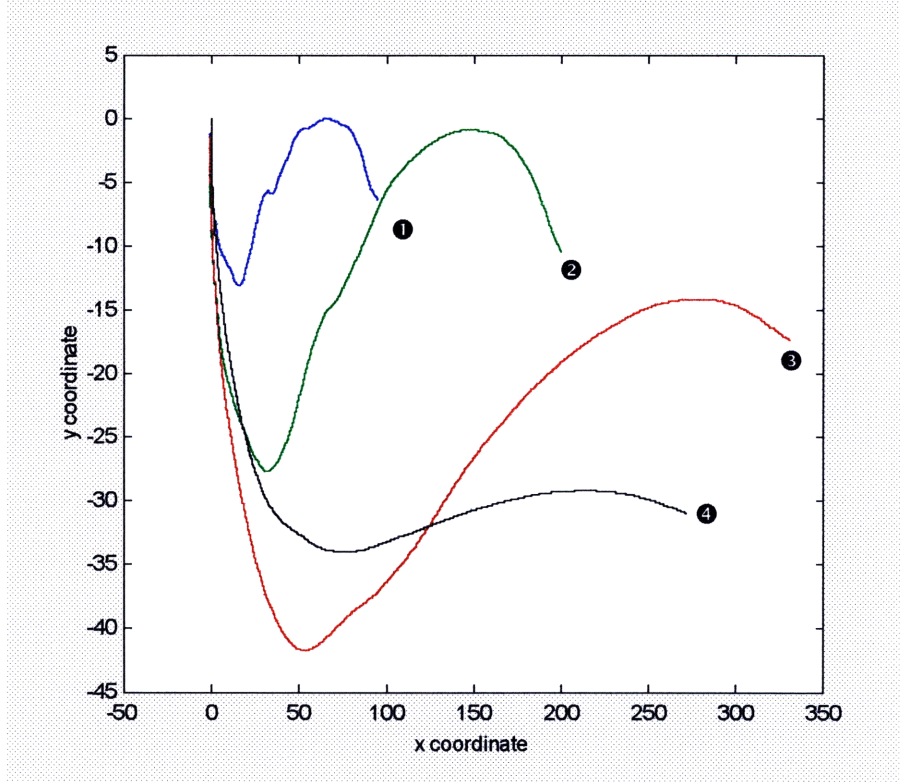
13

Figure 1.7. Sample trajectories showing dependence on correlation time constant. [σ_m^2=0.1, T=0.1, 1024 points, $\alpha_{x,y}$= 1(❶), 1/5(❷), 1/25(❸), 1/125(❹)]

1.1.3 Discrete Time Target Dynamics Model

Since our ultimate objective is to design a discrete time Kalman filter, the continuous time plant model given in (12) must be converted to a discrete time version. This is accomplished as follows. Start with the continuous time (CT) plant given by (12) and repeated here for convenience:

$$\dot{X}_p(t) = A_p(\alpha)X_p(t) + B_pW_p(t) \tag{12}$$

This is a linear time invariant system with dynamic coefficient matrix, A_p, and input coupling matrix, B_p. From (12) we want to get a discrete system of the form:

$$X_p[k+1] = \Phi_p X_p[k] + G_p W_p[k] \tag{16}$$

Using standard techniques [4], the solution to (12) is given by:

$$X_p(t) = e^{(t-t_0)A_p} X_p(t_0) + \int_{t_0}^{t} e^{(t-\tau)A_p} B_p W_p(\tau)d\tau \tag{17}$$

If we choose our sampling time to be T, let $t_0 = kT$, and $t = (k+1)T$, then by substituting into (17) we get:

$$X_p((k+1)T) = e^{A_pT} X_p(kT) + \int_{kT}^{(k+1)T} e^{A_p((k+1)T-\tau)} B_p W_p(\tau)d\tau \tag{18}$$

By suppressing the T in the time index of (18) and comparing to (16) we can see, by inspection, that our discrete time state transition matrix is given by:

$$\Phi_p(\alpha,T) = e^{A_pT} \tag{19}$$

$$= \begin{bmatrix}
1 & T & \frac{1}{\alpha_x^2}(e^{-\alpha_x T} + \alpha_x T - 1) & 0 & 0 & 0 & 0 & 0 & 0 \\
0 & 1 & \frac{1}{\alpha_x}(1 - e^{-\alpha_x T}) & 0 & 0 & 0 & 0 & 0 & 0 \\
0 & 0 & e^{-\alpha_x T} & 0 & 0 & 0 & 0 & 0 & 0 \\
0 & 0 & 0 & 1 & T & \frac{1}{\alpha_y^2}(e^{-\alpha_y T} + \alpha_y T - 1) & 0 & 0 & 0 \\
0 & 0 & 0 & 0 & 1 & \frac{1}{\alpha_y}(1 - e^{-\alpha_y T}) & 0 & 0 & 0 \\
0 & 0 & 0 & 0 & 0 & e^{-\alpha_y T} & 0 & 0 & 0 \\
0 & 0 & 0 & 0 & 0 & 0 & 1 & T & \frac{1}{\alpha_z^2}(e^{-\alpha_z T} + \alpha_z T - 1) \\
0 & 0 & 0 & 0 & 0 & 0 & 0 & 1 & \frac{1}{\alpha_z}(1 - e^{-\alpha_z T}) \\
0 & 0 & 0 & 0 & 0 & 0 & 0 & 0 & e^{-\alpha_z T}
\end{bmatrix}$$

To be precise in the derivation of the discrete process input noise covariance we treat $W_p(t)$ as a true continuous time white noise process that must be integrated over the sampling interval. We thus define the input sequence to be:

$$u_p[k] = \int_{kT}^{(k+1)T} e^{A_p((k+1)T-\tau)} B_p W_p(\tau) d\tau \tag{20}$$

Thus for the purposes of our filter design we have the discrete time model:

$$X_p[k+1] = \Phi_p(\alpha, T) X_p[k] + u_p[k] \tag{21}$$

Note that in our discrete time model the state transition matrix, and, as will be shown in Section 1.1.4, the process noise covariance matrix, are functions of the sampling time, T, and the acceleration model parameters, α and σ_m^2. Thus, if the data sampling interval changes at any time during the filter operation, these matrices must be recalculated. Likewise, if we wish to revise our estimate of either maneuver parameter, we must also update the filter system matrices. Throughout most of this work the two maneuver model parameters are assumed to be equal in all three axis. Also note that in (21) the discrete time input coupling matrix, G_p, is I (identity).

1.1.4 Process Noise Covariance for Target Dynamics Model

To find the process noise covariance matrix for the target dynamics model as defined in (21), we proceed as follows:

$$K_{uu}[k,j] = E\{u_p[k]u_p'[j]\} \tag{22}$$

where E denotes the expectation operator and ' denotes the matrix transpose. Substituting (20) into (22) for $u[\bullet]$, and noting that, for a constant sample time, we can set the interval of integration to $0<\tau<T$, we get:

$$K_{uu}[k,j] = E\{\int_0^T e^{A_p(T-\tau)}B_pW_p(\tau)d\tau\left[\int_0^T e^{A_p(T-s)}B_pW_p(s)ds\right]'\} \tag{23}$$

$$= E\{\int_0^T e^{A_p(T-\tau)}B_pW_p(\tau)d\tau\int_0^T W_p'(s)B_p'e^{A_p'(T-s)}ds\}$$

$$= E\{\int_0^T\int_0^T e^{A_p(T-\tau)}B_pW_p(\tau)W_p'(s)B_p'e^{A_p'(T-s)}d\tau ds\}$$

Interchanging the expectation and integration operations we get:

$$K_{uu}[k,j] = \int_0^T\int_0^T e^{A_p(T-\tau)}B_p E\{W_p(\tau)W_p'(s)\}B_p'e^{A_p'(T-s)}d\tau ds \tag{24}$$

The inner expectation in (24) is the covariance matrix of the continuous time input noise process that drives the acceleration model. We mentioned that in each coordinate these were zero mean, white noise processes with autocorrelation functions given by:

$$R_{xx}(\tau,s) = 2\alpha\sigma_m^2\delta(\tau-s) \tag{25}$$

These processes are assumed to be mutually independent, and thus the continuous time covariance matrix has a diagonal form:

$$K_{ww}(\tau,s) = \begin{bmatrix} 2\alpha_x\sigma_x^2 & 0 & 0 \\ 0 & 2\alpha_y\sigma_y^2 & 0 \\ 0 & 0 & 2\alpha_z\sigma_z^2 \end{bmatrix}\delta(\tau-s) = C\delta(\tau-s) \tag{26}$$

Note that in (26) we have allowed for different noise intensities in each coordinate axis, which may be realistic and desirable. For instance, if we expect the target to mostly remain at a constant altitude, then the maneuver variance in the z-axis would likely be lower than in the x and y axis. In this case, accelerations in the z direction may, for example, be primarily due to wind turbulence. It would also therefore be reasonable to expect the correlation decay time to be different for the z-axis. Substituting (26) into (24) and then integrating over τ, we get:

$$K_{uu}[k,j] = \int_0^T \int_0^T e^{A_p(T-\tau)} B_p C \delta(\tau - s) B_p{}' e^{A_p{}'(T-s)} d\tau ds$$

$$= \int_0^T e^{A_p(T-s)} B_p C B_p{}' e^{A_p{}'(T-s)} ds \qquad (27)$$

Now, let $\qquad M = e^{A_p(T-s)} B_p \qquad (28)$

Thus (27) becomes:

$$K_{uu}[k,j] = \int_0^T M C M' ds \cdot \delta[j,k] \qquad (29)$$

since C is diagonal and not dependent upon s.

The matrix M is given by:

$$M = \begin{bmatrix} \dfrac{1}{\alpha_x^2}(e^{-\alpha_x(T-s)} + \alpha_x(T-s) - 1) & 0 & 0 \\[2mm] \dfrac{1}{\alpha_x}(1 - e^{-\alpha_x(T-s)}) & 0 & 0 \\[2mm] e^{-\alpha_x(T-s)} & 0 & 0 \\[2mm] 0 & \dfrac{1}{\alpha_y^2}(e^{-\alpha_y(T-s)} + \alpha_y(T-s) - 1) & 0 \\[2mm] 0 & \dfrac{1}{\alpha_y}(1 - e^{-\alpha_y(T-s)}) & 0 \\[2mm] 0 & e^{-\alpha_y(T-s)} & 0 \\[2mm] 0 & 0 & \dfrac{1}{\alpha_z^2}(e^{-\alpha_z(T-s)} + \alpha_z(T-s) - 1) \\[2mm] 0 & 0 & \dfrac{1}{\alpha_z}(1 - e^{-\alpha_z(T-s)}) \\[2mm] 0 & 0 & e^{-\alpha_z(T-s)} \end{bmatrix} \qquad (30)$$

Multiplying out the matrices and then performing the integration in (31) results in the following covariance matrix:

define:

$$q_{11}(\alpha_i, T) = \frac{1}{6\alpha_i^5}(3 + 6\alpha_i T + 2\alpha_i^3 T^3 - 6\alpha_i^2 T^2 - 3e^{-2\alpha_i T} - 12\alpha_i Te^{-\alpha_i T})$$ (31)

$$q_{12}(\alpha_i, T) = \frac{1}{2\alpha_i^4}(1 + e^{-2\alpha_i T} + 2\alpha_i Te^{-\alpha_i T} + \alpha_i^2 T^2 - 2\alpha_i T - 2e^{-\alpha_i T})$$ (32)

$$q_{13}(\alpha_i, T) = \frac{1}{2\alpha_i^3}(1 - 2\alpha_i Te^{-\alpha_i T} - e^{-2\alpha_i T})$$ (33)

$$q_{22}(\alpha_i, T) = \frac{1}{2\alpha_i^3}(4e^{-\alpha_i T} + 2\alpha_i T - e^{-2\alpha_i T} - 3)$$ (34)

$$q_{23}(\alpha_i, T) = \frac{1}{2\alpha_i^2}(1 + e^{-2\alpha_i T} - 2e^{-\alpha_i T})$$ (35)

$$q_{33}(\alpha_i, T) = \frac{1}{2\alpha_i}(1 - e^{-2\alpha_i T})$$ (36)

and

$$Q(\alpha_i, T) = \begin{bmatrix} q_{11}(\alpha_i, T) & q_{12}(\alpha_i, T) & q_{13}(\alpha_i, T) \\ q_{12}(\alpha_i, T) & q_{22}(\alpha_i, T) & q_{23}(\alpha_i, T) \\ q_{13}(\alpha_i, T) & q_{23}(\alpha_i, T) & q_{33}(\alpha_i, T) \end{bmatrix} \cdot 2\alpha_i \sigma_i^2$$ (37)

then the noise covariance matrix for target dynamics process is given by:

$$K_{uu}[k, j] = Q_p = \begin{bmatrix} Q(\alpha_x, T) & 0 & 0 \\ 0 & Q(\alpha_y, T) & 0 \\ 0 & 0 & Q(\alpha_z, T) \end{bmatrix} \delta[k, j]$$ (38)

19

1.2 GPS Receiver Clock Model
1.2.1 Continuous Time GPS Receiver Clock Model

As mentioned, in addition to the target position, our filter state vector must include a state for the GPS receiver clock bias. As a result, we require a model for the clock's behavior to include in our filter plant dynamics. One that is fairly commonly employed in GPS receivers[3],[5] is a two-state model which says that we expect both the phase and frequency of the receiver clock oscillator to randomly walk. Thus we start with the continuous time model shown in Figure 1.8. Here the two states are the clock phase (bias), x_p, and the clock frequency, x_f, and the input noise is provided by two independent white noise processes, $w_f(t)$ and $w_p(t)$.
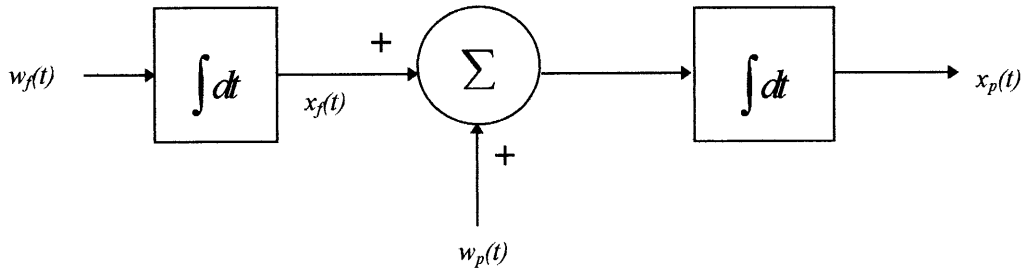

Figure 1.8. Continuous time GPS receiver clock dynamics model.

The continuous time state space model for the clock is thus given by:

$$\begin{bmatrix} \dot{x}_p(t) \\ \dot{x}_f(t) \end{bmatrix} = \begin{bmatrix} 0 & 1 \\ 0 & 0 \end{bmatrix} \begin{bmatrix} x_p(t) \\ x_f(t) \end{bmatrix} + \begin{bmatrix} 1 & 0 \\ 0 & 1 \end{bmatrix} \begin{bmatrix} w_p(t) \\ w_f(t) \end{bmatrix}$$

(39)

Or in matrix notation:

$$\dot{X}_c(t) = A_c X_c(t) + B_c W_c(t)$$

(40)

where the subscript "c" denotes that this is the portion of the plant model that deals with the GPS receiver clock dynamics. The input vector, $W_c(t)$, consists of two mutually independent, zero mean, white noise processes with variances, σ_f^2 and σ_p^2. The tuning of the model to match the actual receiver's clock behavior is accomplished by adjusting these spectral densities appropriately. This may be accomplished by direct observation of the oscillator drift or by deriving the quantities from the Allan variance specifications of the oscillator, if available. A treatment of this second approach is given in ref. [5].

20

1.2.2 Discrete Time GPS Receiver Clock Model

The discrete time clock model is obtained using the same procedure as in Section 1.1.3. Again, we wish to find our discrete time state transition matrix and input sequence such that we have a model of the form:

$$X_c[k+1] = \Phi_c X_c[k] + u_c[k] \tag{41}$$

From (18) we can, once again, deduce that the state transition matrix is:

$$\Phi_C = e^{A_c T} = \begin{bmatrix} 1 & T \\ 0 & 1 \end{bmatrix} \tag{42}$$

and our input sequence is given by:

$$u_c[k] = \int_{kT}^{(k+1)T} e^{A_c((k+1)T-\tau)} B_c W_c(\tau) d\tau \tag{43}$$

1.2.3 Process Noise Covariance for Receiver Clock Model

In a manner similar to the derivation of the target dynamics process noise covariance calculation, the covariance matrix for the GPS receiver clock process noise is derived. We start with the input sequence given by Equation (43), and note that the interval of integration can taken from $\tau=0 \rightarrow T$, and also that the input coupling matrix, B_c, is defined as the 2x2 identity matrix. Thus we can write (43) as:

$$u_c[k] = \int_0^T e^{A_c(T-\tau)} W_c(\tau) d\tau \tag{44}$$

Since, once again, we have assumed $W_c(t)$ is zero mean, the covariance is calculated by:

$$K_{uu}[k,j] = \mathrm{E}\{u_c[k]u'_c[j]\}$$

$$= \mathrm{E}\{\int_0^T e^{A_c(T-\tau)} W_c(\tau) d\tau \left[\int_0^T e^{A_c(T-s)} W_c(s) ds\right]'\}$$

$$= \mathrm{E}\{\int_0^T \int_0^T e^{A_c(T-\tau)} W_c(\tau) W'_c(s) e^{A'_c(T-s)} ds\} \tag{45}$$

$$= \int_0^T \int_0^T e^{A_c(T-\tau)} \mathrm{E}\{W_c(\tau) W'_c(s)\} e^{A'_c(T-s)} ds$$

In the last line of (45) the inner expectation is the covariance of the continuous time noise process. Recall that this vector process was defined to consist of two mutually independent zero mean white noise processes. The covariance matrix for this process is thus given by:

$$\mathrm{E}\{W_c(\tau) W'_c(s)\} = \begin{bmatrix} \sigma_p^2 \delta(\tau-s) & 0 \\ 0 & \sigma_f^2 \delta(\tau-s) \end{bmatrix} \tag{46}$$

Thus substituting (42) and (46) into (45) we get:

$$K_{uu}[k,j] = \int_0^T \int_0^T \begin{bmatrix} 1 & T-\tau \\ 0 & 1 \end{bmatrix} \begin{bmatrix} \sigma_p^2 \delta(\tau-s) & 0 \\ 0 & \sigma_f^2 \delta(\tau-s) \end{bmatrix} \begin{bmatrix} 1 & 0 \\ T-s & 1 \end{bmatrix} d\tau ds \tag{47}$$

$$= \int_0^T \int_0^T \begin{bmatrix} \sigma_p^2 \delta(\tau-s) + (T-s)(T-\tau)\sigma_f^2 \delta(\tau-s) & (T-\tau)\sigma_f^2 \delta(\tau-s) \\ (T-s)\sigma_f^2 \delta(\tau-s) & \sigma_f^2 \delta(\tau-s) \end{bmatrix} d\tau ds$$

Integrating over τ results in:

$$K_{uu}[k,j] = \int_0^T \begin{bmatrix} \sigma_p^2 + \sigma_f^2(T-s)^2 & \sigma_f^2(T-s) \\ \sigma_f^2(T-s) & \sigma_f^2 \end{bmatrix} ds \tag{48}$$

Finally, integrating over s results in the following covariance matrix for the clock model process noise:

$$Q_c = K_{uu}[k,j] = \begin{bmatrix} \sigma_p^2 T + \sigma_f^2 \dfrac{T^3}{3} & \sigma_f^2 \dfrac{T^2}{2} \\ \sigma_f^2 \dfrac{T^2}{2} & \sigma_f^2 T \end{bmatrix} \delta[k,j] \tag{49}$$

1.3 Composite Plant Model

The complete plant model for this filter is the combination of the target dynamics model, developed in Section 1.1, and the GPS receiver clock model, presented in Section 1.2. Combining these two models gives a discrete time system with the state vector:

$$\vec{X}[k] = \begin{bmatrix} x[k] \\ \dot{x}[k] \\ \ddot{x}[k] \\ y[k] \\ \dot{y}[k] \\ \ddot{y}[k] \\ z[k] \\ \dot{z}[k] \\ \ddot{z}[k] \\ b_c[k] \\ f_c[k] \end{bmatrix} \qquad \text{where } b_c = x_p \text{ and } f_c = x_f \text{ from (39)}. \tag{50}$$

Here we have position, velocity, and acceleration in each spatial coordinate, and the receiver clock bias and frequency. The composite discrete time state transition matrix is:

$$\Phi = \begin{bmatrix} \Phi_p(\alpha, T) & 0 \\ 0 & \Phi_c(T) \end{bmatrix} \tag{51}$$

where Φ_p is 9x9 and Φ_c is 2x2.

We have the 11x1 combined process noise vector :

$$u[k] = \begin{bmatrix} u_p[k] \\ u_c[k] \end{bmatrix} \tag{52}$$

which is time uncorrelated (white) with covariance matrix:

$$Q = \begin{bmatrix} Q_p(\alpha, \sigma_m^2, T) & 0 \\ 0 & Q_c(\sigma_p^2, \sigma_f^2, T) \end{bmatrix} \tag{53}$$

where Q_p is 9x9 and Q_c is 2x2.

24

2. GPS Measurement Model

In this section we develop the measurement model for the GPS receiver observables. In order to understand the relationship between the GPS observables and the navigation state vector, the general position solution methodology for GPS is first presented.

2.1 GPS Navigation Solution

The basic principle used by a GPS receiver to determine its position involves the measurement of range to several satellites. Presumably if one can make a range measurement to three different satellites, it should be possible to fix a position in three dimensional space. However, for reasons that will be explained, a minimum of four range measurements are required to fix the receiver's position. Modern GPS receivers utilize a number of techniques to make these range measurements, including C/A (course/acquisition) or P (precise) code phase observations, carrier phase measurements, and differential techniques. Ref. [6] provides further background information on various GPS navigation techniques. The solution method desired in this integration was for a non-military receiver, and thus the measurements that are used are the C/A code phase observables. In this technique, the receiver uses a code correlator to determine the time of arrival of the C/A code signal transmitted by the satellite (SV). The receiver knows that the SV should begin transmission of this signal at a particular GPS system time. If both the satellite and receiver had internal clocks that were perfectly synchronized with system time, all that would be required to measure the range to the SV would be to measure the transit time of the signal and to scale it by the propagation velocity. However, since it is not practical for either the SV or receiver clock to be precisely synchronized to GPS system time, the solution method becomes slightly more complex and is explained below.

All GPS calculations are carried out in an earth-centered, earth fixed (*ECEF*) coordinate frame utilizing the WGS-84 ellipsoid [7]. Denote the user's position in this frame by the vector:

$$U = (u_x, u_y, u_z)$$ (54)

and the position of the ith satellite by:

$$S_i = (x_i, y_i, z_i) \qquad \text{where } i=1..n \text{ for } n \text{ measurements.}$$ (55)
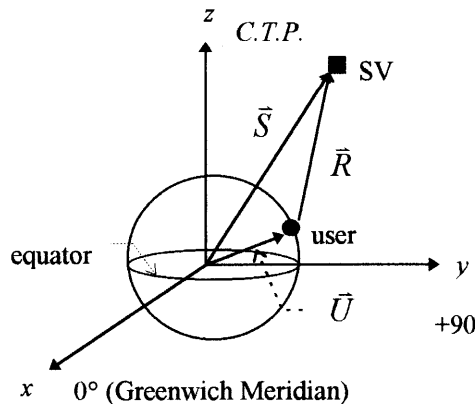

Figure 2.1 GPS earth centered earth fixed coordinate frame.

Then the true range from the receiver to the SV is given by:

$$R_i = |S_i - U| = ((x_i - u_x)^2 + (y_i - u_y)^2 + (z_i - u_z))^{1/2} \qquad i=1..m \qquad (56)$$

Now, if we knew the signal transit time precisely and assumed the propagation velocity was known and constant, then:

$$R_i = c\tau_i \qquad \text{where} \quad c = propagation\ velocity \qquad (57)$$
$$\text{and} \qquad \tau_i = actual\ transit\ time$$

As mentioned, since the receiver and SV clocks are not synchronized, the measurement of signal transit time (scaled by c) is called a pseudo-range measurement. The time that the receiver makes this measurement, as measured by the receiver's clock, is called the "receive epoch" and is denoted by T_R. Since the receiver clock varies from GPS system time we have:

$$T_R = t_R + \Delta t_u \qquad \text{where} \quad t_R = \text{receive epoch in GPS system time} \qquad (58)$$
$$\Delta t_u = \text{receiver clock bias}$$

The time that the SV transmits the signal, as measured by the SV clock, is denoted by T_T. The SV clock also has a bias from GPS system time, and thus:

$$T_T = t_T + \Delta t_{sv} \qquad \text{where} \quad t_T = \text{transmit time in GPS system time} \qquad (59)$$
$$\Delta t_{sv} = \text{SV clock bias}$$

The pseudo-range measurement is thus given by:

$$\rho_i = (T_R - T_T)c$$
$$= [(t_R + \Delta t_u) - (t_T + \Delta t_{sv})]c$$
$$= c\tau_i + c(\Delta t_u - \Delta t_{sv}) \qquad \text{from (57)} \quad t_R - t_T = \tau_i \qquad (60)$$

We expect errors to be introduced in the measurement process as well as from a variety of factors like imprecise knowledge of c, multipath, residual clock and SV position errors, and selective availability, which will be discussed in a subsequent section. To account for this, we add the term ε to (60), which lumps together all these errors. We thus have:

$$\rho_i = c\tau_i + c(\Delta t_u - \Delta t_{sv}) + \varepsilon_i$$
$$= R_i + c\Delta t_u - c\Delta t_{sv} + \varepsilon_i$$
$$= |S_i - U| + c\Delta t_u - c\Delta t_{sv} + \varepsilon_i \qquad (61)$$

In Equation (61) ρ is measured at the receiver and S and Δt_{sv} are calculated by the receiver from parameters that are transmitted from the SV on a signal called the navigation data message. The calculation of these two variables is covered in Appendix A. Equation (61) reveals that for each measurement (i.e. one for each SV in view) we have a non-linear equation. The unknowns to be estimated are:

$$\begin{bmatrix} \vec{U}' & c\Delta t_u \end{bmatrix}' = \begin{bmatrix} u_x & u_y & u_z & c\Delta t_u \end{bmatrix}' \qquad (62)$$

26

Since there are four unknowns to be solved for, this accounts for the requirement that we make pseudo-range measurements to four different satellites in order to get a navigation solution. A solution is obtained by linearizing (61). To linearize (61) we use a Taylor expansion about an estimate of the user's position and clock bias :

Let $\quad \hat{X} = \begin{bmatrix} \hat{U}^T & c\Delta\hat{t}_u \end{bmatrix}$ $\quad$ be our current best estimate of the receiver navigation state vector.

If $\hat{\rho}$ is the pseudo-range from the receiver's estimated position to the SV, then the Taylor expansion about this estimate is:

$$\rho_i = \hat{\rho}_i + \frac{\partial \rho_i}{\partial X}\bigg|_{X=\hat{X}} (X - \hat{X}) + \varepsilon_i \qquad (63)$$

where ε_i now includes errors from the higher order terms and all unknown biases that are not modeled and removed. Taking the partials and rearranging (63), we get an equation in terms of the pseudo-range residual, $\Delta\rho_i$, and the error in our estimate, $[\Delta U^T \quad c(\Delta t_u - \Delta t_u)]$:

$$\Delta\rho_i = \hat{\rho}_i - \rho_i = \begin{bmatrix} \dfrac{-(x_i - \hat{u}_x)}{\left|S_i - \hat{U}\right|} & \dfrac{-(y_i - \hat{u}_y)}{\left|S_i - \hat{U}\right|} & \dfrac{-(z_i - \hat{u}_z)}{\left|S_i - \hat{U}\right|} & 1 \end{bmatrix} \begin{bmatrix} \hat{u}_x - u_x \\ \hat{u}_y - u_y \\ \hat{u}_z - u_z \\ c(\Delta\hat{t}_u - \Delta t_u) \end{bmatrix} + \varepsilon_i \qquad (64)$$

We can rewrite (64) as:

$$\Delta\rho_i = \begin{bmatrix} -\hat{r}_i^T & 1 \end{bmatrix} \begin{bmatrix} \Delta U \\ c(\Delta\hat{t}_u - \Delta t_u) \end{bmatrix} + \varepsilon_i \qquad (65)$$

where $\hat{r}_i$ is the line of sight unit vector from the current estimate of the user's position to the ith satellite, and ΔU is the error in the position estimate. If we make measurements to m different SV's then we can set up the measurement equations:

$$\Delta\rho = H\Delta X + E \qquad (66)$$

where $\quad \Delta\rho = \begin{bmatrix} \Delta\rho_1 \\ \Delta\rho_2 \\ \vdots \\ \Delta\rho_m \end{bmatrix} \quad H = \begin{bmatrix} -\hat{r}_1 \\ -\hat{r}_2 \\ \vdots \\ -\hat{r}_m \end{bmatrix} \quad \Delta X = \begin{bmatrix} \Delta U \\ c(\Delta\hat{t}_u - \Delta t_u) \end{bmatrix} \quad E = \begin{bmatrix} \varepsilon_1 \\ \varepsilon_2 \\ \vdots \\ \varepsilon_m \end{bmatrix}$

and the position error can be obtained from the overconstrained least squares solution:

$$\Delta X = (H^T H)^{-1} H^T \Delta\rho \qquad (67)$$

By adding the solution of (67) to the current best estimate of the state, we have a new estimate of the receiver's position based on the current measurements. This recursive least squares approach to solving for the receiver position is the most common method employed by GPS receivers. Extending this to a Kalman filter is quite straightforward and is explained in the next section.

2.2 GPS Measurement Sensitivity Matrix

In order to fit within the framework of a standard Kalman filter, the measurements should be linearly related to the state vector. The standard Kalman filter measurement equation for a time invariant system is:

$$\vec{Y}[k] = H\vec{X}[k] + \vec{V}[k] \tag{68}$$

In (68) the vector Y is the measurement, the matrix H is the measurement coupling matrix (often referred to as the sensitivity matrix in filtering literature), X is the state vector, and V is the measurement noise. Referring back to Equation (61), we have the following relationship between a GPS measurement and the state vector:

$$\rho_i = \left| S_i - U \right| + c\Delta t_u - c\Delta t_{sv} + \varepsilon_i \tag{61}$$

This is a single measurement to the ith SV. Expanding (61) we get:

$$\rho_i = \sqrt{(x_i - u_x)^2 + (y_i - u_y)^2 + (z_i - u_z)^2} + c\Delta t_u - c\Delta t_{sv} + \varepsilon_i \tag{69}$$

In (69) the measurements are clearly not a linear function of the state vector. This fact requires the implementation of an extended Kalman filter. If we stack up measurements to m different SV's we can rewrite the measurement equation as:

$$\vec{\rho} = h(\vec{X}) - c\Delta\vec{t}_{sv} + \vec{E} \tag{70}$$

where $\quad \vec{\rho} = \begin{bmatrix} \rho_1 \\ \rho_2 \\ \vdots \\ \rho_m \end{bmatrix}, \quad \vec{X} = \begin{bmatrix} u_x & \dot{u}_x & \ddot{u}_x & u_y & \dot{u}_y & \ddot{u}_y & u_z & \dot{u}_z & \ddot{u}_z & c\Delta t_u & f_c \end{bmatrix}^\dagger$

and using the notation from Section 1.3: $\quad b_c = c\Delta t_u$

In the extended Kalman filter we use a Taylor series expansion to linearize the measurement about the current estimate of the state, in an identical manner to that shown in Equation (63). Thus the measurement coupling matrix is given by:

$$H_G = \left. \frac{dh(\vec{X})}{d\vec{X}} \right|_{X = \hat{X}^-} \tag{71}$$

where $\hat{X}^-$ is the *a priori* estimate of the current state, i.e. the filter's prediction of the state at the current epoch, prior to incorporation of the current measurement.

29

Taking the partials yields the matrix:

$$
H_G = \begin{bmatrix}
\dfrac{-(x_1 - \hat{u}_x^-)}{\left| S_1 - \hat{U}^- \right|} & 0 & 0 & \dfrac{-(y_1 - \hat{u}_y^-)}{\left| S_1 - \hat{U}^- \right|} & 0 & 0 & \dfrac{-(z_1 - \hat{u}_z^-)}{\left| S_1 - \hat{U}^- \right|} & 0 & 0 & 1 & 0 \\[4mm]
\dfrac{-(x_2 - \hat{u}_x^-)}{\left| S_2 - \hat{U}^- \right|} & 0 & 0 & \dfrac{-(y_2 - \hat{u}_y^-)}{\left| S_2 - \hat{U}^- \right|} & 0 & 0 & \dfrac{-(y_2 - \hat{u}_y^-)}{\left| S_2 - \hat{U}^- \right|} & 0 & 0 & 1 & 0 \\[4mm]
\vdots & \vdots & \vdots & \vdots & \vdots & \vdots & \vdots & \vdots & \vdots & \vdots & \vdots \\[4mm]
\dfrac{-(x_m - \hat{u}_x^-)}{\left| S_m - \hat{U}^- \right|} & 0 & 0 & \dfrac{-(y_m - \hat{u}_y^-)}{\left| S_m - \hat{U}^- \right|} & 0 & 0 & \dfrac{-(z_m - \hat{u}_z^-)}{\left| S_m - \hat{U}^- \right|} & 0 & 0 & 1 & 0
\end{bmatrix} \qquad (72)
$$

Note that (72) consists of the line-of-sight unit vectors from the current estimate of the user's position to each of the SV's, augmented with a column of ones. This matrix is usually referred to as the "geometry" matrix.

30

2.3 GPS Measurement Errors
2.3.1 GPS Measurement Error\Noise Model

The fundamental measurement equation for a single SV, given in (61), was:

$$\rho_i = \left| S_i - U \right| + c\Delta t_u - c\Delta t_{sv} + \varepsilon_i \tag{61}$$

Once again, we are estimating the user position, U, and clock bias, Δt_u. The satellite position, S_i, and the SV clock bias, Δt_{sv}, are calculated from broadcast data, as explained in Appendix A. All remaining errors were lumped into the term, ε_i. A more careful look at the errors that occur during the typical measurement results in the following pseudo-range equation:

$$\rho_i = \left| S_i - U \right| + c\Delta t_u - c\Delta t_{sv} + \Delta S_i \cdot \vec{r} + R_{SA} + I + T + M + N \tag{73}$$

These error contributions are:

SV Ephemeris Errors: The term given by $\Delta S \cdot r$ is the result of any inaccuracies in the calculation of the satellite position, primarily due to errors in the broadcast ephemeris data. ΔS, which is the actual offset in the SV position, will result in a ranging error equivalent to the projection of that offset onto the line-of-sight vector, $\vec{r}$, to that SV. As might be expected, these errors tend to be highly time correlated.

SV Clock\Selective Availability: R_{SA} in (73) represents what is by far the largest error contributor. As described in the navigation solution, knowledge of the SV's clock bias is crucial to obtaining an accurate range measurement. At propagation velocities, every 3 nanoseconds of clock error translates to about one meter of ranging error. This term includes any inaccuracy in the knowledge of the SV clock bias. The clock bias term is calculated by the receiver, as described in Appendix A, from parameters transmitted on the navigation data message. It turns out that the reason that the SV clock bias cannot be determined accurately is due to a policy implemented by the US Government called Selective Availability (SA). The purpose of this policy is to deliberately degrade the accuracy of real-time navigational information available to civilian users of the GPS. The method used to implement SA is to add a deliberate, continuously varying, "random" error to the value that is calculated from the clock correction parameters. As can be seen from the error budget in Table 2.1, this error component is an order of magnitude larger than all the others and essentially determines the accuracy of a single receiver C/A code GPS user. (Military users have access to decryption information which allows them to reverse this deliberate error.) The ranging error due to the R_{SA} is highly non-white with a small uncorrelated noise-like component.

Atmospheric Effects: The next two terms in (73), I and T, are due to variations in the propagation velocity of GPS signals as they travel through the ionosphere and troposphere. Since accurate knowledge of the propagation speed is germane to the ranging process, these variations contribute directly to range errors. Ionospheric errors are predominantly non-white with a small white component. Tropospheric errors are generally small with an equal time correlated and uncorrelated component.

Multipath: Multipath errors, denoted by the M term in (73), are caused by GPS signals bouncing off of reflective surfaces near the receiver antenna, and causing the correlator to lock to them. This means that the receiver will not be measuring the true direct path range, and will instead have an error offset. As would be expected for a stationary receiver, this error is predominantly a bias. For a moving receiver, with a properly located antenna, this error is fairly small, with an equal uncorrelated component.

Receiver Measurement Noise: The last error term in (73), N, is due to any inaccuracies in the measurement process caused by receiver electronics and software. The exact nature of these errors is dependent upon the particular receiver's implementation. In most cases, modern receiver technology limits this error source to a very minor contribution.

Error Source	Bias (σ, meters)	Uncorrelated (σ, meters)	Total (σ, meters)
Ephemeris	2.1	0.0	2.1
SV Clock/ SA	20.0	0.7	20.0
Ionospheric	4.0	0.5	4.0
Tropospheric	0.5	0.5	0.7
Multipath	1.0	1.0	1.4
Receiver Noise	0.5	0.2	0.5
Total	20.5	1.4	20.6

Table 2.1. GPS ranging error budget[8].

Table 2.1 shows a typical C/A code receiver's expected ranging error budget. In this initial filter design, it is intended that the GPS measurements be made with this kind of receiver. In order to fit within the framework of a Kalman filter, the noise process represented by $V[k]$ in Equation (68) should be time uncorrelated (white). From Table 2.1 we can see that a receiver of this type is dominated by highly non-white errors that are predominantly the result of Selective Availability.

There are at least three approaches that could be taken in this particular application to deal with this problem. The first approach involves incorporating a dynamic model into the filter to track SA. Although the details of how SA is implemented are classified, long term observation of the behavior of these errors by the civilian user community seems to indicate that a reasonably good model for SA is a second order Gauss-Markov process[9]. A state space model for this process would require the addition of two states for every satellite being used. Since it is typical for a minimum of 5 SV's, and often 8 or more, to be in view, this approach would more than double the size of the state vector and significantly increase the filter's computational burden. Although, in some circumstances, this may be an acceptable and practical approach, in this filter implementation it was not considered optimal.

The second approach involves the use of military GPS equipment. A military receiver gains an advantage over a typical C/A code receiver in several ways. First, the effects of SA can be completely removed, and thus the error contribution due to the SV clock is solely a result of inaccuracies in the tracking and prediction of the SV's atomic clock. This results in ranging errors caused by the SV clock to be typically 2.0 m bias and 0.7 m uncorrelated noise[8]. The second way in which a military receiver gains an advantage is through the use of dual frequency tracking. A military receiver uses a different ranging signal, called the P-code, which is transmitted on two different L-band carriers. By making dual frequency correlations, the P-code receiver is able to remove a large part of the ionospheric error by solving for the frequency dependent delay this effect causes. The result is to reduce ionospheric errors to 1.0 m bias and 0.7 m uncorrelated noise[8]. The resulting total ranging error for a military receiver is typically 3.3 m bias and 1.5 m uncorrelated noise[8]. The use of a military GPS receiver in implementing this filter is not covered in this work but is likely to be included in future extensions.

The third approach to dealing with the highly time correlated nature of pseudo-range errors utilizes a technique called differential corrections. This technique involves the use of a second GPS reference receiver at the data processing site, and results in the removal of the largest amount of time correlated error component. This is the approach used in the design of this filter and is discussed in detail the next section.
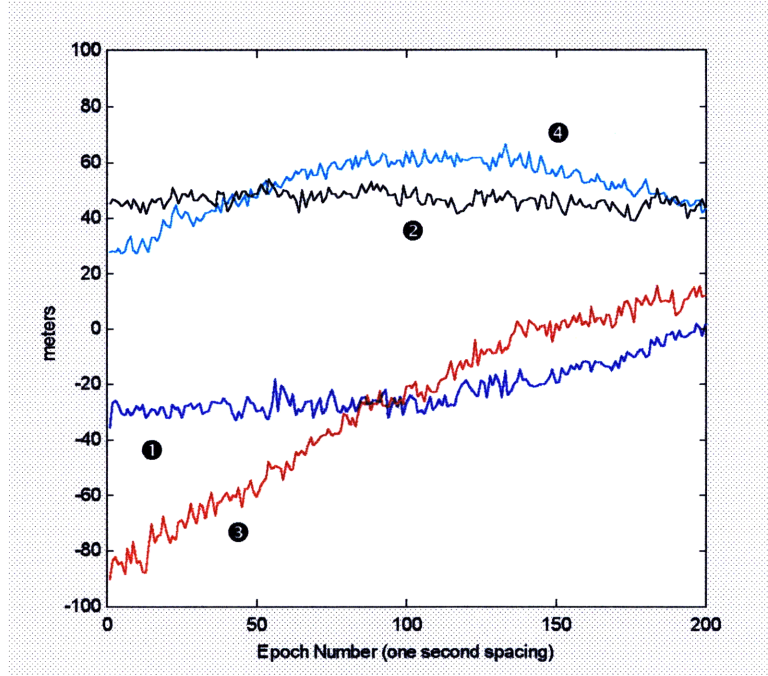
Figure 2.2. Pseudo-range errors for 200 second interval collected from sv19(❶),sv9(❷),sv17(❸),sv23(❹).

In Figure 2.2 above, the error\noise component of the pseudo-range measurements for four different satellites is plotted over a 200 second interval. This data was collected with an Ashtech Ranger model 6M C/A code tracking receiver located at an accurately surveyed point. The errors were determined by calculating the predicted pseudo-range based on the known receiver location and information on the SV position and clock error. In this figure we can see that the errors essentially consist of a small white noise component, on the order of a couple of meters as given in Table 2.1, and a slowly varying bias, which is mostly due Selective Availability. There is also a small bias component present in all plots, due to an error in the receiver clock prediction. This bias is common to all SV's and does not affect the position solution.

If unmodeled, the highly time correlated nature of the biases, caused primarily by the first three error sources in Table 2.1, will cause the Kalman Filter to track these variations as if they were plant dynamics. This necessitates their removal, which is accomplished in this filter through the differential correction technique discussed next.

33

2.3.2 Differential Correction Technique

The underlying principle behind the differential technique is that most of the highly time correlated errors discussed in the previous section are also correlated over distance. This means that two receivers within a certain distance of each other will be subject to essentially the same errors when making ranging measurements to the same satellite. The differential technique, illustrated in Figure 2.3, is thus to locate a reference receiver at a surveyed site. This receiver makes pseudo-range measurements to all SV's in view and then by using the receiver's known position, calculates what each pseudo-range should be. The differences are correction factors which can be applied to any other receiver's (within a certain range) pseudo-range measurements to the same satellites, resulting in a dramatic increase in the accuracy of those measurements. Since errors are significantly correlated only for a limited time and distance, the corrections should be applied quickly, and only to receivers within a certain range from the reference location. For the purposes of this application positioning accuracy of 10 m or less are considered quite acceptable, since we are often tracking targets whose size itself exceeds this amount. It turns out that if we locate the reference receiver within 1000 km of the airborne unit, and apply the corrections within 10 seconds, this level of accuracy is attainable[10].
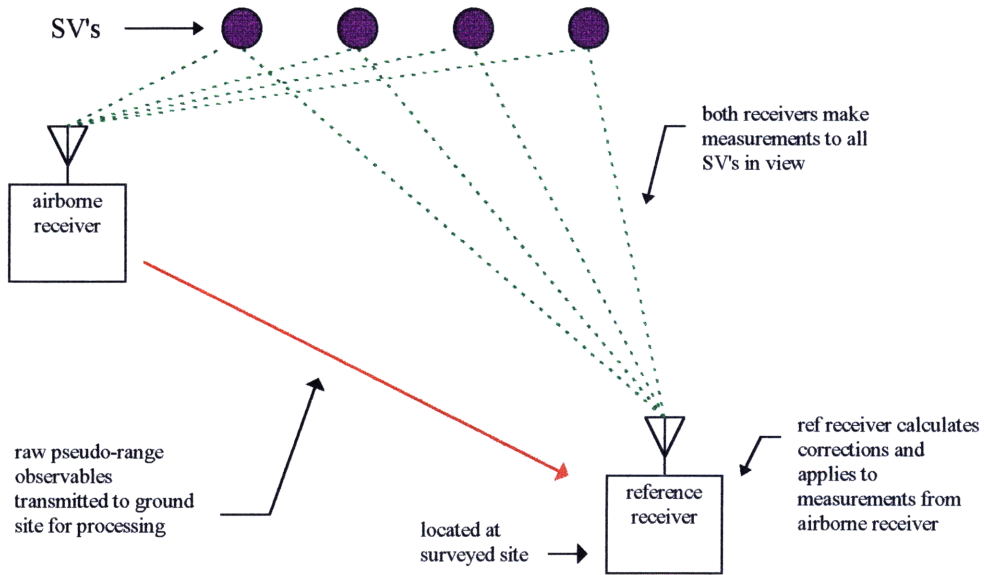

Figure 2.3. Differential correction scenario.

The application of differential corrections is as follows. The reference receiver depicted in Figure 2.3 is located at a surveyed site and we know its position vector, U_R. Recall that the basic pseudo-range equation to the ith SV as given by (61) is:

$$\rho_{R_i} = \left| S_i - U_R \right| + c\Delta t_{Ru} - c\Delta t_{sv_i} + \varepsilon_{Ri} \tag{74}$$

where the subscript R refers to the reference receiver.

Since we know U_R, using the values S_i and Δt_{sv} calculated from the ephemeris data, and an estimate of the receiver's clock bias, we can calculate a predicted value for the first three terms on the right hand side of (74). If this value is subtracted from the actual value of ρ_{Ri} measured by the reference receiver, we end up with an estimate of the error component ε_{Ri}.

34

That is:

$$\varepsilon_{Ri} \approx \rho_{Ri} - \left| S_i - U_R \right| + c\Delta t_{Ru} - c\Delta t_{sv_i} = \Delta\rho_i \qquad (75)$$

Equation (75) defines the basic pseudo-range correction for the ith SV. The reference receiver will make this calculation for all SV's it collects measurements on. At the same time, the airborne receiver makes a pseudo-range measurement to the same SV's. Each of these measurements consists of:

$$\rho_{A_i} = \left| S_i - U_A \right| + c\Delta t_{Au} - c\Delta t_{sv_i} + \varepsilon_{Ai} \qquad (76)$$

Since the assumption is that a large part of the error component in (76) is common to the error in (74), we have:

$$\varepsilon_{Ai} = \varepsilon_{Ri} + v_i \qquad (77)$$

where v_i is the uncorrelated part of the error.

Thus, if we subtract the pseudo-range correction in (75) from (76) the error component in the corrected pseudo-range is reduced to v, which has a significantly reduced bias and is much more predominantly white noise. The corrected airborne measurement is thus given by:

$$\rho c_{A_i} = \rho_{Ai} - \Delta\rho_i = \left| S_i - U_A \right| + c\Delta t_{Au} - c\Delta t_{sv_i} + v_i \qquad (78)$$

This correction process is applied to every pseudo-range measurement made by the airborne receiver that is common to the reference receiver. Only corrected ranges are then used in the filter. Note that in the above calculation we used an estimated value of the receiver clock bias. The particular value used in the determination of the pseudo-range correction is not critical since any offset here will be common to all the measurements to each SV, and thus will end up being removed from the final position solution[10].
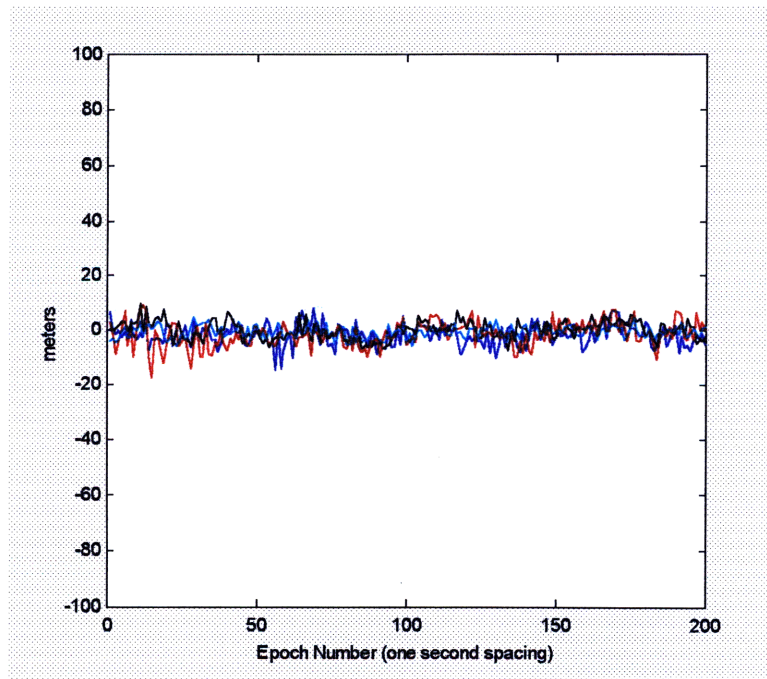

Figure 2.4. Pseudo-range errors after differential correction (same interval and SV's as Figure 2.2).

35

In Figure 2.4 above, we see the result of applying the differential corrections technique to the pseudo-range measurements whose errors were plotted in Figure 2.2. As desired, the result is to eliminate most of the time-correlated bias component, leaving predominantly white noise like errors. A GPS-only extended Kalman filter was run on both the uncorrected and corrected data sets to illustrate the effect of the unremoved bias on the position solution. Figure 2.5 shows the position estimation error in the x coordinate for a filter run on both data sets. As might be expected for the uncorrected data, the time-correlated bias in the pseudo-ranges is tracked by the filter and shows up as a slowly varying position error. In fact, without any attempt to model the bias component in the filter, this is indistinguishable from target movement. For the filter run on the differentially corrected data, we see a dramatic decrease in estimation error and we achieve the desired affect of having an unbiased estimator.
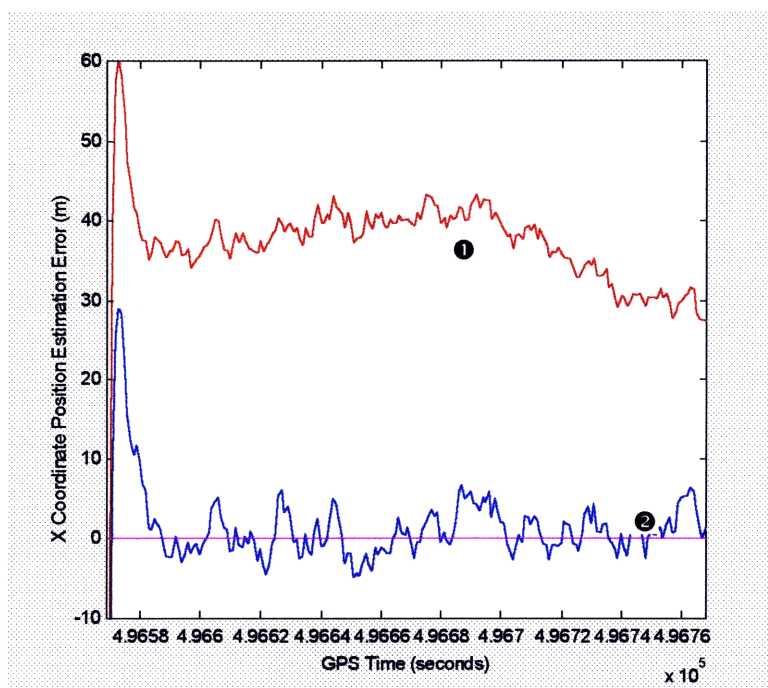

Figure 2.5. Position estimation error in x coordinate for an extended Kalman filter run on uncorrected(❶) and differentially corrected(❷) data.

2.3.3 GPS Measurement Noise Covariance Matrix

Once the differential correction process described in Section 2.3.2 is applied to the GPS measurements, the remaining errors are due predominantly to receiver noise and multipath and are on the order of 1-3 meters. These errors may be modeled in the filter as independent, zero mean, white noise processes with expectation of reasonable results. The resulting measurement noise covariance matrix would then be:

$$R_G = \mathrm{E}\{V_G[j]V_G{}'[k]\} = \mathrm{E}\{\begin{bmatrix} v_1 \\ v_2 \\ \vdots \\ v_m \end{bmatrix} \begin{bmatrix} v_1 & v_2 & \cdots & v_m \end{bmatrix}\} \tag{79}$$

With the assumption that these are independent identical processes then we get:

$$R_G = \sigma_\rho^2 I \tag{80}$$

where I is the *mxm* identity matrix (assuming m measurements) and :

$$\sigma_\rho^2 = \mathrm{E}\{v_i v_i\} \tag{81}$$

3. Radar Measurement Model

The intent in this filter design is to integrate position (tracking) data on an airborne target, obtained from a ground-based radar sensor, with position data obtained from a GPS receiver. The type of radar used to track aircraft in a cooperative scenario such as this would typically be a microwave pulse radar. This type of radar transmits pulses at the target which are, either actively or passively, bounced back from the target. This enables the radar system to measure the direction and range to the target. A passive system relies on what is called "skin" return, which is simply the electromagnetic energy reflected off the target's body, for a signal to track. Since we have already assumed that the aircraft being tracked is cooperative on account of its requirement to transmit GPS data, it might also be reasonable to expect that a radar transponder would be used. A transponder is a device carried aboard the target that transmits a return pulse to the radar system whenever it receives a pulse from the ground. This provides a more reliable "active" return signal for the radar to track. In both of the above cases, the measurement set is identical and the types of errors are very similar. This section derives the model for the radar sensor measurements.

3.1 Radar Position Measurements

The measurements that are obtained from the tracking radar are normally given in a spherical coordinate system and consist of the *azimuth* and *elevation* angle, and the *range* to the target. These coordinates are given relative to a topocentric frame such as the one shown in Figure 3.1. The topocentric coordinate frame is a right handed system with it's origin on the earth's surface and its axis pointing to *East, True North, and Up*. By *True North,* we mean that this is the direction toward the *Conventional Terrestrial North Pole*, which is the point where the *z axis* of the *ECEF* frame, defined in Figure 2.1, intersects the reference ellipsoid. The *East* axis points along the direction of the latitude lines, and the *Up* axis is normal to the plane formed by the *East* and *North* axis, which is essentially the local vertical direction. This local radar coordinate system has its origin at the radar location and is abbreviated as the *ENU* frame. The *Azimuth (Az)* angle is given clockwise from the *North* axis and the *Elevation (El)* angle is positive relative to the *E-N* plane.
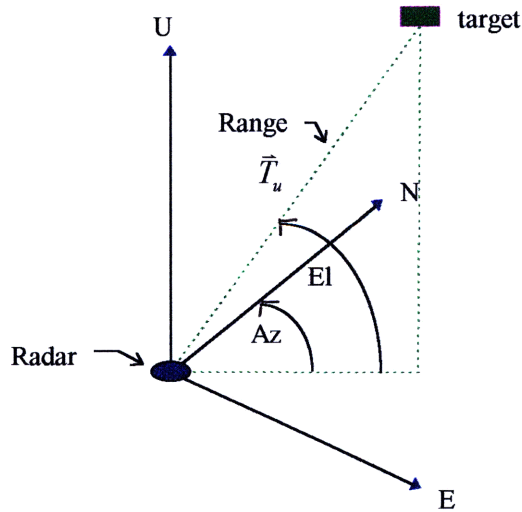

Figure 3.1. Radar Measurements and Local (ENU) Coordinate System.

38

If we define the target position vector in the *ENU* frame to be:

$$\vec{T}_U = \begin{bmatrix} E \\ N \\ U \end{bmatrix} = \begin{bmatrix} x_u \\ y_u \\ z_u \end{bmatrix} \tag{82}$$

then from Figure 3.1, we see that the relationships between the measurements and the Cartesian (*ENU*) coordinates are given by:

$$Az = \tan^{-1}(\frac{x_u}{y_u}) \tag{83}$$

$$El = \tan^{-1}(\frac{z_u}{\sqrt{x_u^2 + y_u^2}}) \tag{84}$$

$$Rng = \sqrt{x_u^2 + y_u^2 + z_u^2} \tag{85}$$

3.2 Radar Measurement Sensitivity Matrix

In order to derive the radar measurement coupling matrix for the extended Kalman filter, we need to derive the relationship between these measurements and the state vector. Recall that the state vector gives the target position in *ECEF* coordinates. Thus, to find the sensitivity matrix, we need to first find the function $h(X)$, in the basic measurement equation, which relates these *ECEF* coordinates to the radar measurements. The form of the radar measurement equation is:

$$Y_R[k] = h_R(X[k]) + V_R[k] \tag{86}$$

where $Y_R[k] = \begin{bmatrix} Az[k] \\ El[k] \\ Rng[k] \end{bmatrix}$, $X[k]$ is the state vector as given in (50), and V_R is the radar measurement

noise vector.

Let the target position vector in the *ECEF* frame, which corresponds to the appropriate elements of the state vector, be given by:

$$\vec{P}_E = \begin{bmatrix} x_P \\ y_P \\ z_P \end{bmatrix} \tag{87}$$

Referring to Figure 3.2, the target position vector, given in *ECEF* coordinates, from the radar frame *(ENU)* origin is given by:

$$\vec{T}_E = \begin{bmatrix} x_T \\ y_T \\ z_T \end{bmatrix} \tag{88}$$

The radar antenna phase center is at the local *ENU* frame origin and its location is usually accurately surveyed. We assume here that we know the *ECEF* coordinates of this frame origin. This vector is given by:

$$\vec{S}_E = \begin{bmatrix} x_R \\ y_R \\ z_R \end{bmatrix} \tag{89}$$

Thus:

$$\vec{T}_E = \vec{P}_E - \vec{S}_E = \begin{bmatrix} x_P - x_R \\ y_p - y_R \\ z_p - z_R \end{bmatrix} \tag{90}$$
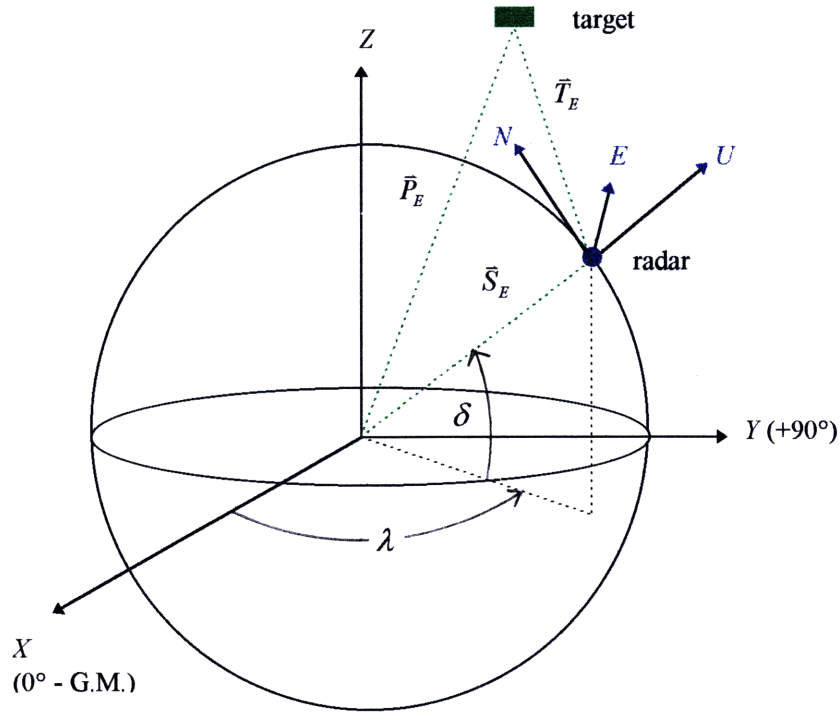
Figure 3.2. Relationship between radar (*ENU*) frame and *ECEF* frame.

Equation (90) gives us the target position vector relative to the radar frame origin in *ECEF* coordinates. In order to relate that vector to the measurements, we need to rotate the *ECEF* vector into the *ENU* frame. In addition to knowing the radar frame origin in *ECEF* coordinates $(\vec{S}_E)$, we assume we know, or have derived, the geodetic latitude, δ, and longitude, λ, of the origin. (The relationships between the *ECEF* coordinates and the geodetic latitude and longitude are derived in Appendix B.) Using this information we perform the frame rotations as follows. We start with the *U, E, N axis* of the radar frame aligned with the *X, Y, Z axis* of the *ECEF* frame in that order, and rotate around the *Z axis* by the angle λ, where the longitude angle is measured positive in an easterly direction from the zero meridian (*X axis*). This gives the first rotation matrix:

$$R_1 = \begin{bmatrix} -\sin\lambda & \cos\lambda & 0 \\ 0 & 0 & 1 \\ \cos\lambda & \sin\lambda & 0 \end{bmatrix}$$

(91)

Next we rotate about the *E axis* by the angle δ, where North latitude angles are measured positive. This gives the second rotation matrix:

$$R_2 = \begin{bmatrix} 1 & 0 & 0 \\ 0 & \cos\delta & -\sin\delta \\ 0 & \sin\delta & \cos\delta \end{bmatrix}$$

(92)

Combining these two rotations with equation (90), the target position vector from the radar frame origin, in *ENU* coordinates, is given by:

$$\vec{T}_U = \begin{bmatrix} x_u \\ y_u \\ z_u \end{bmatrix} = R_2 R_1 (\vec{P}_E - \vec{S}_E)$$

$$= \begin{bmatrix} -\sin\lambda & \cos\lambda & 0 \\ -\sin\delta\cos\lambda & -\sin\delta\sin\lambda & \cos\delta \\ \cos\delta\cos\lambda & \cos\delta\sin\lambda & \sin\delta \end{bmatrix} \begin{bmatrix} x_P - x_R \\ y_P - y_R \\ z_P - z_R \end{bmatrix} \tag{93}$$

or more explicitly:

$$E = x_u = -\sin\lambda(x_P - x_R) + \cos\lambda(y_P - y_R) \tag{94}$$

$$N = y_u = -\sin\delta\cos\lambda(x_P - x_R) - \sin\delta\sin\lambda(y_P - y_R) + \cos\delta(z_P - z_R) \tag{95}$$

$$U = z_u = \cos\delta\cos\lambda(x_P - x_R) + \cos\delta\sin\lambda(y_P - y_R) + \sin\delta(z_P - z_R) \tag{96}$$

Substituting (94) - (96) into (83) - (85) gives the measurements *(Az, El, Rng)* in terms of the states *(x_P, y_P, z_P)*. Thus our equation for the radar measurements is:

$$\begin{bmatrix} Az \\ El \\ Rng \end{bmatrix} = \begin{bmatrix} \tan^{-1}[\dfrac{E}{N}] \\ \tan^{-1}[\dfrac{U}{\sqrt{E^2 + N^2}}] \\ \sqrt{E^2 + N^2 + U^2} \end{bmatrix} + \begin{bmatrix} v_a \\ v_e \\ v_r \end{bmatrix} \tag{97}$$

where *E,N* and *U* are defined by (94)-(96) and v_a, v_e, and v_r are the measurement noise processes. Clearly our measurements are not a linear function of the state variables, and thus, as with the GPS measurements, the radar coupling matrix for the filter is the Jacobian of the vector function *h(X)* in Equation (97). The coupling matrix is thus given by:

$$H_R = \frac{\partial h_R(X)}{\partial X}\bigg|_{X = \hat{X}^-} \tag{98}$$

$$= \begin{bmatrix} \dfrac{\partial[\tan^{-1}(E/N)]}{\partial x_{P:}} & 0 & 0 & \dfrac{\partial[\tan^{-1}(E/N)]}{\partial y_{P:}} & 0 & 0 & \dfrac{\partial[\tan^{-1}(E/N)]}{\partial z_{P:}} & 0 & 0 & 0 & 0 \\[3mm] \dfrac{\partial[\tan^{-1}(U/\sqrt{E^2+N^2})]}{\partial x_P} & 0 & 0 & \dfrac{\partial[\tan^{-1}(U/\sqrt{E^2+N^2})]}{\partial y_P} & 0 & 0 & \dfrac{\partial[\tan^{-1}(U/\sqrt{E^2+N^2})]}{\partial z_P} & 0 & 0 & 0 & 0 \\[3mm] \dfrac{\partial[\sqrt{E^2+N^2+U^2}]}{\partial x_p} & 0 & 0 & \dfrac{\partial[\sqrt{E^2+N^2+U^2}]}{\partial y_p} & 0 & 0 & \dfrac{\partial[\sqrt{E^2+N^2+U^2}]}{\partial z_p} & 0 & 0 & 0 & 0 \end{bmatrix}$$

where:

$$\frac{\partial[\tan^{-1}(E/N)]}{\partial x_P} = \frac{-\sin\lambda \cdot N + \sin\delta\cos\lambda \cdot E}{N^2 + E^2} \tag{99}$$

$$\frac{\partial[\tan^{-1}(E/N)]}{\partial y_P} = \frac{\cos\lambda \cdot N + \sin\delta\sin\lambda \cdot E}{N^2 + E^2} \tag{100}$$

$$\frac{\partial[\tan^{-1}(E/N)]}{\partial z_P} = \frac{-\cos\delta \cdot E}{N^2 + E^2} \tag{101}$$

$$\frac{\partial[\tan^{-1}(U/\sqrt{E^2+N^2})]}{\partial x_P} = \frac{\sqrt{E^2+N^2} \cdot \cos\lambda\cos\delta + \dfrac{U(\sin\lambda \cdot E + \cos\lambda\sin\delta \cdot N)}{\sqrt{E^2+N^2}}}{E^2 + N^2 + U^2} \tag{102}$$

$$\frac{\partial[\tan^{-1}(U/\sqrt{E^2+N^2})]}{\partial y_P} = \frac{\sqrt{E^2+N^2} \cdot \sin\lambda\cos\delta - \dfrac{U(\cos\lambda \cdot E - \sin\lambda\sin\delta \cdot N)}{\sqrt{E^2+N^2}}}{E^2 + N^2 + U^2} \tag{103}$$

$$\frac{\partial[\tan^{-1}(U/\sqrt{E^2+N^2})]}{\partial z_P} = \frac{\sqrt{E^2+N^2} \cdot \sin\delta - \dfrac{U \cdot \cos\delta \cdot N}{\sqrt{E^2+N^2}}}{E^2 + N^2 + U^2} \tag{104}$$

$$\frac{\partial[\sqrt{E^2+N^2+U^2}]}{\partial x_p} = \frac{-\sin\lambda \cdot E - \sin\delta\cos\lambda \cdot N + \cos\delta\cos\lambda \cdot U}{\sqrt{E^2+N^2+U^2}} \tag{105}$$

43

$$\frac{\partial[\sqrt{E^2 + N^2 + U^2}]}{\partial y_p} = \frac{\cos\lambda \cdot E - \sin\delta\sin\lambda \cdot N + \cos\delta\sin\lambda \cdot U}{\sqrt{E^2 + N^2 + U^2}} \qquad (106)$$

$$\frac{\partial[\sqrt{E^2 + N^2 + U^2}]}{\partial z_p} = \frac{\cos\delta \cdot N + \sin\delta \cdot U}{\sqrt{E^2 + N^2 + U^2}} \qquad (107)$$

where, once again, E, N, and U are functions of the state vector, given by (94)-(96). Note that δ and λ are constants determined by the "fixed" location of the radar site. Thus, in the expressions above, all the trigonometric functions are constants that may be pre-computed off-line.

3.3 Radar Measurement Error\Noise Model

Since the Kalman filter framework requires that we are able to characterize the errors in our observables as white noise processes we once again desire to fit the radar measurement model into the form of equation (86), where $V[k]$ is such a process. As we might expect, it turns out that most radar measurements also have significant time correlated components, and we once again have a measurement of the form:

$$y[k] = \begin{bmatrix} Az \\ El \\ Rng \end{bmatrix} = h(X[k]) + \begin{bmatrix} b_a \\ b_e \\ b_r \end{bmatrix} + \begin{bmatrix} v_a[k] \\ v_e[k] \\ v_r[k] \end{bmatrix} \tag{108}$$

where b represents the bias component and $v[k]$ the white noise component of each measurement. The exact nature of these errors is, naturally, highly dependent on the particular type of radar sensor being used. However, some generalizations can be made to present a reasonable initial model for use in the filter. It is expected that, at implementation, calibration data from the particular radar being used will allow fine tuning of the model.

The type of radar typically being employed for aircraft tracking is called a "monopulse" tracking radar. In this type of radar, a range measurement is made by bouncing an electromagnetic pulse off the target and measuring the round-trip travel time to the target. Scaling by an assumed propagation velocity gives the range to the target. The bias component in the range measurement would be expected to consist of fixed latencies which were most likely due to the electronics, and also a slowly time varying component. In some cases there are deliberate latencies added to the system, as is the case with a transponder aided tracker. In that case, the transponder is typically programmed to add a delay of the order of several microseconds (thousands of meters) between the time it receives a radar pulse until it replies. Fixed, or constant latencies, are either known or measurable beforehand and it is assumed here that they can simply be subtracted from the measurements. Slowly time varying error components that might also be present in range measurements can be due to effects such as multipath. In this case we have no a-priori knowledge of the bias and we cannot simply remove it. Multipath effects tend to be present primarily when tracking low altitude targets.

The bearing angle to the target is typically measured by making a phase comparison of the signal returned to two closely spaced antenna elements. A signal nulling process is used to steer the antenna, either electronically or physically, so that it is pointing at the target. In the case of a physically steered antenna, the azimuth and elevation angles may, for example, be read off resolvers on the antenna pedestal. Here we would also expect there to be fixed angle errors which may be measured and subtracted off, and some slowly time varying components which would not be removable.

Since it can be expected that the exact nature and amount of the range and angle biases will vary greatly not only from one mechanization to another, but also between two different sensors of identical type, the general approach to modeling radar biases will be to obtain calibration data on each sensor which can be used to remove any fixed errors. In this initial implementation of the filter, the slowly varying time correlated radar errors due to phenomena such as multipath will not be removed.

The remaining error component will essentially be an uncorrelated noise process that we will model as independent white noise added to each measurement. In the case of both bearing and range measurements, these types of errors are caused primarily by the electronics involved with discrimination process. For the range measurement, the radar receiver may have a detector that is attempting to find the edge of a received pulse, and for the bearing measurement, a discriminator may be used to find a signal null. In both these cases we can expect the quality of the detection to depend directly on the received signal-to-noise ratio. That is, the magnitude of the errors expected are inversely proportional to the signal to noise ratio.

45

A common rule of thumb for the magnitude of radar errors is given by[11]:

$$\sigma \approx \frac{k}{\sqrt{S/N}}$$ (109)

where S/N is the peak-signal to mean-noise ratio out of a matched filter detector and k is a proportionality constant that depends on the particular mechanization of the radar sensor. We can use (109) to derive a simple expression for the spectral density of the noise processes, v, in (108). Starting with the expression for the signal to noise ratio out of a receiver[12]:

$$\frac{S_o}{N_o} = \frac{S_i/N_i}{F}$$ (110)

where S_o/N_o = Signal power to noise power ratio out of radar receiver.

              S_i/N_i = Signal power to noise power ratio into radar receiver.

              F = Noise figure of receiver.

For the input noise power we can substitute the idealized expression:

$$N_i = K_B TB \quad \text{(watts)}$$ (111)

where K_B = Boltzman constant (J/degK).

              T = Temperature in degrees Kelvin.

              B = Receiver bandwidth (Hz).

Also, using a simple form of the radar range equation, the input signal power at the radar receiver is given by[12]:

$$S_i = \frac{P_t GA_e \sigma_{cs}}{(4\pi)^2 R^4}$$ (112)

where P_t = Transmitted Power (W).

              G = Antenna gain.

              A_e = Antenna effective aperture (m^2).

              σ_{cs} = Target radar cross section (m^2).

              R = Target range (m).

Substituting (111) and (112) into (110) we get the following expression for the signal-to-noise ratio at the output of the receiver (i.e. used by the detector):

$$\frac{S_o}{N_o} = \frac{P_t GA_e \sigma_{cs}}{(4\pi)^2 K_B TBFR^4}$$ (113)

In Equation (115) it is reasonable to assume all the factors, with the exception of range, are constant for a given tracking scenario. The result is then that, for a particular radar sensor, the received signal-to-noise is inversely proportional to the fourth power of the range. That is:

$$S_o/N_o = \frac{k}{R^4}$$ (114)

where k now is a proportionality constant that incorporates all the physical parameters of the particular radar sensor being employed. If we now take Equation (114) and substitute it into (109) we get the following relationship for the standard deviation of our measurement errors:

$$\sigma = kR^2$$ (115)

where k now incorporates the square root of the proportionality constant in (114) and the proportionality constant used in (109). The above derivation is not meant to serve as a rigorous, ironclad method for determining the process noise variance in our radar measurement model, since there are many simplifications made, and a large number of physical parameters to include in an actual calculation. Rather, it is meant to demonstrate, from first principles, that we might expect the measurement noise variance to vary with the target's range from the radar sensor. It would therefore be reasonable to incorporate some range dependence into the measurement noise covariance matrix of the filter. This range dependence would typically not be expected to be monotonic over the entire operating range of the radar, and in fact many radars suffer from certain degradations that occur at short ranges as well[12]. It is believed that the best approach to handling this would be to obtain calibration data from the radar sensor and to formulate a polynomial fit in range for the magnitude of the noise variance. Thus we would expect to have a measurement noise covariance matrix that is given by:

$$E\{V_R[k]V_R'[j]\} = R_R = \begin{bmatrix} \sigma_{Az}^2 & 0 & 0 \\ 0 & \sigma_{El}^2 & 0 \\ 0 & 0 & \sigma_{Rng}^2 \end{bmatrix} = \begin{bmatrix} f_a(\hat{Rng}) & 0 & 0 \\ 0 & f_e(\hat{Rng}) & 0 \\ 0 & 0 & f_r(\hat{Rng}) \end{bmatrix}$$ (116)

where $\hat{Rng}$ is the filter's best estimate of the current range of the target, obtained by taking the magnitude of $\vec{T}_E$ in Equation (90).

4. Filter Description

The structure of the filter employed in this work is essentially a discrete time extended Kalman filter with non-linearity only in the measurements. That is, since the chosen process model has a linear state evolution equation, the only linearization that needs to be performed is on the measurements. As seen in Sections 2 and 3, measurements from both sensors are non-linear functions of the state vector. It is assumed the reader is familiar with Kalman filtering concepts and Section 4 primarily describes details specific to this implementation. For more background on general Kalman filtering the reader is referred to [5] and [13].

4.1 Matrix Definitions

The general form of this filter is shown in Figure 4.1, using the following matrix definitions:

X[k]: **(11x1)** The state vector which consists of position, velocity, and acceleration for each spatial coordinate in an *Earth Centered Earth Fixed* coordinate system, and the phase and frequency of the GPS receiver clock. Defined in Equation (50).

$\Phi(\alpha,T)$: **(11x11)** The plant dynamics state transition matrix. This matrix, which defines the discrete time behavior of the plant, is a combination of the target dynamics state transition matrix given in Equation (19), and the GPS clock model state transition matrix given in Equation (42). Note that this matrix is a function of two parameters: α, the acceleration model correlation time constant, and T, the discretization sample period. In this filter, it is generally assumed that α will be fixed for a class of targets being tracked and will not change in real-time. However, a possible extension to this filter would be to employ an adaptive algorithm that allows α to change in response to perceived target dynamics. Since the parameter T may vary if the data fed into the filter is not evenly sampled in time, the state transition matrix is recalculated in response to this. Defined in Equation (51).

$Q(\alpha,\sigma_m^2,\sigma_p^2,\sigma_f^2,T)$: **(11x11)** The process noise covariance matrix. This matrix defines the statistics for the noise driving the plant model, and again is a combination of the covariance matrices for the target dynamics, defined by Equation (38), and the GPS clock model, defined in Equation (49). This matrix is also a function of the target acceleration model parameters, α and σ_m^2, which, as mentioned above, are not expected to vary during the filter operation. The two parameters, σ_p^2 and σ_f^2, which define the spectral densities of the noise processes driving the continuous time clock model, are determined by the chosen receiver hardware, and do not vary during filter operation. This covariance matrix is also a function of the sample period, T, and like the state transition matrix, must be recalculated if the data sample time changes. Defined in Equation (53).

H[k]: **(m+3x11)** This is the linearized measurement sensitivity matrix which defines the relationship between the measurements and the state vector. The filter's measurement vector has the form:

$$Y[k]=\begin{bmatrix} Az[k] \\ El[k] \\ Rng[k] \\ \rho_1[k] \\ \vdots \\ \rho_m[k] \end{bmatrix} \tag{117}$$

where the ρ's are the pseudo-range measurements to the "m" satellites that are available, and the three radar observables are *Azimuth, Elevation, and Range.* The H matrix is the combination of the GPS

48

measurement coupling matrix defined in Equation (72), and the radar measurement coupling matrix, defined in Equations (98-107). Thus H is given by:

$$H[k] = \begin{bmatrix} H_R[k, X[k|k-1]] \\ H_G[k, X[k|k-1]] \end{bmatrix}$$ (118)

Since the H matrix is a function of the current *a-priori* state estimate, it must be updated at every filter epoch. In addition, the size of the matrix will vary depending upon the number of measurements available to the filter at a given epoch.

$R(\hat{r})$: **((m+3)x(m+3))** This is the filter measurement noise covariance matrix and is a combination of the GPS measurement noise covariance matrix, R_G, and the radar measurement noise covariance matrix, $R_R(r)$. All GPS observables are assumed to have independent, identical, and stationary statistics and thus R_G is an *(mxm)* constant matrix. As described in Section 3, however, the radar observables typically do not have stationary noise statistics and thus the *(3x3)* matrix, $R_r(Rng)$, is updated as the estimated target range varies. Thus R has the form:

$$R(\hat{Rng}) = \begin{bmatrix} R_R(\hat{Rng}) & 0 \\ 0 & R_G \end{bmatrix}$$ (119)

P and K: (11x11) and (11x(m+3)): These are the normal state estimation error covariance and Kalman gain matrices and are defined in Figure 4.1.

4.2 Implementation Description

The general form of an Extended Kalman Filter with only non-linear measurements is shown in Figure 4.1. This section outlines details particular to this specific implementation of the general filter shown there. In the subsequent description, the filter epochs are assumed to be driven by the GPS data, which is available at a one second spacing. Radar data, which is typically available at a much higher rate, is sampled to coincide with these epochs. With the exception of the initialization, the following steps are performed recursively:

Initialization: This step is generally performed by assigning to the initial state estimate the first position fix on the target, available from any source. This fix could be calculated independently from either sensor's data. For example, it could be a single epoch least squares GPS solution. However, simulations indicate the filter should be quite robust to initial position errors, and will converge fairly rapidly even from extremely large distances. The error covariance matrix must also be assigned some initial value, and this normally should indicate to the filter the magnitude of the initial position estimation error. It is expected that, regardless of how these two matrices are initialized, the filter should converge properly. The real issue to be determined in initialization is how quickly the filter converges and how long the initial filter transients take to die out. One exception is that assigning the initial state estimate to zero causes the filter to attempt inverting a singular matrix. Obviously, this should be avoided and the filter code should have some method of detecting this condition.

State and Covariance Extrapolation: This is the normal Kalman filter procedure of taking the current state estimate and error covariance and predicting forward one time step. The navigation state vector is projected forward using the target dynamics model represented by the state transition matrix Φ, and the error covariance matrix is projected forward using Φ and Q, the process noise covariance. Note that since both these matrices are functions of the data sampling time, a routine for recalculating them is invoked if the filter detects a change in T. In initial simulations of the filter on real data, changes in sample time occurred occasionally due to missed GPS data epochs and were detected from time stamping

49

available on the data. Note that, depending on the data rates available from the particular sensors used, different data sampling schemes could be employed. For example, it is not necessary that data from both sensors be available at each epoch. The filter can be driven by whichever data is available at a desired sample time.

Calculate Measurement Coupling Matrix: Using the *a-priori* state estimate, the measurement coupling matrix is computed. For the GPS measurements this involves using the current position estimate and the computed SV positions to calculate the geometry matrix given in Equation (72), and for the radar measurements the matrix defined by Equation (98) is calculated. The size of the matrix depends upon the number of measurements available at the current epoch. Note that when calculating *H*, it is convenient to also calculate the predicted observables needed for the filter innovation used in the update step. For example, when computing the line-of-sight vectors to each SV, the predicted pseudo-ranges can be calculated simply by using the SV clock bias and estimated receiver clock bias. Similarly, the predicted radar measurements are easily calculated from the values of *E,N, and U,* that are computed to find the radar measurement sensitivity matrix.

Calculate Filter Gain Matrix: The Kalman gain matrix is computed using the current values of *H, R,* and *P[k|k-1]*. The current value of the measurement noise covariance matrix, *R,* is obtained using the predicted radar range.

Measurement Update: In this final step the current measurements are incorporated. In the actual filter implementation, care must be taken when calculating the innovation, $y[k] - \hat{y}[k]$, since two of the radar measurements involve angles. The innovation term thus contains azimuth and elevation angle differences, which if not treated properly can cause the filter to behave unstably. For example, if the estimate is converging on the true target position in azimuth from one side and then at the next measurement crosses over, the innovation must be corrected in sign and magnitude so the filter is steered back in the appropriate direction. If not accounted for, the modulo 2π nature of the angle innovation may steer the filter in azimuth all the way around 360° again. This can be handled simply by ensuring that the innovation is always corrected to be in the range 0 - π, with the appropriate sign. After the new state estimate is calculated, the updated error covariance is calculated.
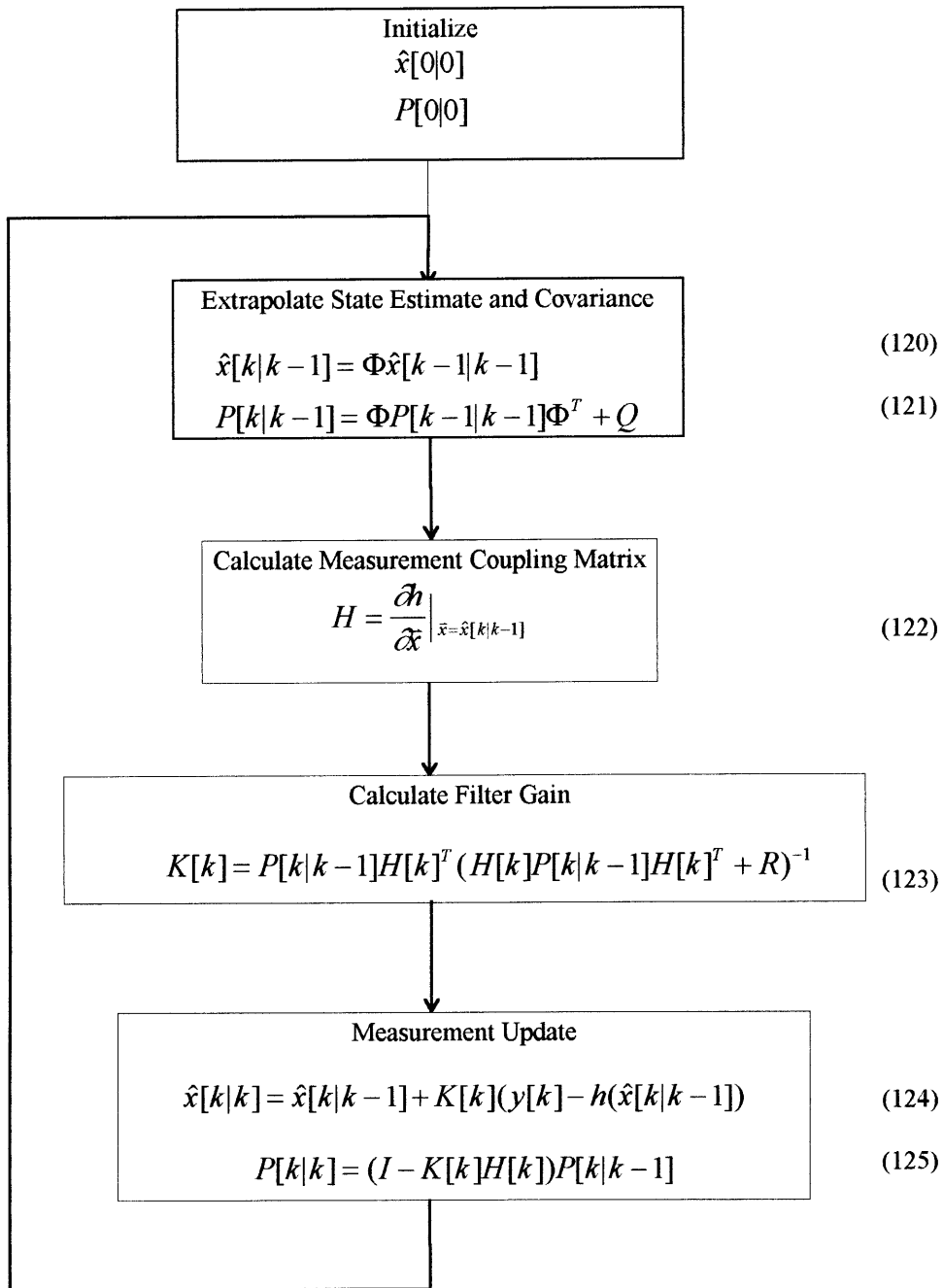
```
Initialize
x̂[0|0]
P[0|0]
```

Extrapolate State Estimate and Covariance

$$\hat{x}[k|k-1] = \Phi \hat{x}[k-1|k-1] \qquad (120)$$

$$P[k|k-1] = \Phi P[k-1|k-1]\Phi^{T} + Q \qquad (121)$$

Calculate Measurement Coupling Matrix

$$H = \left.\frac{\partial h}{\partial x}\right|_{\bar{x} = \hat{x}[k|k-1]} \qquad (122)$$

Calculate Filter Gain

$$K[k] = P[k|k-1]H[k]^{T}(H[k]P[k|k-1]H[k]^{T} + R)^{-1} \qquad (123)$$

Measurement Update

$$\hat{x}[k|k] = \hat{x}[k|k-1] + K[k](y[k] - h(\hat{x}[k|k-1])) \qquad (124)$$

$$P[k|k] = (I - K[k]H[k])P[k|k-1] \qquad (125)$$

Figure 4.1. Flow chart for an extended Kalman filter with non-linear measurement equation.

5. Filter Simulation and Test

Verification of the filter design presented in this work was conducted in several stages. First, a set of two-dimensional (planar) simulations was run using various target trajectories and measurement sets. These studies, which allowed manipulation of the target dynamics and filter parameters, provided considerable insight into the accuracy and convergence of the filter under a variety of scenarios. Next, the full three dimensional form of the filter described in the previous sections was implemented using Matlab[27], and tested using data collected from actual GPS receivers combined with simulated radar data. The results of these tests are presented below. Future testing will include actual implementation of this filter into a tracking system at MIT-Lincoln Laboratory, where airborne kinematic GPS data will be available in conjunction with instrumentation radar tracking data.

5.1 2D Simulations
5.1.1 2D Planar Radar-Only Filter Simulations

This set of simulations was conducted with a two dimensional formulation of the filter that utilized only radar measurements. At first the target was kept stationary and a Monte Carlo analysis was conducted to examine the convergence of the filter under different initial conditions and values of the model parameters. It was found that, with one exception, the filter converged to a steady state solution about the real target position for all tested values. The one exception was if the filter was started with a zero state vector which represents an equilibrium point for the system. As would be expected, the values chosen for the initial conditions and model parameters affected the rate of convergence, i.e. the dissipation of the initial filter transients. Figure 5.1 shows the ensemble mean error variance for the x coordinate position, velocity, and acceleration for a set of 20 simulation runs with a stationary target. No dimensions were assigned for these simulations. Figure 5.2 shows the ensemble mean estimation error, for all the state variables, for the same simulations. From these results, it can be seen that the filter is convergent, in the sense that it reaches a steady state position error, and that the estimate is unbiased.
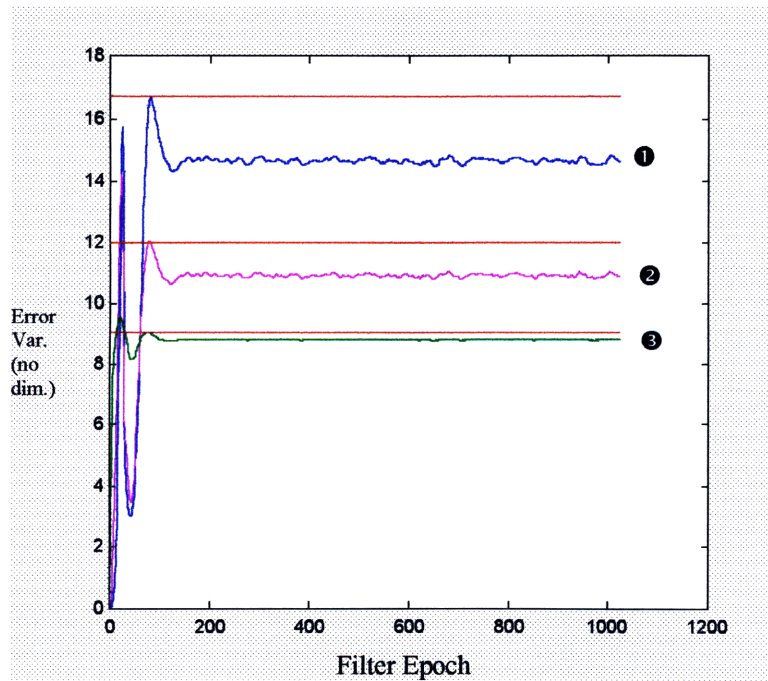

Figure 5.1. Mean error variance for x pos.(❶), x vel.(❷), x acc.(❸) with predicted steady state values in red. {$T=0.1$, $\alpha=1$, $\sigma_m^2=10$ (for x and y), target range = 500+v_r ($v_r{\sim}N[0,1]$), target bearing=$\pi/4$+ v_b ($v_b{\sim}N[o,.001]$), number samples = 1024}

With a standard Kalman filter the steady state error covariance, P_∞, can be accurately predicted from the steady state solution of the matrix Riccati equation:

$$\Phi P_\infty \Phi^T + GQG^T - \Phi P_\infty H^T (HP_\infty H^T + R)^{-1} HP_\infty \Phi^T = P_\infty \qquad (126)$$

For the extended Kalman filter, although the error covariance is still propagated by the Riccati equation, the value of the measurement coupling matrix, H, is a function of the current state estimate. Since the state estimate is a random variable, H is not known beforehand and, strictly speaking, the actual value of the error covariance cannot be precomputed. However, when conducting simulations, the trajectory of the target is known in advance, and we can therefore compute a nominal point by point solution to Equation (126), by using the value of H evaluated along this trajectory. This technique was employed, and it turns out that in all these simulations, the solution always closely predicted the behavior of the error covariance, although the predicted value was always slightly larger. This nominal prediction was extremely useful in determining whether the filter was behaving reasonably under dynamic target simulations, where, as will be shown below, the error covariance appears divergent. In Figure 5.1 the error covariance predicted by this method is shown in red just above each plot.
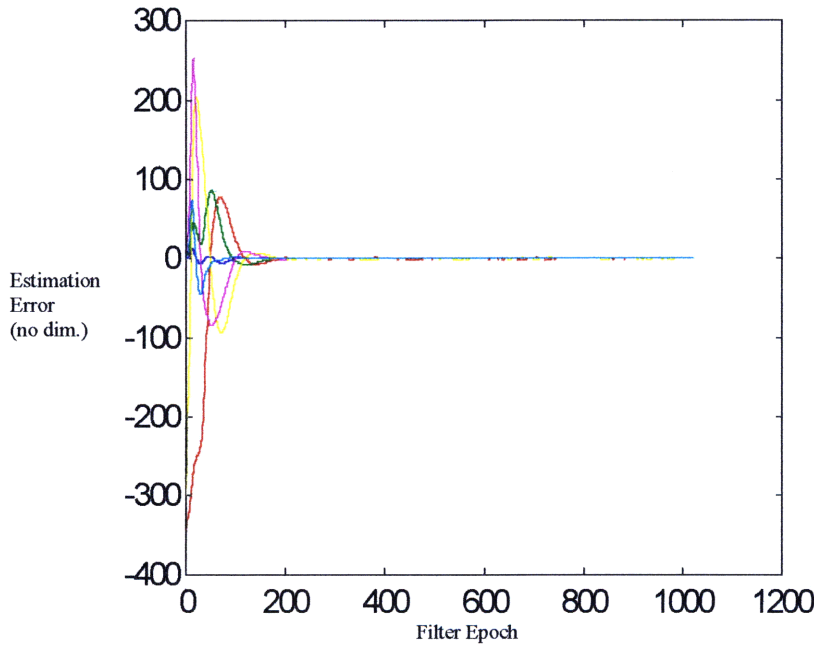
Figure 5.2. Ensemble mean estimation error for all state variables *(x,y)* for stationary target.
{Same parameters as Figure 5.1}

The next set of simulations investigated the behavior of the 2D radar-only filter with a moving target. With a dynamic target, several issues arise that are not apparent in the static case. Selected results are shown below for a simulation of a target with linearly increasing range and bearing angle. The trajectory is thus a spiral outward from the radar site. Once again, a properly tuned filter tracked the target quite well. Figure 5.3 shows a typical target and filter trajectory for these simulations. The filter was initialized with a small position error, and the target and filter plots are virtually identical except for the initial acquisition phase. The most interesting results here come from examination of the estimation errors for this trajectory. Figure 5.4 shows the ensemble average error covariance plot for the x coordinate the filter with the predicted values in red. This plot shows that the estimation errors are increasing in magnitude and appear to be sinusoidally modulated. It turns out that for this particular measurement set, there is a structural dependence of the error covariance on the range and bearing of the target. This can be understood by looking at the situation depicted in Figure 5.5.
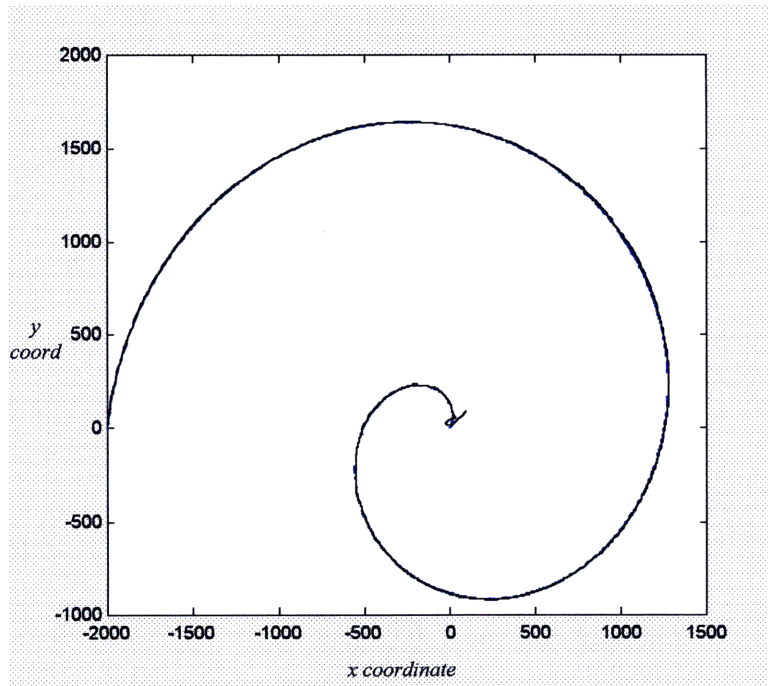
53

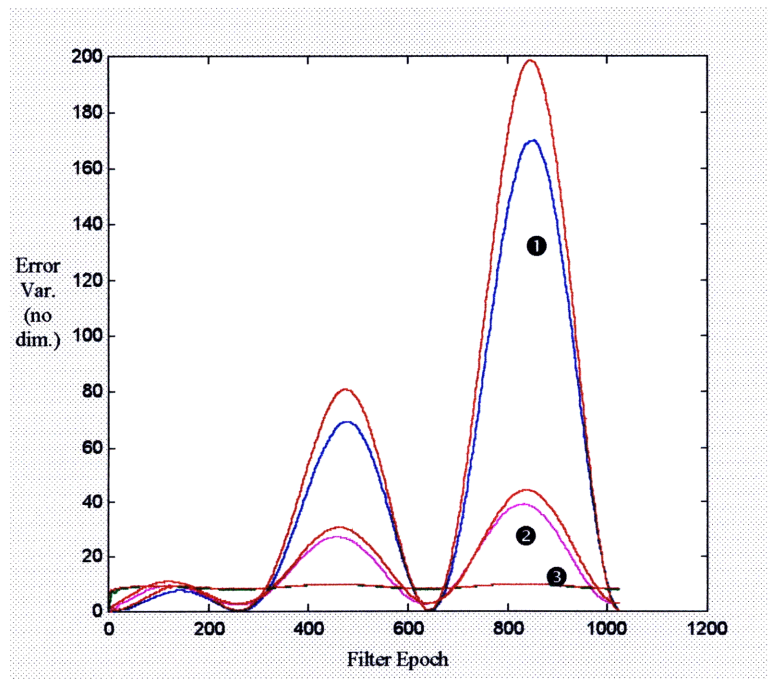Figure 5.3. Target and filter trajectories for moving target simulation.

Figure 5.4. Ensemble average x pos(❶), x vel(❷), x acc(❸) error variance for above simulation with predicted values in red.
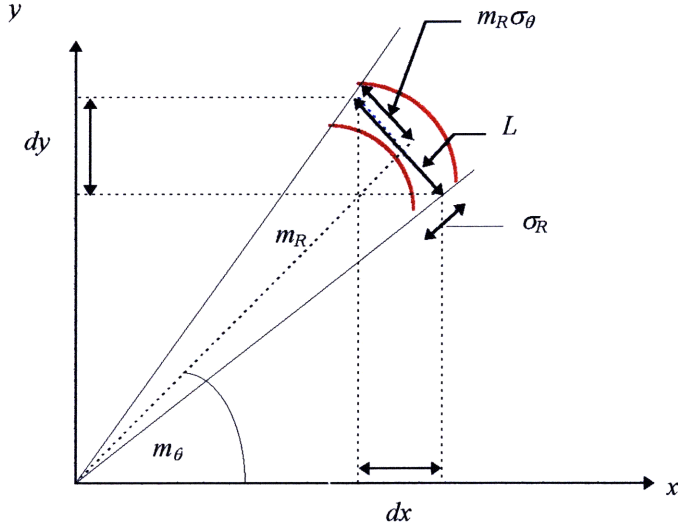
Figure 5.5. Structural dependence of positional uncertainty on target position.

In the above figure we depict a target located at position $(R, \Theta) = (m_R, m_\theta)$. Any particular measurement of that target position is characterized by a region of uncertainty based on the magnitude of the noise variances. For a range/bearing measurement this region takes the approximate shape of the arc between the red lines in Figure 5.5. The thickness of this arc is set by σ_R and the arc length at the center is determined by $m_R\sigma_\theta$, where m_R is $E\{R\}$. In this scenario we make the assumption that $m_R\sigma_\theta > \sigma_R$, i.e. the range is sufficiently large so that the arc of uncertainty is longer than it is thick. With the assumption that σ_θ is small, the arc length is approximately the straight blue line at $R=m_R$, with say length L. The measurements are statistically characterized by:

$$\Theta \approx N(m_\Theta, \sigma_\Theta^2) \qquad \text{and} \qquad R = N(m_R, \sigma_R^2) \tag{127}$$

where m_R and m_Θ correspond to the true trajectory of the target. The projection of the line L onto the x and y axis are approximately given by:

$$dx = L\sin(m_\Theta) \qquad \text{and} \qquad dy = L\cos(m_\Theta) \tag{128}$$

Now since L is proportional to the angle variance, i.e.

$$L \propto m_R\sigma_\Theta \qquad \text{then from (128)} \quad dx \propto m_R\sigma_\Theta \sin(m_\Theta) \tag{129}$$
$$\text{and} \quad dy \propto m_R\sigma_\Theta \cos(m_\Theta) \tag{130}$$

Thus since dx and dy represent the uncertainty in position variables x and y we can conclude:

$$\sigma_x^2 \propto m_R^2 \sin^2(m_\Theta)\sigma_\Theta^2 \qquad \text{and} \qquad \sigma_y^2 \propto m_R^2 \cos^2(m_\Theta)\sigma_\Theta^2 \tag{131}$$

What the above essentially says is that, even using a range/bearing measurement with stationary statistics, (i.e. R, the measurement noise covariance matrix (different from the R used above), is constant,) we would expect to see the uncertainty in x and y position vary with the target position and thus with time for a moving target. In fact, if the target is moving away from the radar, we can expect position uncertainty to grow proportional to the square of the range. For targets with an angle rate, we can expect to see a

55

sinusoidal modulation on the x and y error covariance. Equations (131) predict the behavior of position errors for the above simulations quite well.

The above heuristic explanation of the behavior of the error covariance points out that range and angle measurements in themselves cause an inherent degradation of positioning accuracy even with the assumption of stationarity in measurement noise. When this effect is combined with the range dependence of the radar measurement noise model presented in Section 3.3, the deterioration of position estimates can be considerable at large ranges.

5.1.2   2D Planar Radar+GPS Filter Simulations

In this set of simulations, the effect of augmenting the radar-only filter, described in Section 5.1, with a single GPS observable was examined. As discussed in Section 2, a GPS receiver obtains a position solution by making ranging measurements to a number of satellites. If we require a navigation solution from a GPS sensor only, we need a minimum of four different satellites, and any number of measurements less than this would not be sufficient for the GPS-only filter to converge. Since the intent of this filter study is to explore a low level integration of measurements from the two types of sensors (GPS and radar), this set of simulations looked at the utility of combining a single GPS range measurement with radar.

Once again, a variety of static and dynamic simulations were conducted, and the filter was observed to converge to the target trajectory in all cases. For these simulations the GPS range measurement noise was chosen to be the same magnitude as the radar range measurement noise. (This, in fact, turns out to be an approximately realistic assumption for real-world radar and GPS sensors.) The most significant effect of the combined measurement set can be seen by looking at simulations with the spiral trajectory used for the radar-only filter. With the radar-only filter we saw a significant degradation in estimation accuracy with increasing range. By augmenting the radar-only filter with a single GPS observable, we can almost completely remove this effect. Figures 5.6 and 5.7 compare the estimation errors and error covariances from typical simulation of the radar-only filter and of the GPS augmented filter for the same spiral trajectory.
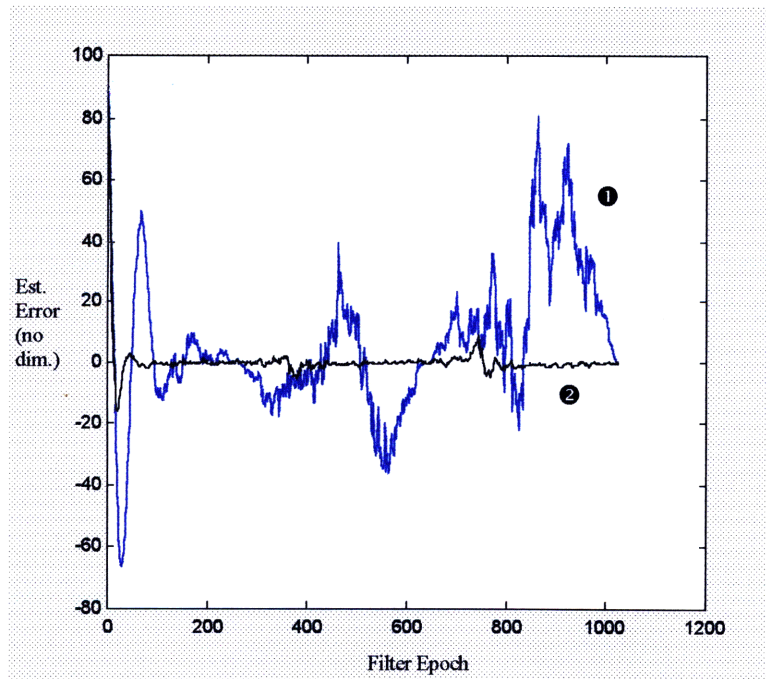

Figure 5.6. Estimation errors in x coordinate from typical simulation of radar-only filter (❶) compared to radar + single GPS range filter (❷) for spiral trajectory.
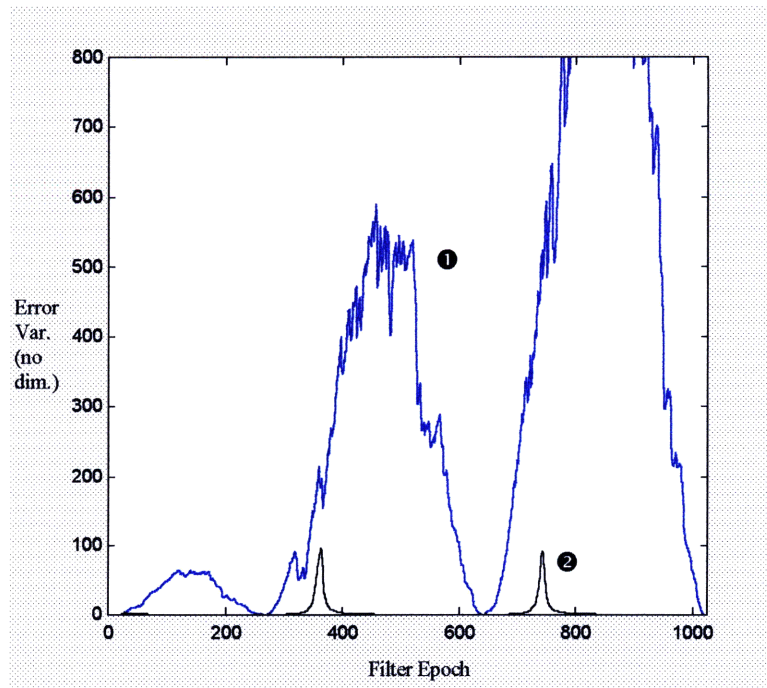
56

Figure 5.7. Estimation error variance in *x* coordinate from typical simulation of radar-only filter (❶) compared to radar + single GPS range filter (❷) for spiral trajectory.

In Figure 5.6 we see the expected increase in estimation errors as the target increases in range for the radar-only filter. In comparison, however, the filter augmented with a single GPS measurement shows almost no such degradation. This is confirmed by looking at the error variance plot in Figure 5.7. The radar-only filter displays the expected range and angle dependence, whereas the GPS augmented filter has almost constant error variance. The small spikes occur when the two range measurements are aligned, i.e. when the radar, target, and satellite are all collinear. Once again, as a means of verifying the performance of the filter, the steady state solution to the algebraic Ricatti equation was calculated along the known trajectory. This nominal performance is compared to the actual (ensemble mean) error covariance of the augmented filter in Figure 5.8, and we can see that the filter does indeed appear to behave reasonably.

57
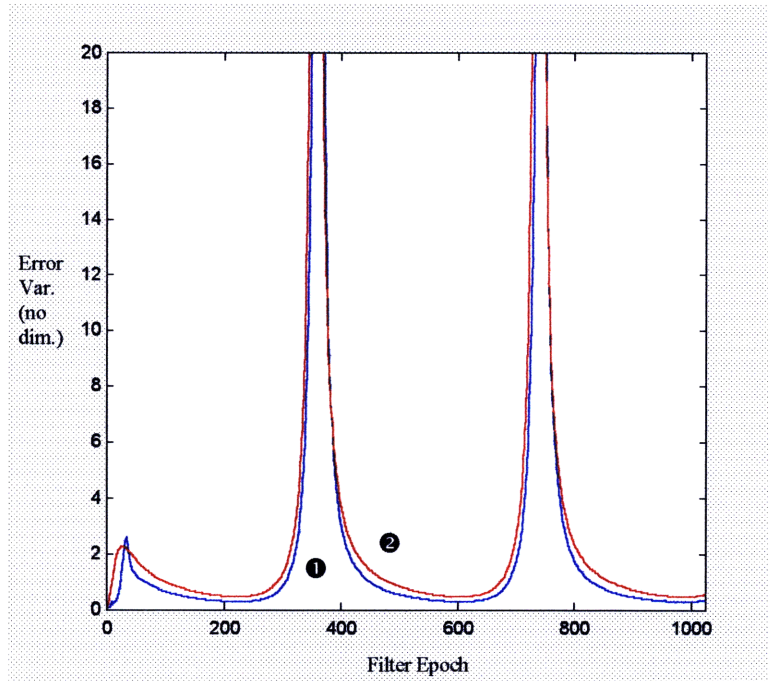
Figure 5.8. Ensemble mean error variance in *x* position (❶) versus predicted steady state solution (❷) for GPS augmented filter.
{T=0.1, α=0.1, σ_m^2=100 (for x and y), radar range noise: (v_r~N[0,1]), bearing noise: (v_b~N[0,0.01]), GPS range noise:(v_{rg}~N[0,1]), number samples = 1024}

5.1.3   Summary of 2D Planar Simulations

Examination of the radar-only 2D filter simulations served as a base-line performance metric for the study of this filter integration. As was shown, a radar-only filter can be constructed that serves, when properly tuned, as an unbiased position estimator. However, when using the standard radar measurement set, the estimation error has a geometric dependence which results in significant degradation of performance with increasing range. By augmenting the radar-only filter with a single GPS range measurement we were able to almost completely remove any geometric degradation in filter performance. Apart from any robustness issues that may be addressed by such an integration, these results indicate a significant benefit in combining sensor data even when only a partial measurement set is available from GPS. Further investigation of the benefits of combining different measurements was conducted and the results are presented in Section 5.3.

5.2 Filter Tuning

An important issue, whose relevance is highlighted when simulating dynamic targets, is that of filter tuning. By tuning, we refer primarily to the setting of the model parameters α and σ_m^2 which are appropriate for the dynamics of the target we expect to track. Assuming we have properly characterized the sensor errors and our process model is correct, these parameters will essentially determine the filter's ability to track. One way to think about this is to realize that the dynamics of our plant model are governed by these parameters. In other words, the aircraft model "flying" in our filter is only capable of the dynamics we assign to it. If we set the model parameters to correspond to a slow flying, less maneuverable aircraft, and we subsequently try to track a fast, highly maneuverable aircraft, we might expect to see the filter diverge. However, modeling a highly maneuverable target in the filter can result in the filter being too sensitive to measurement noise, which it interprets as reasonable target dynamics. In a real application we might hope to track a wide variety of target dynamics reasonably well, and we would thus be driven by a trade-off between performance and flexibility. Much work in the literature has focused on the problem of adaptively changing the target model in response to perceived dynamics.

In addition to the target dynamics model, we also have two parameters that tune the GPS receiver clock model, σ_p^2 and σ_f^2. It turns out that due to the stability of most clocks used in GPS receivers, the clock bias, although large, varies relatively slowly. The result is that there is a fair degree of latitude in selecting these parameters without adversely affecting the position solution. These spectral densities can be derived from an Allan variance plot of the clock behavior[5], however, quite acceptable results can be obtained using values that have been derived for a whole class of clock oscillators. For example, in all the tests conducted in this work, values of α and σ_m^2 were used that apply to all temperature compensated crystal oscillators.

Tuning of the target dynamics model is somewhat more critical. The figure below shows an example of filter divergence due to improper setting of the filter these parameters. Here, the maneuver variance used in the filter process model is much too small for the dynamics of this spiral trajectory, and the filter track can clearly be seen to diverge from the target. Qualitatively, this is an example of the filter process model not being able to keep up with the aircraft.
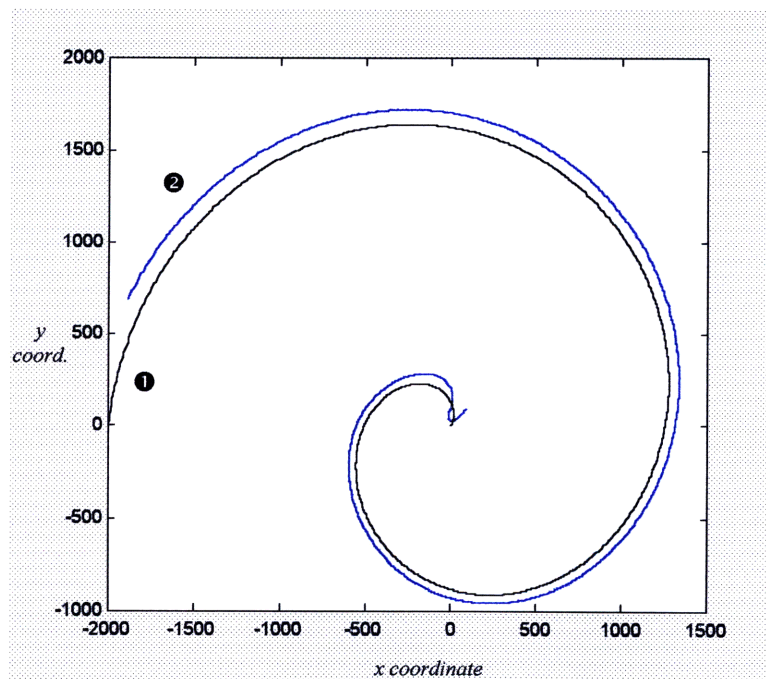

Figure 5.9. Sample divergence of an improperly tuned filter. Target (❶) Filter (❷).

The position estimation errors for the *x* coordinate for two different filter tunings are shown in Figure 5.10. The more central blue plot corresponds to a filter which is correctly tuned. As discussed previously, the magnitude of the errors will increase with range and be sinusoidally modulated, but they should remain unbiased. This is essentially the case for the properly tuned filter shown below. However, the red plot in Figure 5.10 corresponds to a mistuned filter. Here the estimation errors are clearly biased. Note that the bias is also a function of position.
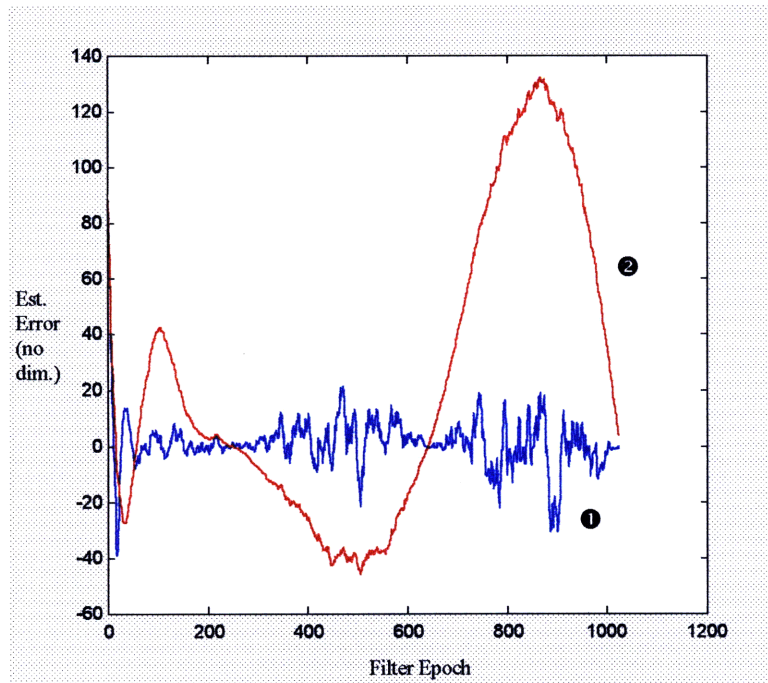
Figure 5.10. Estimation errors for *x* coordinate for properly (❶) and improperly (❷) tuned filter.

As might be expected, there is a trade-off in tuning the maneuver variance of the filter. As shown, if we improperly model the aircraft dynamics, we can expect the filter to develop a bias error. However, in our effort to ensure the filter remains unbiased by increasing the maneuver variance, we also the cause the filter to start paying more attention to noise, thereby increasing the error covariance. Figures 5.11 and 5.12 demonstrate this trade-off. Figure 5.11 plots the estimation errors for a range of values of σ_m^2, while Figure 5.12 shows the error variance of the *x* position for the same values. The correlation time constant was fixed at $\alpha=1/30$ for all these simulations.
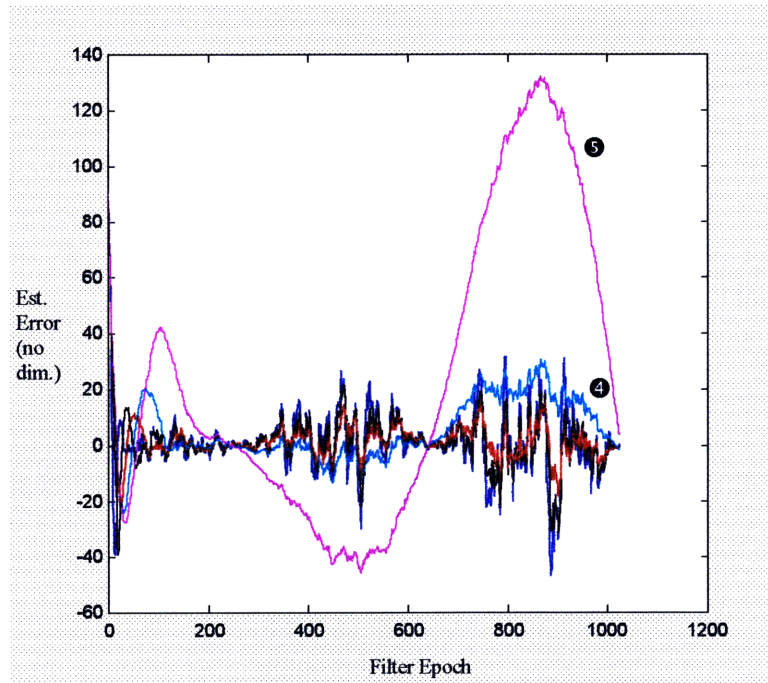
Figure 5.11. Estimation error in x position for $\sigma_m{}^2$= 1000 , 100 , 10, 1(❹), 0.1(❺) .

Time Averaged of Estimation Errors from Figure 5.11

$\sigma_m{}^2$	1000	100	10	1	0.1
avg. est. err. X	.9	.9	1.4	5.8	25.7

In Figure 5.11 it is a little difficult to distinguish the behavior of the different plots, but the essential idea is that for the small maneuver variance (0.1) we have the outlying sinusoidally modulated plot, which displays a low noise component and a large bias. As the maneuver variance increases the bias decreases, but the magnitude of noise component increases. As an indicator of the bias in the above plots, a time average of the estimation error was calculated for a section of the trajectory. These are tabulated above and confirm that the larger the maneuver variance, the less the bias. In Figure 5.12 we can see how the magnitude of the error variance is directly proportional to the maneuver variance.

61
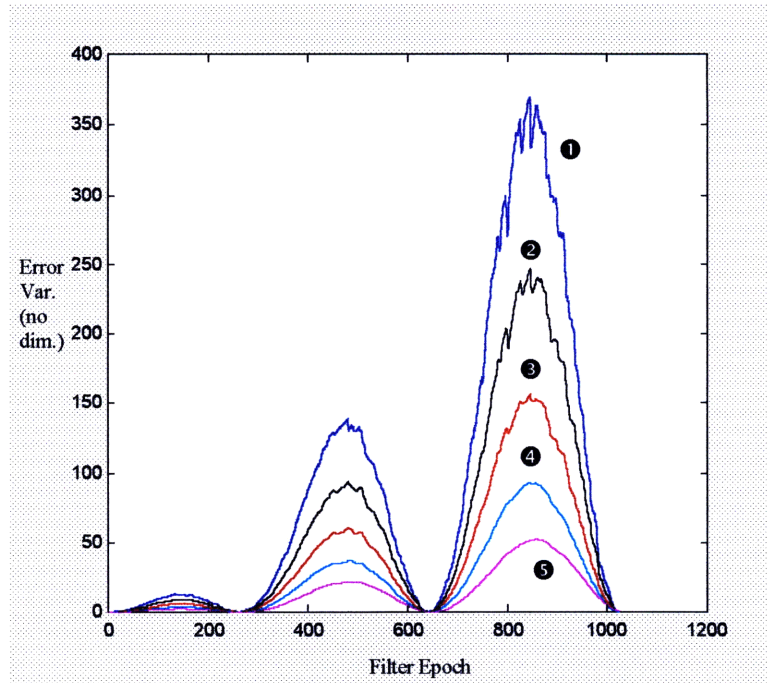
Figure 5.12. Error variance in x position for $\sigma_m^2 = 1000(\mathbf{❶})$, $100(\mathbf{❷})$, $10(\mathbf{❸})$, $1(\mathbf{❹})$, $0.1(\mathbf{❺})$.

Tuning the filter correctly also involves determining the appropriate value of acceleration time constant, α. To illustrate the effect of α on the filter performance, a target trajectory was created with an instantaneous turn maneuver. i.e. the target makes a perfect 90° left turn. This corresponds to an impulsive acceleration, which, of course, would be impossible for a real aircraft. This, however, serves to demonstrate the dependence of filter behavior on the α parameter. Figure 5.13 shows the filter trajectory, while attempting to track the left turn, for three different values of α. The filter was run with noiseless measurements for these simulations, and thus the filter is tracking the target perfectly before going into the turn.

 The best way to understand the behavior in Figure 5.13 is to realize that the filter is modeling real aircraft dynamics, and thus it would not expect or be able to track an infinite acceleration. As a result, the filter will execute turns within the limitations of the dynamics assigned to its process model. For a longer acceleration correlation time (smaller α) the filter is slower to react (slower to decorrelate previous acceleration components) and when it goes into a turn, the turn is wider and it stays in it longer (longer correlation of new accelerations). This results in overshooting of the desired trajectory very similar to filter ringing. In this example, the dynamics are unrealistic and thus the filter will never track perfectly. However, the value of α can most likely be set optimally for a realistic set of dynamics. Once again, there is a trade-off in adjusting α. We cannot make α arbitrarily large (short correlation time) in an attempt to allow it to track any possible quick dynamics, since increasing α will also increase the error covariance, although the dependence is not monotonic as in the case of σ_m^2. Figure 5.14 shows the x position estimation error for the trajectories in Figure 5.13.
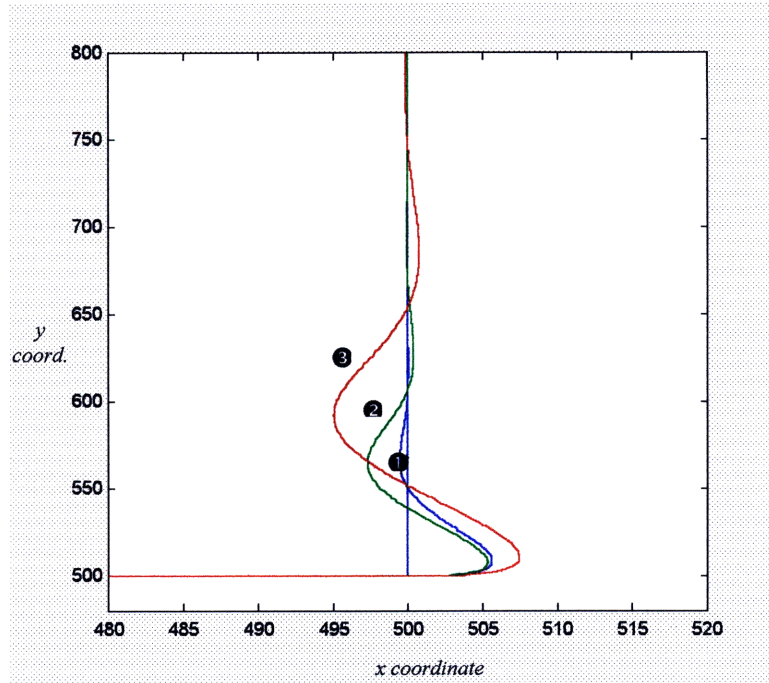
62

Figure 5.13. Filter trajectory for 90° left turn for α= 1(❶) , 0.1(❷) , .01(❸).

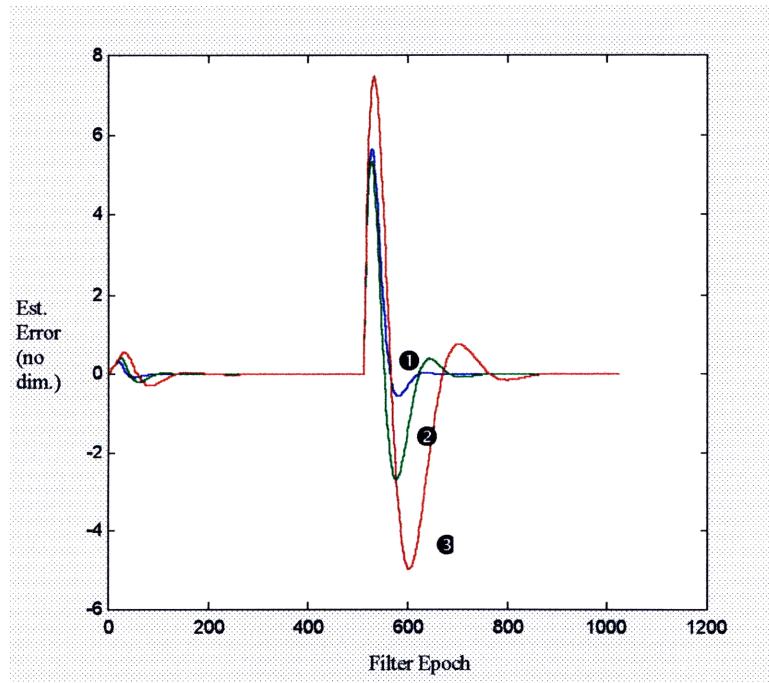Figure 5.14. *x* position estimation error for 90° left turn for α= 1(❶), 0.1(❷) , .01(❸).

5.3 3D Filter Simulation and Testing

In this section a full three dimensional implementation of the filter is tested. In order to determine the usefulness and effects of the integration, first a single sensor version of the filter is tested for both radar and GPS. This helps establish a baseline for filter performance and enables us to verify proper filter construction for each measurement type.

5.3.1 3D GPS-Only Filter

Using the measurement model developed in Section 2 and the target dynamics and GPS clock models presented in Section 1, an Extended Kalman Filter for GPS only was implemented. The filter was tested using static measurement data that was collected using two Ashtech Ranger XII GPS receivers. Both receivers were placed at accurately surveyed sites, with one receiver simulating the target and the other used as a differential reference station. These tests validated the formulation of the GPS filter and served as an indicator of GPS-only estimator performance.

The filter was first run using data collected from the target receiver without applying corrections from the reference receiver. The target dynamics model was set with all three axis using:

$$\sigma_m^2 = 0.1 \qquad (m/s^2)^2$$
$$\alpha = 1/10 \qquad s^{-1}$$

and the clock dynamics model was set with the phase and frequency noise spectral densities at:

$$\sigma_p^2 = 0.0090 \quad m^2$$
$$\sigma_f^2 = 0.0355 \quad (m/s)^2$$

which were derived from a table of typical Allan variances for temperature compensated crystal oscillators[5]. The GPS measurement noise covariance was set to:

$$\sigma_\rho^2 = 2.0 \qquad m^2$$

which reflects the level of uncorrelated noise. The target receiver was located at *ECEF* coordinates:

$$[x\,y\,z] = [1510885.9 \quad -4463462.6 \quad 4283902.5] \quad (meters, \ ECEF)$$

The filter was initialized with several hundred meters of position error, no target motion, and a fairly large initial error covariance. Figure 5.15 shows the filter's estimate of the x coordinate for a 200 second interval as compared to the receiver's internal point by point least squares position solution. Seven satellites were in view during this interval and the filter was set to utilize all available measurements. For comparison purposes, the uncorrected filter solution was adjusted to compensate for ionospheric and tropospheric bias models that are applied in the receiver solution, but not necessary when differential corrections are used in the filter. Figure 5.15 shows that the filter does indeed converge and tracks the receiver's least squares solution fairly closely. There is some minimal smoothing apparent in the filter's solution as a compared to the receiver's. If desired, this smoothing could be increased by tuning the filter for stationary dynamics, but, for comparison purposes, the dynamics model parameters were kept closer to a range we might expect for a moving target. Note that both solutions contain an error (in this instance on the order 10 meters) that results from the unremovable bias caused by Selective Availability as explained in Section 2.3. In Figure 5.16 the position error variances are plotted indicating that the filter is reaching a steady state solution. The gradual increase in the position error variance apparent in this plot is a result of changes in the satellite geometry which effect positioning accuracy. This is explained in Section

64

5.3.1.1. The covariance predictor described in Section 5.1.1 is shown in black, once again validating that the filter is not actually diverging but appears to be behaving reasonably.
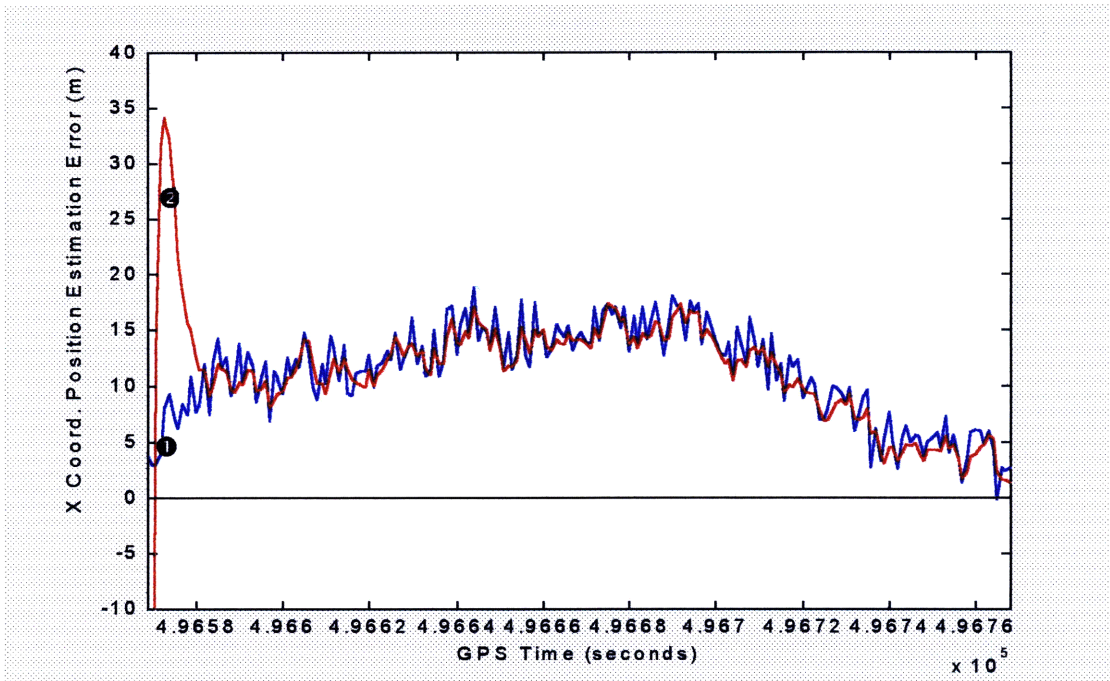

Figure 5.15. Estimation error of x position coordinate: receiver point by point least squares(❶); GPS-only Kalman filter using uncorrected (no differential) pseudo-ranges(❷).
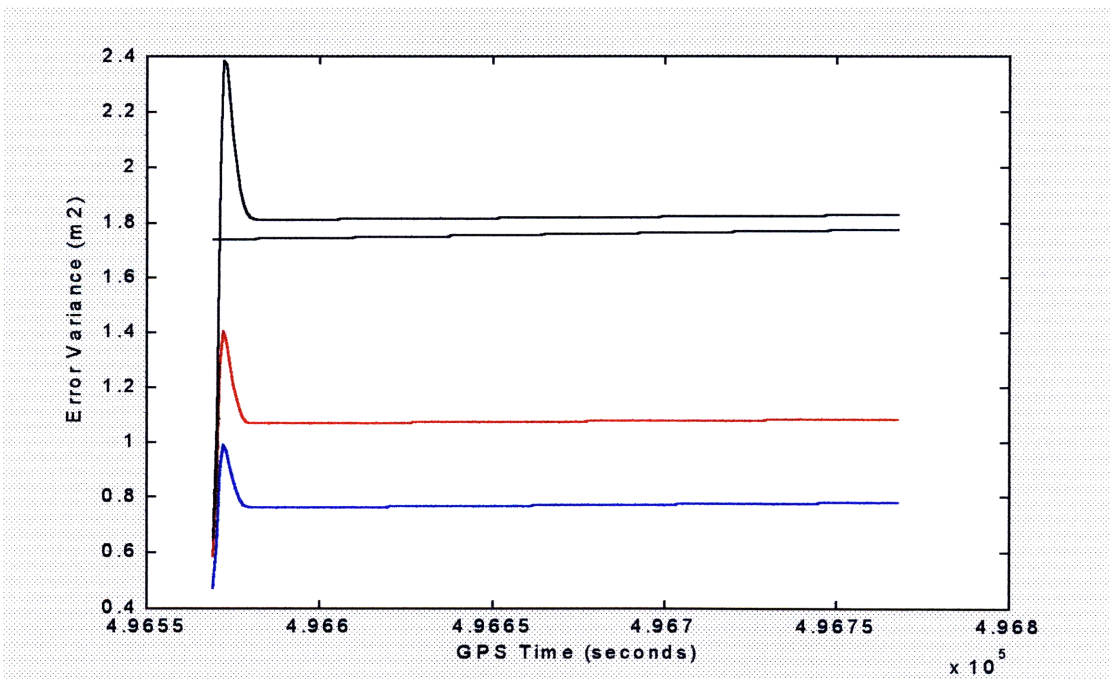

Figure 5.16. GPS-only filter error variance for x(❶),y(❷), and z(❸) position (x predictor in black).

The same filter was run on data sets that were differentially corrected utilizing a reference receiver in the manner explained in Section 2.3.2. Figure 5.17 compares the filter's position estimation accuracy with uncorrected data (corrected only for SV clock bias), differentially corrected data, and the receiver's internal least squares solution which is smoothed and corrected with models for propagation delays. The GPS-only filter plots in Figures 5.15 and 5.17 are identical with the exception that in Figure 5.15 the ionospheric correction model used in the receiver's least squares solution is also applied to the filter solution for comparison purposes. In Figure 5.17 we can see that the uncorrected filter solution has a large bias as a result of Selective Availability and other unmodelled errors. Some improvement is gained in the receiver by applying propagation delay correction models, but only the differentially corrected filter attains an essentially unbiased solution.
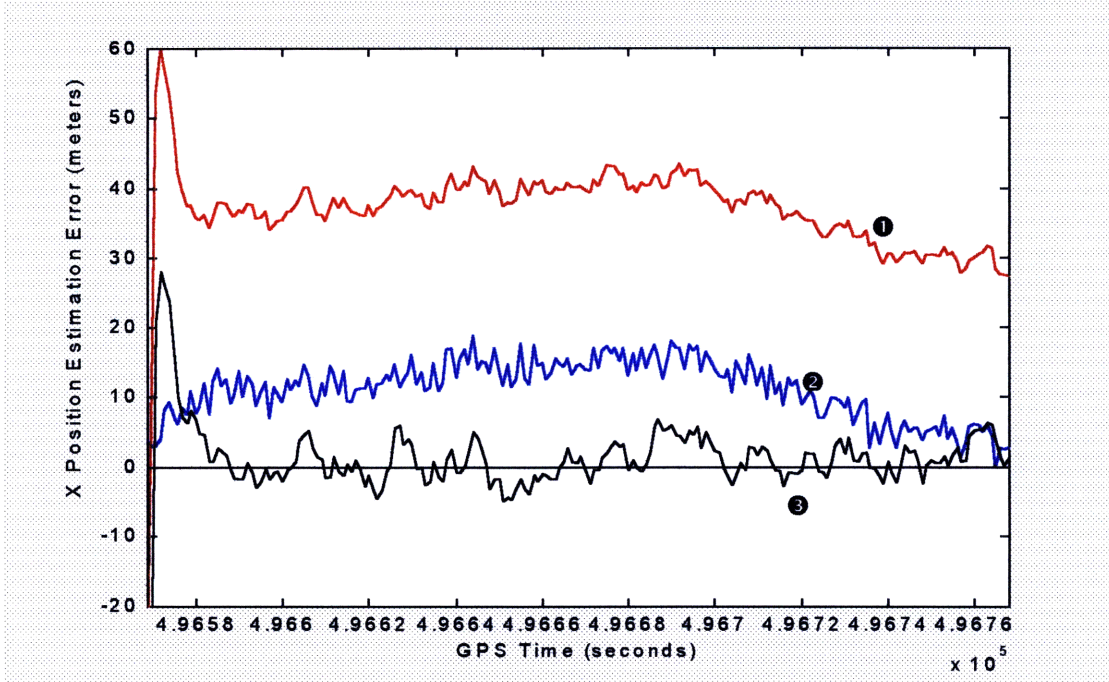

Figure 5.17. *x* position estimation errors for uncorrected GPS-only Kalman filter(❶), receiver least squares with internal 200 second smoothing(❷), differentially corrected GPS-only Kalman filter(❸).

5.3.1.1 Geometric Dependence of Error Covariance (GPS-Only Filter)

It turns out that, similar to the structural dependence noted with the radar-only filter, there is a dependency of the GPS-only filter's error covariance on the satellite geometry. Although somewhat more difficult to analyze rigorously, this effect is well understood and has been described extensively by the phenomenon known geometric dilution of precision[14]. To understand the basic idea, refer back to Figure 4.1. By substitution of Equation (123) into (125), the *a-posteriori* error covariance (current time step after incorporation of measurement) is given by:

$$P[k|k] = P[k|k-1] - P[k|k-1]H^T (HP[k|k-1]H^T + R)^{-1} HP[k|k-1] \qquad (132)$$

where *P[k|k-1]* is given by Equation (121).

In (132) we can see that the error covariance propagation in the filter is a function of the measurement sensitivity matrix, *H*. Recall that the *H* matrix for the GPS measurements, given by Equation (72), consists of the line of sight vectors from the current position estimate to each of the SV's. It would thus be natural to expect that error covariance would vary as the geometry relating the receiver and the satellites

66

changes. Even if the receiver remains stationary, due to the orbital motion of the GPS satellites and the rotation of the earth, the relative geometry will constantly change. The result is that, when observing what we might expect to be the steady state error covariance of the filter, we can expect to see gradual variation with time. The effect of satellite geometry on the accuracy of the position solution depends on how the particular receiver implements its navigation solution. A receiver that utilizes the required minimum of four satellites will typically search all possible sets of SV's in view to obtain the best geometry. An ideal geometry utilizing four SV's has three satellites spaced equally (120° apart in azimuth) on the horizon, and one directly overhead. Any geometry where satellites tend to be bunched together in the sky is much less favorable. A navigation solution method that incorporates all available SV's, such as the Kalman filter presented here, would be less susceptible to degradation due to geometry. This is due to the fact that the GPS satellite constellation is designed such that there is almost always a reasonable spread of satellites around the sky, and a filter utilizing all SV's in view would benefit from the best geometry. However, under certain situations such as when the receiver antenna may be masked, we might expect to see positioning accuracy degrade considerably. This is demonstrated in Figure 5.18, where the error variance in the x position is plotted for a GPS-only filter run with four different sets of SV's. The lowest trace corresponds to the filter being run with all available satellites and the other traces represent different sets of four. (In the GPS constellation satellites are identified by an ID number, between 1 and 32, called their PRN code, which is a reference to that SV's particular signal.)
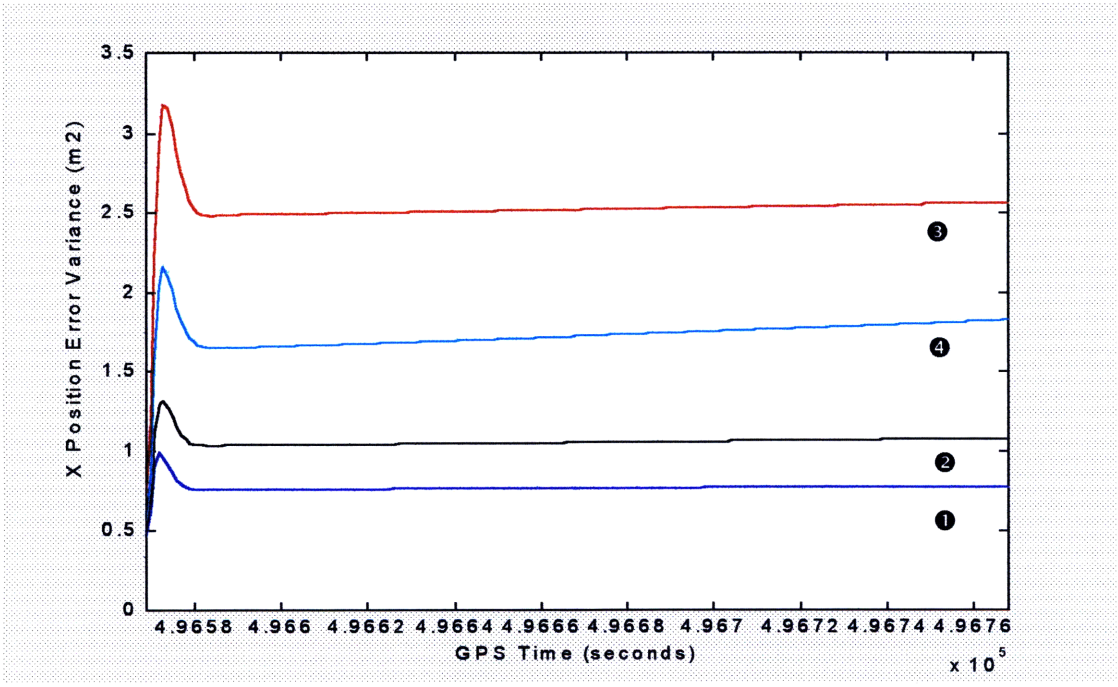

Figure 5.18. Error variance for x position coordinate for GPS-only filter run with different satellite sets: All Available [1 5 9 17 21 23 26](❶), [1 5 9 17](❷), [17 21 23 26](❸), [1 9 21 26](❹).

The magnitude of the estimation error for the x position coordinate is plotted in Figure 5.19 for two of the filter runs shown in Figure 5.18.
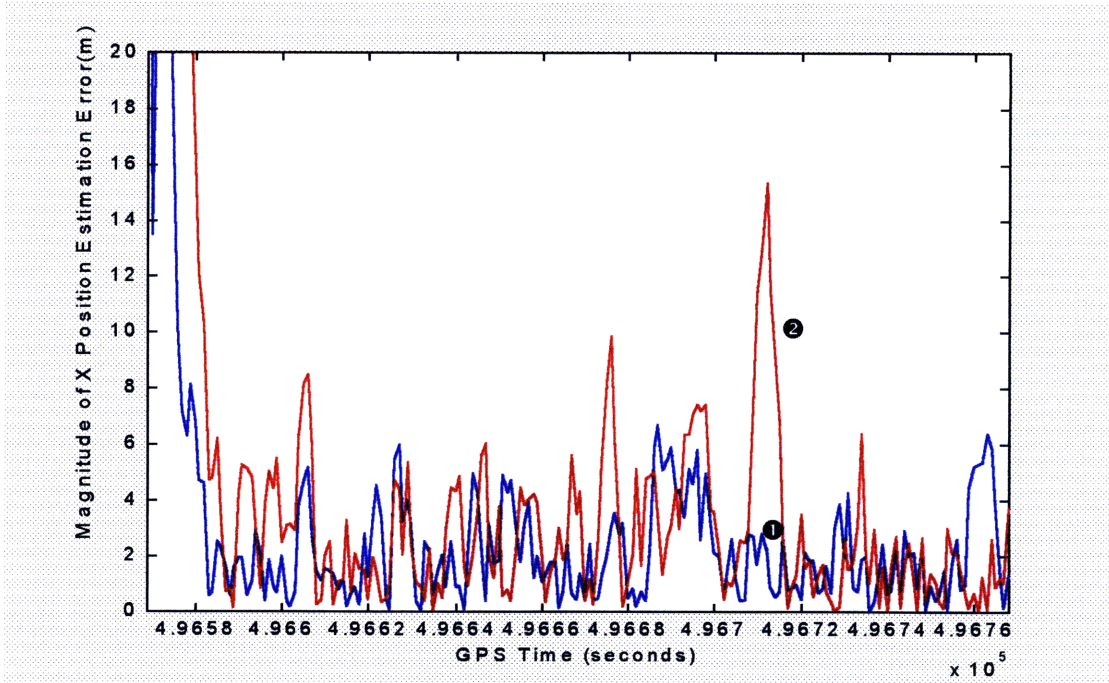
Figure 5.19. Magnitude of x position estimation error for GPS-only filter run with different SV sets.
{ [1 5 9 17 21 23 26](❶), [17 21 23 26](❷) }

5.3.1.2 Observability Conditions (GPS-Only Filter)

As described in Section 2.1, a full GPS position solution in three dimensions (with no other information available) is only possible with measurements to a minimum of four satellites. It seems intuitive then that this requirement would define observability for the system. Since the measurement coupling matrix, H, is a function of the current state estimate, the linearized system given by $\{\Phi, H\}$ is not time invariant. Thus, as a means to verify observability, the rank of observability matrix given by:

$$O_n[k] = \begin{bmatrix} H[k] \\ H[k]\Phi[k] \\ H[k]\Phi^2[k] \\ \vdots \\ H[k]\Phi^n[k] \end{bmatrix} \qquad \text{where } n=11. \qquad (133)$$

was evaluated at each time step during the filter runs[4]. As might be expected, for all cases where at least four SV's were available, the pair $\{\Phi, H\}$ was observable, and for all cases where less then four SV's were used, the pair was unobservable. i.e.

$$rank(O_n[k]) = \begin{cases} n & \forall k: m \geq 4 \\ <n & \forall k: m < 4 \end{cases} \qquad \text{where } m = \text{number of measurements.} \qquad (134)$$

The result for all tests conducted was that whenever less than four SV's were available, the GPS-only filter diverged. Figure 5.20 shows the x position estimate for two tests of the filter. In the first case four

measurements are used, and in the second case one SV is removed, leaving only three measurements. When the filter is run with three measurements only, it clearly diverges.
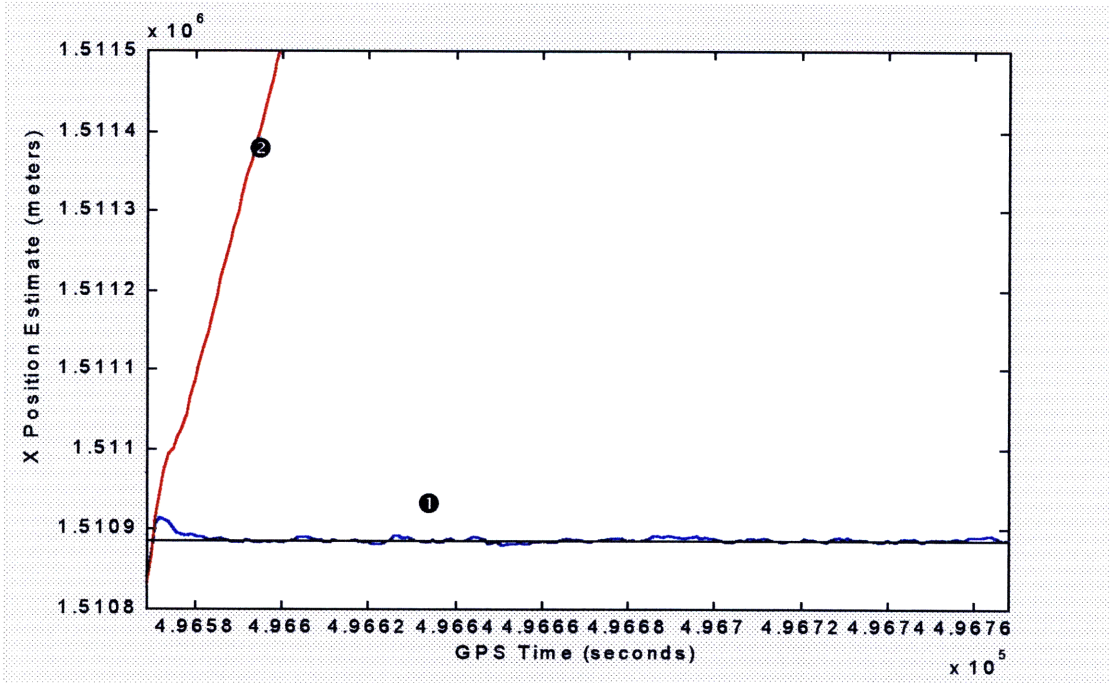

Figure 5.20. *x* position estimate for GPS-only filter test with four SV's [1 5 9 17](❶) and three SV's [1 5 9] (❷). (Position truth dotted black line.)

Although the test given in (133) does not strictly define observability for a time varying system, in this application it turns out to be a useful tool for determining which sets of measurements by themselves will allow the filter to work over any useful time period. However, momentary loss of observability as defined by this measure, does not necessarily mean that the filter will immediately become divergent.

3.2   3D Radar-Only Filter Simulation

Primarily for the purpose of verifying convergence, a filter utilizing the radar measurement model presented in Section 3, was simulated. These simulations were conducted by synthesizing radar measurements from a sensor located 10 km from the GPS test receiver site (stationary target). The same target dynamics parameters were used as in Section 5.3.1 and the radar measurements were assigned the following noise intensities:

$$\sigma^2_{AZ} = 0.02 \times 10^{-3} \;\; (rad^2) \;\; (0.25° \text{ std. dev.})$$

$$\sigma^2_{EL} = 0.02 \times 10^{-3} \;\; (rad^2) \;\; (0.25° \text{ std. dev.})$$

$$\sigma^2_{Rng} = 2.0 \;\; (m^2)$$

The range measurement noise variance was chosen to be the same magnitude as the GPS pseudo-range measurement noise variance. The filter was observed to converge to the target position with a steady state error variance from all initialized positions (again, with the exception of the origin). Figure 5.21 shows a typical plot of the x position estimate overlaid with the apparent noisy radar position measurements. The position estimates appear quite noisy in this plot, considering the relatively small measurement noise variances. But, as mentioned in the 2D simulations, the uncertainty in each coordinate is strongly dependent upon geometry. To see that the estimator is actually working quite reasonably, the position coordinate as measured by the radar is shown in red in Figure 5.21.
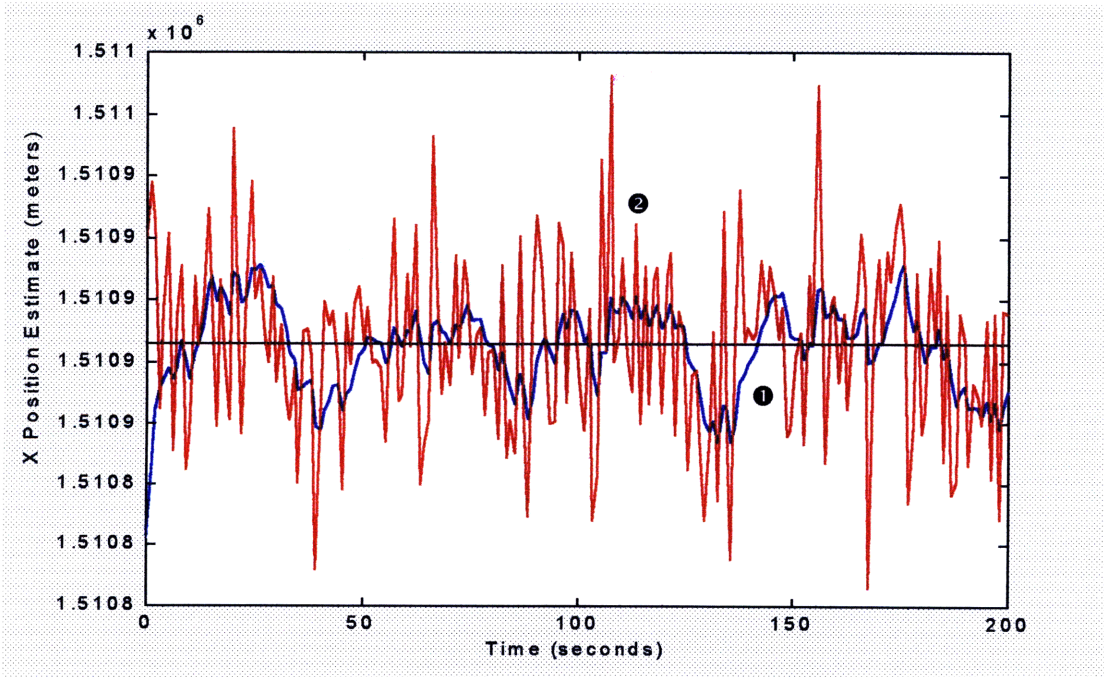

Figure 5.21. *x position estimate* (❶) for radar-only filter with noisy measurements (❷). (Truth in black.)

The estimation error variance in each position coordinate for the above filter simulation is shown in Figure 5.22. The strong range and angle dependence discussed in Section 5.1.1 is carried over to the three dimensional situation and is apparent in these plots by the large error variance.
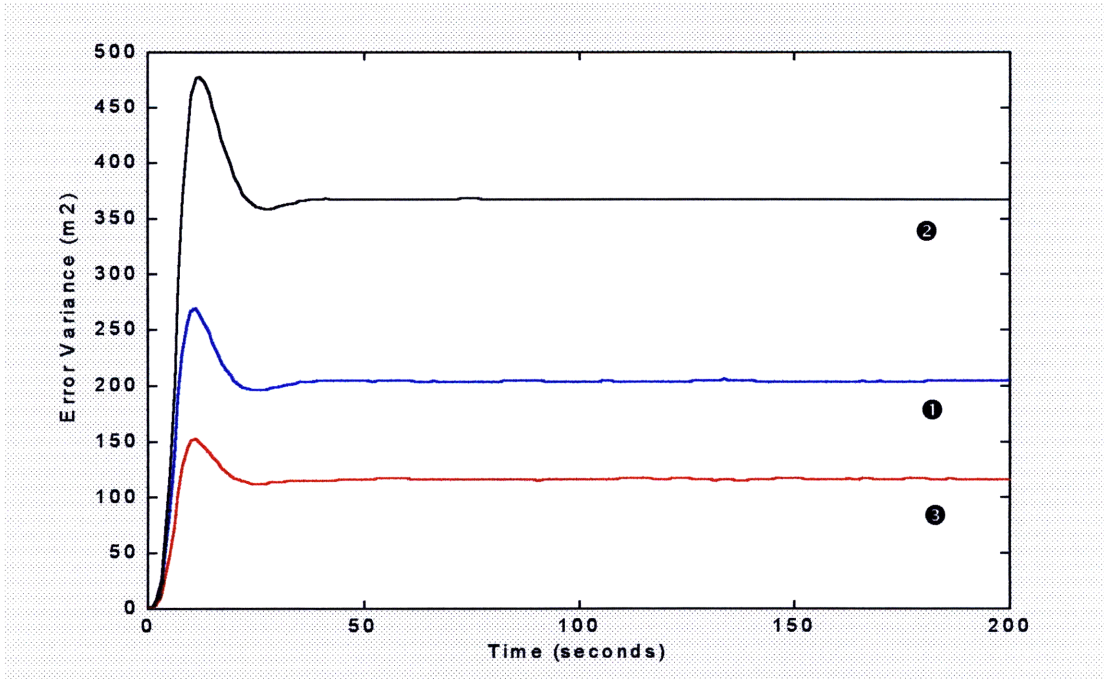
Figure 5.22. Error variance in x(❶), y(❷), and z(❸) position estimates for radar-only filter.

5.3.2.1 Observability Conditions (Radar-Only Filter)

If we use the observability condition defined by $rank\{O_n[k]\}=n$, where $O_n[k]$ is given by Equation (133) and $n=9$ (since we are not concerned with the GPS clock states in the radar-only filter), then strictly speaking we must have all three measurements to ensure observability under all dynamics. i.e. for any subset of measurements in these filter simulations, we have $rank\{O_n[k]\}<n$ for all k. The use of angle only measurements, sometimes referred to as passive tracking, has been the subject of considerable study. It has been established that target motion is observable, in angle only tracking, if and only if the sensor platform accelerates under certain constraints[15]. In the problem of concern here, it is assumed that the radar sensor position is fixed, and thus the requirement that we have all three measurements (azimuth, elevation, and range) is applicable.

5.3.3 Combined 3D Radar+GPS Filter Tests

The final set of tests conducted in this work involved the complete filter that combined both the radar and GPS measurement models. These tests confirm, as would be expected, that the filter is convergent. They also demonstrate the synergy that occurs by using a filter that combines, at a low level, both sensors. This synergy allows the combined estimator to converge with partial measurements from either sensor which would normally constitute an unobservable situation in a single sensor filter. In addition, in situations where the geometry is unfavorable for either sensor, inclusion of measurements from the other sensor can significantly reduce the estimation errors.

Throughout all the combined filter tests the following dynamic model parameters were used, where the acceleration noise processes were considered to be independent and identically distributed:

$$\sigma_m^2 = 0.1 \qquad (m/s^2)^2$$
$$\alpha = 1/10 \qquad s^{-1}$$
$$\sigma_p^2 = 0.0090 \quad m^2$$
$$\sigma_f^2 = 0.0355 \quad (m/s)^2$$

The target was stationary and located at the surveyed location:

$$[x\,y\,z] = [1510885.9 \quad -4463462.6 \quad 4283902.5] \quad (meters,\ ECEF)$$

The measurement noise statistics were set to:

$$\sigma_\rho^2 = 2.0 \qquad m^2$$
$$\sigma_{AZ}^2 = 0.02 \times 10^{-3} \ (rad^2)\ (0.25° \text{ std. dev.})$$
$$\sigma_{EL}^2 = 0.02 \times 10^{-3} \ (rad^2)\ (0.25° \text{ std. dev.})$$
$$\sigma_{Rng}^2 = 2.0 \ (m^2)$$

5.3.3.1 Full Radar and GPS Measurement Sets

The first set of tests verifies the functionality of the combined filter with a full complement of measurements. For these tests we had seven satellites available, resulting in a fairly low geometric dilution of precision. As expected, the filter converged to an essentially unbiased steady state estimate around the true target position. Since the error covariance will vary as a function of the continuously changing satellite geometry, by "steady state", we mean that the effects of initial conditions have dissipated and are negligible. The position estimates in each coordinate for a typical test run are shown in Figure 5.23.

Figures 5.24-5.26 give a comparison of the position estimation error variances for the combined filter and the single sensor filters. In general, when a full complement of satellites is available the GPS solution is less susceptible to geometric degradation and the filter performance will be driven primarily by the GPS measurements. In this case we can see that we have a slight improvement in the estimation accuracy of the combined filter over GPS alone. The largest performance gain is over the radar-only filter. In some cases where satellite geometry is good, there may be some degradation in accuracy of the combined filter, as opposed to the GPS-only filter, due to the incorporation of very noisy radar measurements.
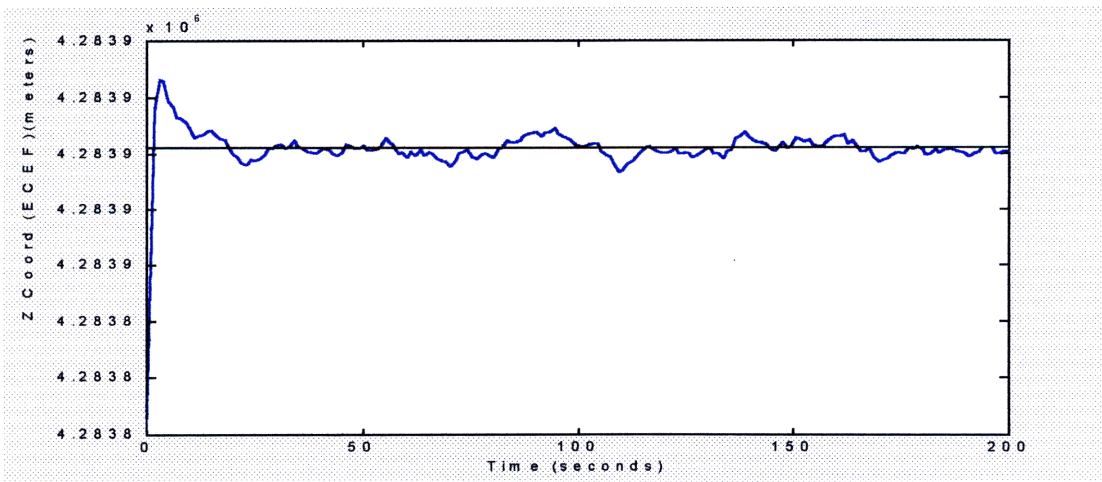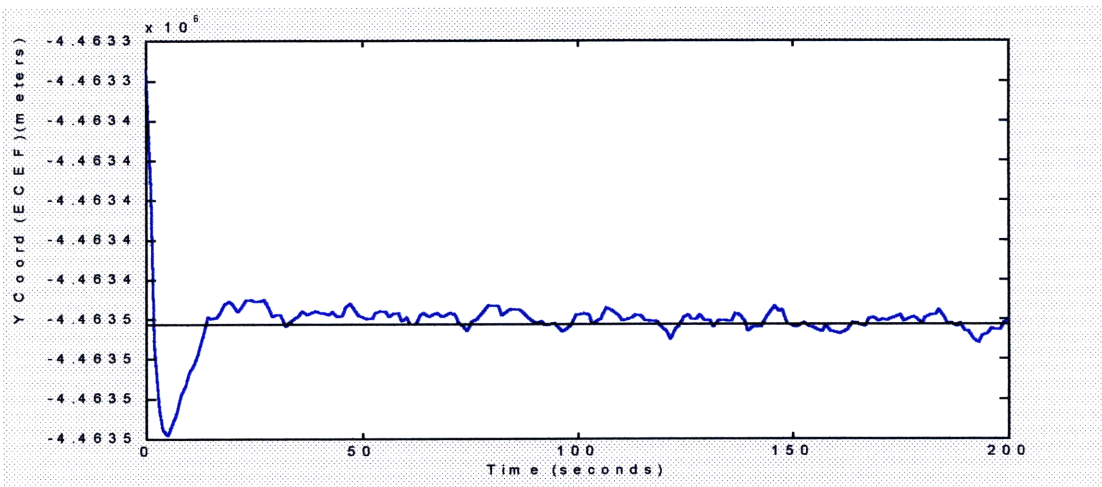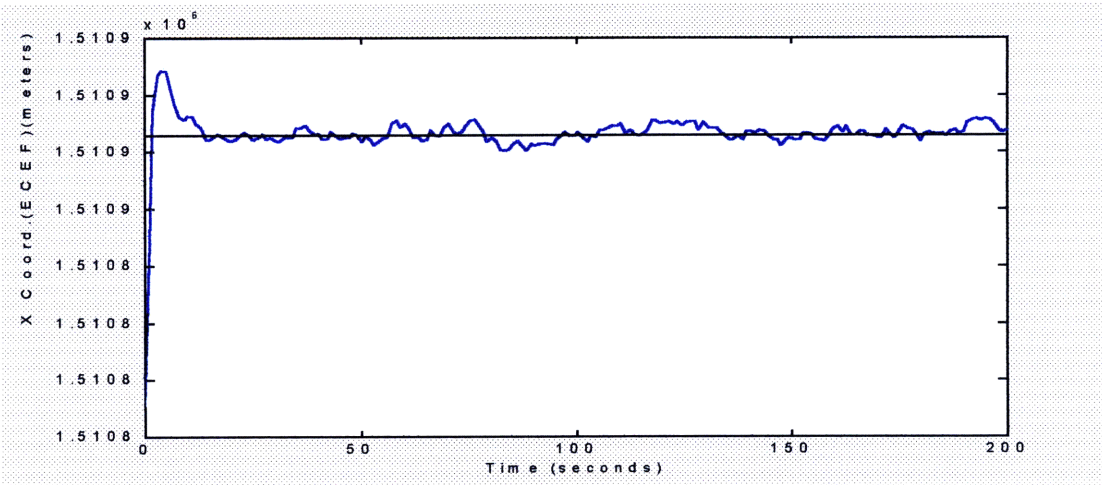
Figure 5.23. Combined filter position estimates in each coordinate *(ECEF)*. (Position truth in black).
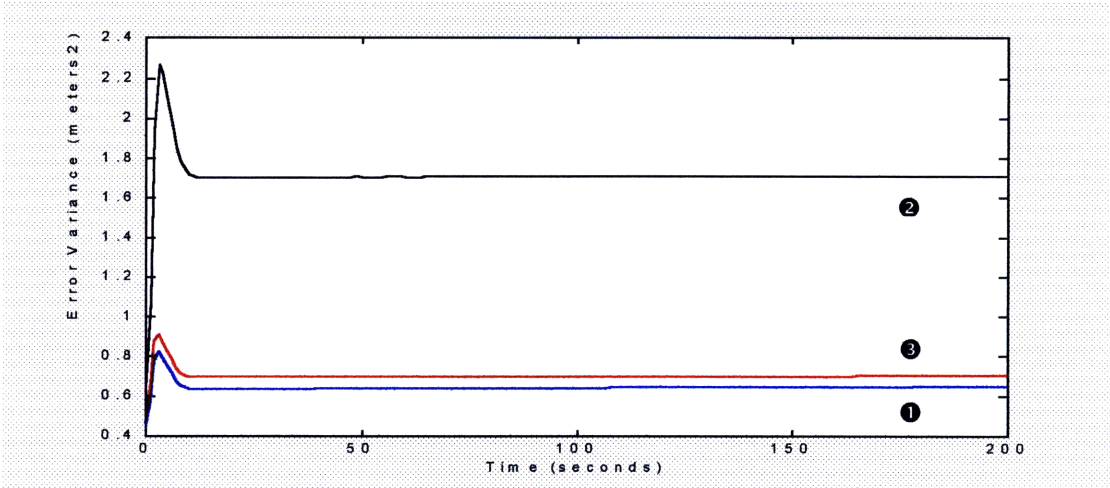
Figure 5.24. Position estimation error variance in x(❶), y(❷), & z(❸) coordinate for combined filter.
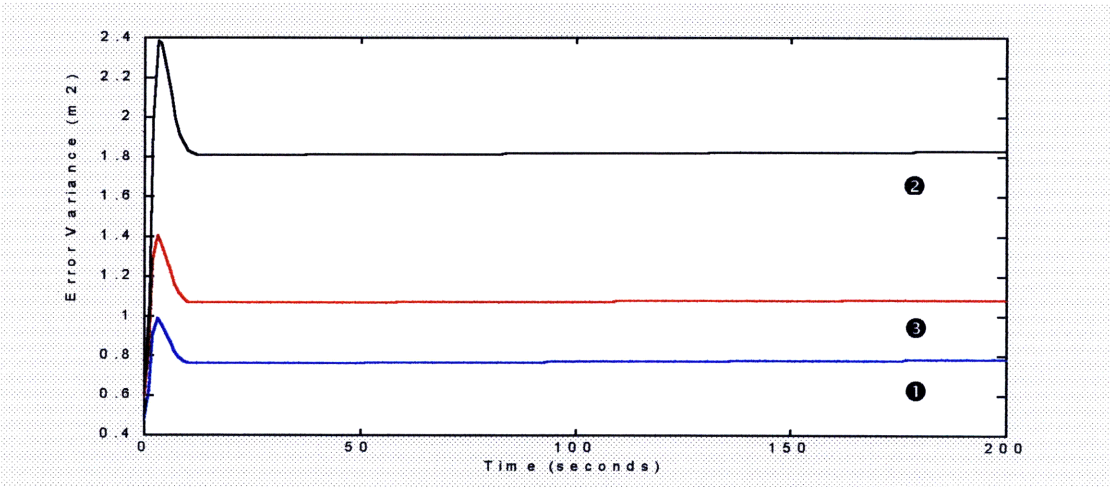

Figure 5.26. Position estimation error variance in x(❶), y(❷), & z(❸) coordinate for GPS-only filter.
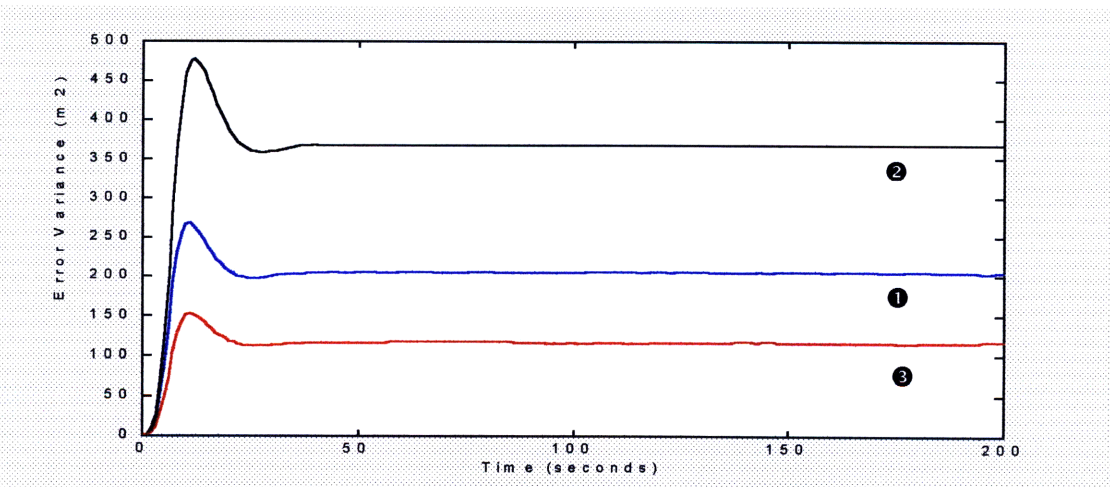

Figure 5.25. Position estimation error variance in x(❶), y(❷), & z(❸) coordinate for radar-only filter.

74

5.3.3.2 Partial Radar or GPS Measurement Set

In this set of tests, the convergence and estimation error were examined for the filter run with only a partial measurement set from either one or the other sensor. That is, we have either a full set of GPS measurements (four or more satellites) and only a partial set of radar observables, or we have all three radar observables (azimuth, elevation, and range) and less than four GPS measurements. In both these cases the advantage of combining the sensor data in a single Kalman filter is evident since a stand-alone Kalman filter for either sensor with partial measurements would typically not converge. Here we are able to take advantage of some information from the other sensor to improve the estimator's performance even if a complete position solution could not be obtained from that information alone.

Figure 5.26 shows the x position estimate error variance for three different runs of the filter with a full radar measurement set and partial GPS measurements. The filter was run with one, two, and three pseudo-range measurements respectively. In all three cases, not enough information would be present for a GPS-only filter to converge. However, when this information is used to augment the radar measurements, a distinct improvement over the radar-only filter is achieved. The actual amount of improvement will depend on the geometric relationship between the satellites and the radar sensor. In Figure 5.26 we can see that even a single GPS observable results in a significant decrease in the estimation error variance. For this particular geometry, adding the second pseudo-range results in a dramatic drop in error variance in the x coordinate.
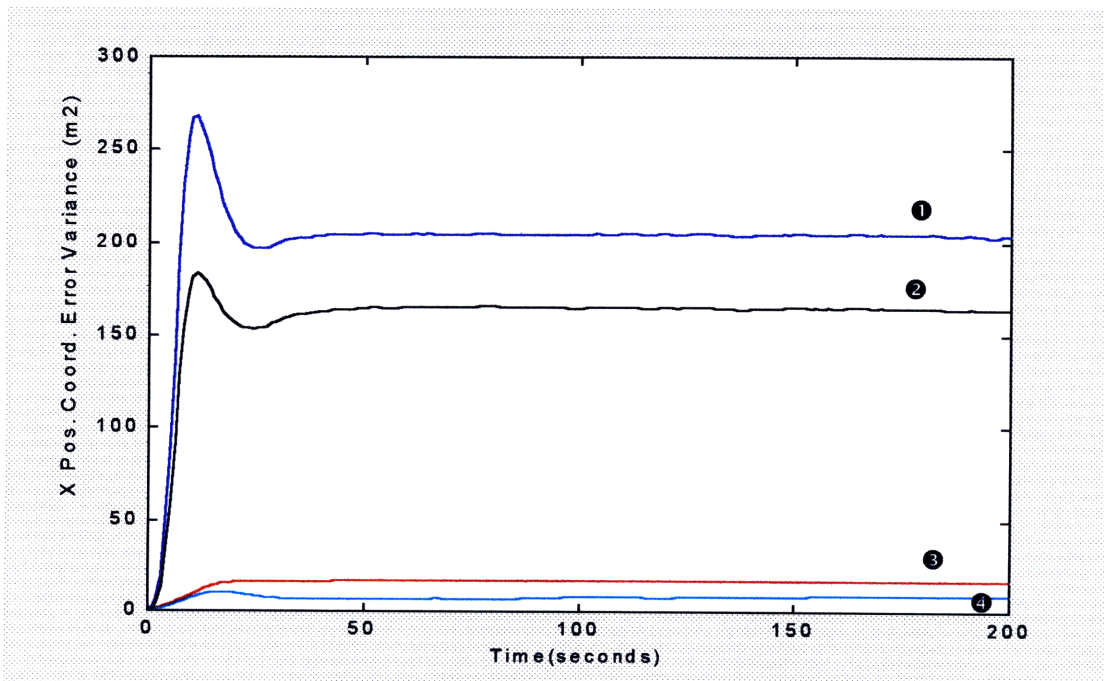
Figure 5.26. x position coordinate estimation error variance for radar-only filter(❶) and combined filter with one(❷), two(❸), and three(❹) GPS pseudo-range measurements.

Testing of the combined filter was also conducted with a full set of GPS observables and partial radar measurements. In these tests, four pseudo-range measurements were used, which would be enough to ensure a GPS position solution, combined with a variety of different radar measurements. Figure 5.27 is a plot of the x coordinate error variance comparing a GPS-only filter run with four pseudo-range measurements and a combined filter with the same measurements plus a radar range measurement. As can be seen, the addition of the single radar observable to the GPS measurement set reduces the estimation error significantly. Adding this range measurement has a similar effect to adding another GPS observable

to the measurements, and the amount of improvement will vary with the relative target/satellite/radar geometry. It turns out that this is the only partial radar measurement that yields any discernible improvement in the performance of the combined filter. Angle measurements, whether both are present or just one, appeared to have no effect on filter performance in these tests. Also, a single angle measurement combined with a radar range measurement did not improve the combined filter performance over just adding the range measurement itself.
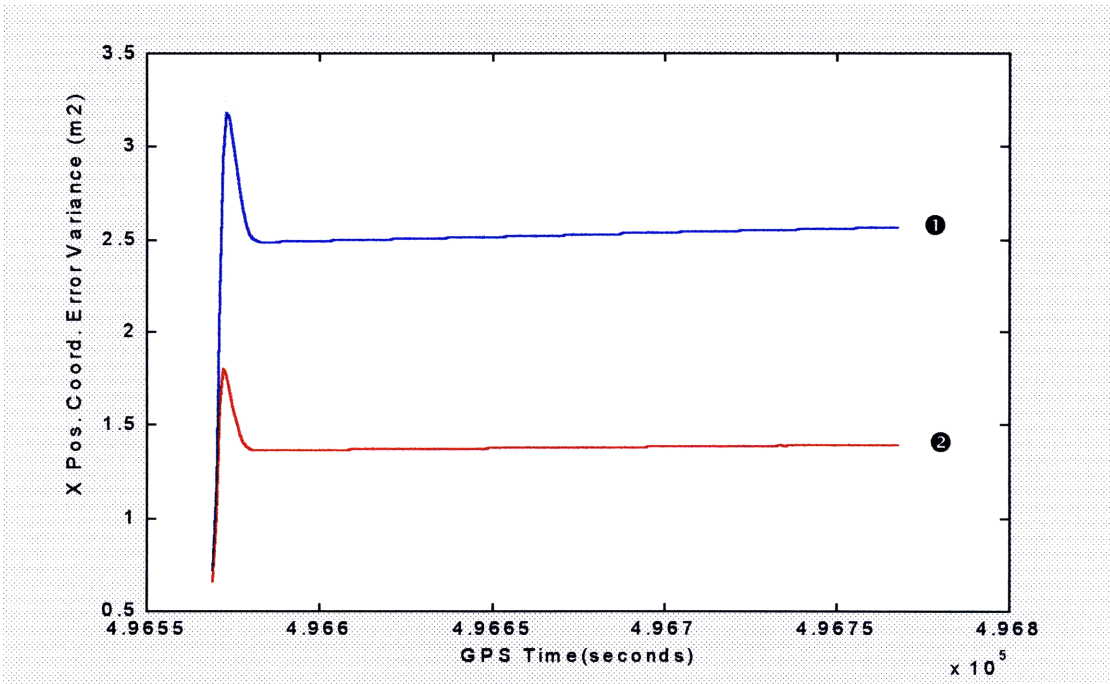

Figure 5.27. *x* position coordinate error variance for combined Filter (❷) with four GPS pseudo-range measurements only (SV's [17,21,23,26]) plus radar range measurement and GPS-only filter (❶) using the same four SV's.

5.3.3.3 Partial GPS and Radar Measurements

The final set of tests conducted with the combined filter looked at filter behavior with partial measurements from both sensors. In these situations we do not have sufficient information from either sensor alone for a position solution, i.e. the system is unobservable as defined by *rank $O_n[k]<n$ for all k* with just one sensor. However, certain combinations of partial measurements from both sensors will provide observability and allow the filter to converge.

The observability condition for the filter run with partial measurements can be summarized by saying that a minimum of four measurements must be present. Recall that the GPS pseudo-range measurements are not true ranges and must be corrected by the estimate of the receiver clock bias. Thus, whenever we are utilizing GPS observables, we are required to have at least four measurements present in order to get an estimate of this bias. Any combination of four, it turns out, will suffice, but the performance of the filter is highly dependent upon the particular geometry. This results in some combinations of measurements providing an unbiased position estimate but having large error variances. Figure 5.28 summarizes a subset of tests by showing the *x* position estimation error variance for all the observable sets of measurements. In this particular geometry, the combination of three GPS pseudo-ranges plus a radar elevation angle measurement had much larger error variances. The combination of three pseudo-ranges plus a radar range and angle measurement produced the best performance. However, removing the angle measurement resulted in virtually the same level of error variance. Also note that in the tests where we have two GPS

76

measurements and a radar range and angle measurement (plots ❺ and ❽), we can again see the strong dependence of the error variance on the relative geometry. In this case, incorporation of the radar elevation angle results in significantly better filter performance than if we use the azimuth angle to complete the measurement set.
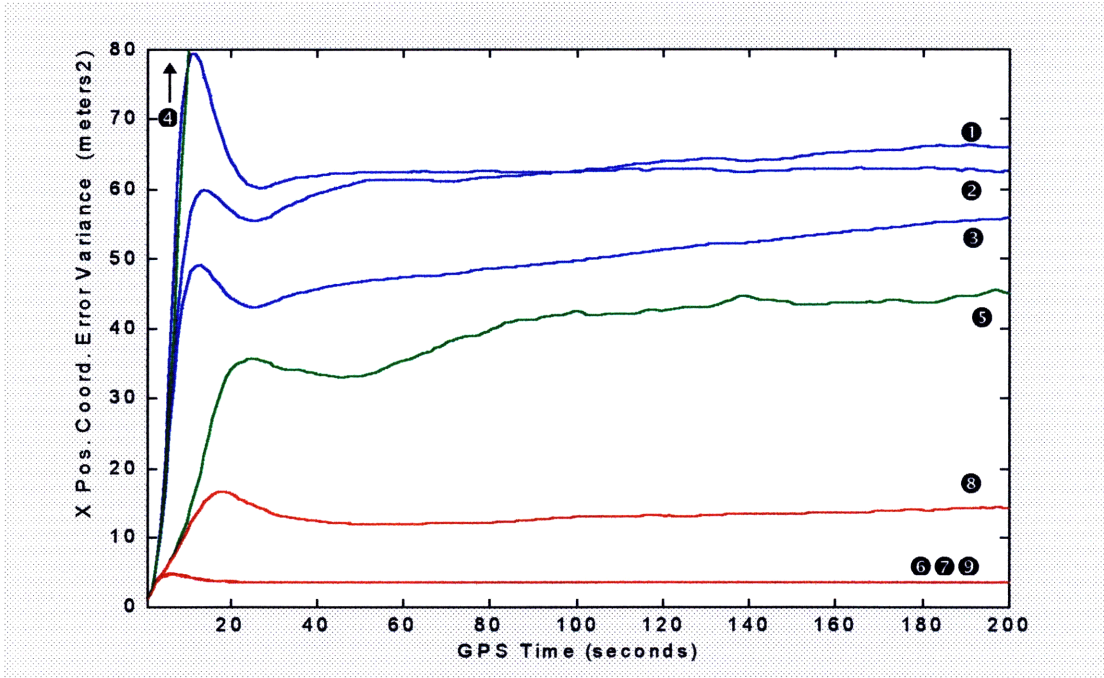
Figure 5.28. *x* position coordinate error variance for combined filter run with partial measurements.

Plot Key

blue	green	red
$3\rho+Az$ (❶)	$3\rho+El$ (❹)	$3\rho+R$ (❼)
$2\rho+Az+El$ (❷)	$2\rho+Az+R$ (❺)	$2\rho+El+R$ (❽)
$3\rho+Az+El$ (❸)	$3\rho+Az+R$ (❻)	$3\rho+El+R$ (❾)

(ρ=GPS pseudo ranges, Az=radar azimuth angle, El=radar elevation angle, R=radar range)

Conclusions

The Kalman filter developed in this thesis is a methodology for the fusion of tracking data from two quite different sensors which are now commonly employed separately to obtain aircraft position. The radar sensor has been the mainstay of airborne target tracking for a considerable time and is still in general use. The newer Global Positioning System is quickly gaining popularity in many traditional radar applications and may eventually completely replace radar in cooperative tracking scenarios. However, during the period that both sensors remain in common use, the question of how useful it is to combine these data and what methodology might be used is a relevant one. This thesis presents answers to both these questions.

The methodology chosen here was an extended Kalman filter which is essentially a low level fusion of raw measurements from each sensor. Alternate methods might involve employing separate position estimators for each sensor, the outputs of which may be combined in some manner to give a composite target position estimate. In this situation, we might be expecting that the sensors are robust to failure and the implementation of separate estimators in different hardware would aid in the robustness of the system to failures in the computational hardware. However, in situations where we would more likely expect partial sensor failures, the centralized filter approach presented in this thesis has distinct advantages. By partial sensor failure we mean that, although a target position estimate may not be obtainable from that sensor alone, a subset of measurements is still available. In these situations, separate position estimates from the failed sensor would typically be of no use. However, in the extended Kalman filter approach presented here, it is shown that this partial information can be utilized to improve the accuracy of the position estimate over that which we would get from the other single sensor only. In addition, if both sensors have partial failures, we would have no usable position estimate available from a separate, decentralized filter approach, whereas the combined filter is often able to provide an accurate position estimate even with these partial measurements.

To obtain a position estimate from a GPS sensor alone, we need to have a minimum of four satellite measurements. For a radar sensor, we need to have both angles and a range measurement present to acquire the target's position. With either of these sensors, if we have less than this minimum of measurements for any period of time we can expect the outputs of any individual position estimator to diverge. In this thesis it is shown that with the centralized Kalman filter we can utilize any remaining subset of four measurements to obtain an unbiased position estimate. Also, as mentioned, incorporating partial measurements from one sensor will improve performance of the filter over that which would be obtained with measurements from the other sensor only. For example, with a full set of radar measurements, incorporation of even a single GPS observable can significantly increase the accuracy of a position estimate over that which we would obtain from the radar only. Likewise, even if we have enough GPS observables to get a position solution, due to less then optimal satellite geometry we can often improve this position estimate by incorporating a radar range measurement. In many cases incremental improvements can be gained in accuracy with the inclusion of each new measurement.

It is expected that the work begun in this thesis will continue with the actual development of a combined radar and GPS tracking system at MIT Lincoln Laboratory. In this future work, issues related to fitting the dynamic models presented here to actual targets will be addressed, and measurement noise models will be formulated for specific radar sensors. In addition, the problem of dealing with different sensor data rates will have to be more carefully examined. The implementation of this filter in a real world system will provide the opportunity to test the performance of this filter under realistic conditions and compare the results with individual sensor tracking systems.

Appendix A: Calculation of SV Position and Clock Error

In order to obtain a position solution as described in Section 2.1, two important components must be calculated: the position of the SV at the time of transmission of the ranging code signal and the SV's clock bias. Both of these may be computed from parameters that are transmitted on a navigation data signal available to all receivers[24]. The broadcast ephemeris gives parameters which describe the orbit of the SV quite accurately for a small region around the point at which they are determined. The SV clock correction parameters give coefficients to a polynomial which may be used to calculate the clock correction at the desired time. The following section outlines the procedure used in this filter to calculate these quantities.

We start with essentially two measurements from the receiver: the receiver epoch, T_R, and the pseudo range to the SV of interest, ρ. Recall that the receiver epoch or receive time is measured as per the receiver's clock and can be expected to vary considerably from GPS system time. Once again:

$$T_R = t_R + \Delta t_u \qquad \text{where} \quad t_R = \text{receive epoch in GPS system time}$$

$$\Delta t_u = \text{receiver clock bias} \qquad (\text{a1})$$

Also recall that the SV begins transmission of the code sequence at T_T, which is also according to its own biased clock:

$$T_T = t_T + \Delta t_{sv} \qquad \text{where} \quad t_T = \text{transmit time in GPS system time}$$

$$\Delta t_{sv} = \text{SV clock bias} \qquad (\text{a2})$$

Since we actually want the position of the SV at t_t, which is the transmit time according to GPS system time, we proceed as follows:

Our pseudo-range measurement is defined as:

$$\rho = c(T_R - T_T) \qquad (\text{a3})$$

Rrearranging, we get:

$$T_T = T_R - \rho/c \qquad (\text{a4})$$

Substituting this in (a2) results in:

$$t_t = T_R - \rho/c - \Delta t_{sv} \qquad (\text{a5})$$

From (a5) we see that in order to find the transmit time we need the SV clock correction, Δt_{sv}. The polynomial used to calculate Δt_{sv} is:

$$\Delta t_{sv} = af_0 + af_1(t_t - t_{oc}) + af_2(t_t - t_{oc})^2 + \Delta t_r \qquad (\text{a6})$$

In (a6) the coefficients, af_0, af_1, and af_2, and the clock data reference time, t_{oc}, are given by the navigation data message. Δt_r is a relativistic clock correction term that is dependent upon certain orbital parameters. It is calculated along with the SV position covered further along in this appendix. It can be seen immediately that (a5) and (a6) are dependent, i.e. we need Δt_{sv} to find t_t, and vice versa. Also we have the term Δt_r that is calculated in the orbit determination procedure, for which we are trying to find t_t. These

interdependencies require us to proceed recursively to calculate both the clock correction and the SV position.

We initialize the recursion by calculating an estimate to Δt_{sv} and t_t:

$$\Delta t_{sv} \approx af_0 + af_1(T_T - t_{oc}) + af_2(T_T - t_{oc})^2 \tag{a7}$$

where T_T is obtained from (a4). It turns out that equation (a6) is not highly sensitive to t_t, thus this estimate is fairly good. Now we can obtain an estimate of t_t from (a5). We then proceed recursively, as shown in Figure A1. The first item calculated is T_k, which is the time of transmission relative to the ephemeris data reference time t_{oe}. We then calculate the SV position at T_k using the broadcast ephemeris data and the procedure described next in this appendix. This will yield the SV position (x,y,z) in ECEF coordinates and the relativistic correction term, Δt_r. We now use (a6) to calculate a new estimate to Δt_{sv} and then (a5) to obtain an updated t_t. This, in turn, is used to update T_k, and the recursion continues until sufficient convergence occurs.

In the iteration described above and shown in Figure A1, the second step is to compute the SV's ECEF coordinates and relativistic correction term, at the time T_k. For a filter such as the one described in this thesis, this calculation must be done repetitively and in real time. The method used in most applications is fairly standard and utilizes a set of parameters, referred to as the "broadcast ephemeris", that describe the orbit of the SV quite accurately for a short period of time. All SV's are tracked from the ground by the control segment and the parameters describing each ones orbit are continually updated. Since each receiver utilizing GPS signals needs to calculate the position of the appropriate SV's at its own particular time, the parameters are used to extrapolate the elliptical path of the satellite about a reference point. A list of the clock correction parameters and the broadcast ephemeris are given in Table A1. The calculation of SV position and relativistic correction factor is described below.

Parameter	Description	Units
t_{oc}	SV clock correction data reference time	seconds
af_0	constant coefficient for SV clock correction polynomial	
af_1	1st order coefficient	
af_2	2nd order coefficient	
t_{oe}	ephemeris data reference time	seconds
A	semi-major axis	meters
e	eccentricity	
M_0	mean anomaly at reference time	radians
Δn	mean motion correction	rad/sec
ω	argument of perigee	radians
C_{uc}	amplitude of cosine 2nd harmonic correction term for argument of latitude	radians
C_{us}	amplitude of sine 2nd harmonic correction term for argument of latitude	radians
C_{ic}	amplitude of cosine 2nd harmonic correction term for inclination angle	radians
C_{is}	amplitude of sine 2nd harmonic correction term for inclination angle	radians
C_{rc}	amplitude of cosine 2nd harmonic correction term for SV radius	meters
C_{rs}	amplitude of sine 2nd harmonic correction term for SV radius	meters
i_0	inclination angle at reference time	radians
$\dot{i}$	rate of change of inclination angle	rad/sec
Ω_0	longitude of ascending node at GPS weekly epoch	radians
$\dot{\Omega}$	rate of right ascension	rad/sec

Table A1. Ephemeris and clock parameters broadcast on navigation data message.

Initialize

$$\Delta t_{sv} = af_o + af_1(T_T - t_{oc}) + af_2(T_T - t_{oc})^2$$
$$t_t = T_R - \rho/c - \Delta t_{sv}$$

Calculate Input Time for SV Orbit Determination

$$T_k = t_t - t_{oe}$$

Calculate SV ECEF Coordinates & Relativistic Correction Term at T_k

SV Position (x, y, z)

Δt_r

Update SV clock Correction

$$\Delta t_{sv} = af_o + af_1(t_t - t_{oc}) + af_2(t_t - t_{oc})^2 + \Delta t_r$$

SV Clock Corr. Δt_{sv}

Update Transmit Time

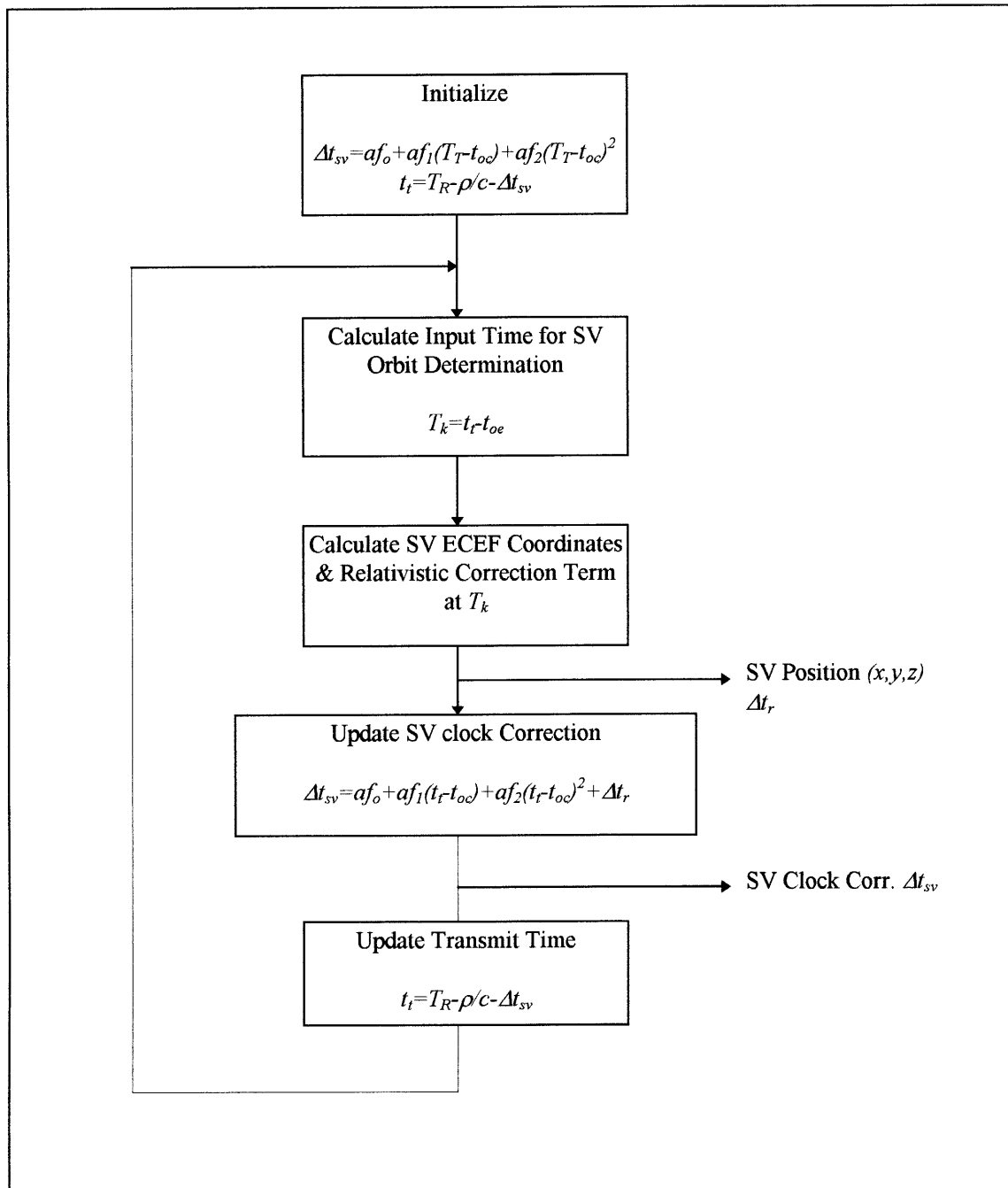$$t_t = T_R - \rho/c - \Delta t_{sv}$$

Figure A1. Iteration for calculating SV position and clock correction.

Several constants which are utilized in these calculations are:

μ = WGS-84 value of earth's universal gravitational parameter (m^3/s^2).

$\dot{\Omega}_e$ = WGS-84 value of earth's rotation rate (rad/sec).

c = Propagation velocity (m/s).

We start by fixing the position of the SV along an elliptical path in an orbital plane which is tilted relative to the ECEF frame. Figure A2 shows such an elliptical path and some of the relevant quantities. The ellipse is described by a semi-major axis, A, and eccentricity, e. The ephemeris data provides A, and from this we compute the mean (angular) motion of the SV along the ellipse in radians per second and apply a correction factor:

$$n = \sqrt{\frac{\mu}{A^3}} + \Delta n \qquad \text{corrected mean motion (rad/sec)} \qquad \text{(a8)}$$

From n we can compute the mean anomaly at time T_k, M_k, which is actually a fictitious angle measured from perigee through which the SV would have traveled assuming it is moving at the angular rate given by the corrected mean motion:

$$M_k = M_0 + nT_k \qquad \text{mean anomaly (rad)} \qquad \text{(a9)}$$

where M_O is the mean anomaly at reference time, t_{oe}.

We next compute the eccentric anomaly at time T_k, E_k. This angle is defined by projecting the SV's position on the ellipse out to an auxiliary circle along a normal to the semi-major axis. The auxiliary circle coincides with the ellipse at perigee and has a radius of A. The angle E_k is defined relative to perigee. The eccentric anomaly may be computed using a variety of equations. The method chosen here involves iterating the following equations until the value of the mean anomaly computed in the iteration is within a desired tolerance of the value computed by (a9).

We first estimate E_k and M_k by:

$$\hat{E}_k = M_k + e\sin(M_k) + \frac{1}{2}e^2 \sin(2M_k) \qquad \text{(a10)}$$

$$\hat{M}_k = E_k - e\sin(E_k) \qquad \text{(a11)}$$

Next we iterate the following equations until the value of M_k computed below matches the value computed in (a9) within a desired tolerance:

$$\hat{E}_k = \hat{E}_k + \frac{(M_k - \hat{M}_k)}{1 - e\cos(\hat{E}_k)} \qquad \text{(a12)}$$

$$\hat{M}_k = \hat{E}_k - e\sin(\hat{E}_k) \qquad \text{(a13)}$$

When the desired tolerance is achieved:

$$E_k = \hat{E}_k \qquad \textit{eccentric anomaly (rad)} \qquad\qquad (a14)$$
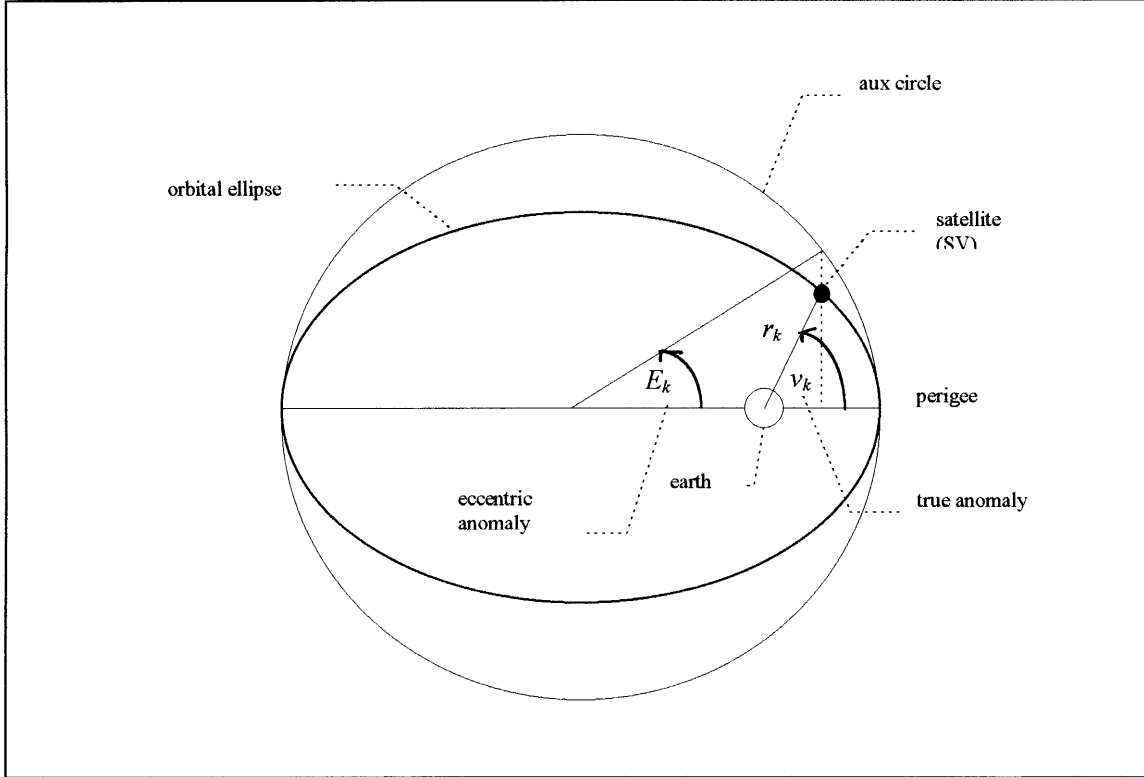

Figure A2. Elliptical orbit

From the *eccentric anomaly* we determine the *true anomaly* at time T_k, v_k. This is the angle from perigee to the radius vector from the earth center to the SV position on the ellipse:

$$v_k = \tan^{-1}\left[\frac{\sqrt{1-e^2}\,\sin(E_k)}{\cos(E_k)-e}\right] \qquad \textit{true anomaly (rad)} \qquad\qquad (a15)$$

We have now fixed the angular displacement of the SV in its orbital plane relative to perigee. i.e. the *true anomaly*, v_k, is the angle between perigee and the SV radius vector as shown in Figure A3. We want to determine the position of the SV in its orbital plane. To do this we define a 2D coordinate frame with x'-axis from the earth center through a point called the ascending node, which will be explained shortly, and a corresponding y'-axis perpendicular to this. Now, if we find the angle between our x'-axis and the radius vector we can easily find the (x',y') coordinates of the SV in this frame. To find this angle we need to add the angle known as the *argument of perigee*, and labeled ω in Figure A3, to the *true anomaly*. (The *argument of perigee* is transmitted as part of the broadcast ephemeris.) Thus the angle from the x'-axis to the SV radius vector at time T_k, called the *argument of latitude*, is given by:

$$\Phi_k = v_k + \omega \qquad \textit{uncorrected argument of latitude (rad)} \qquad\qquad (a16)$$

83

As mentioned, our (x', y') coordinate system for the position of the SV in the orbital plane is defined relative to the ascending node. The ascending node corresponds to the point on the ellipse where the orbital plane intersects the x-y plane of the GPS ECEF coordinate system, which is essentially the earth's equatorial plane. This can be seen in Figure A4.

A simple relationship exists between the SV radius vector, r_k, and the *eccentric anomaly*, E_k :

$$r_k = A(1 - e\cos(E_k))$$ *uncorrected SV radius (m)*   (a17)

However, before using Φ_k and r_k to determine the SV coordinates in the orbital plane, we need to apply a set of correction factors due to second harmonic perturbations in the orbit. These perturbations are detected by the control segment and characterized by the six subscripted coefficients, C, in the equations below. We compute three quantities, a correction term for the *argument of latitude*, the *SV radius*, and also a quantity known as the *inclination angle*, which will be explained subsequently.

The corrections are computed as follows:

$$\delta u_k = C_{us}\sin(2\Phi_k) + C_{uc}\cos(2\Phi_k)$$ *argument of latitude correction (rad)*   (a18)

$$\delta r_k = C_{rs}\sin(2\Phi_k) + C_{rc}\cos(2\Phi_k)$$ *radius correction (m)*   (a19)

$$\delta i_k = C_{is}\sin(2\Phi_k) + C_{ic}\cos(2\Phi_k)$$ *inclination correction (rad)*   (a20)

The new *argument of latitude* and *radius* thus become:

$$u_k = \Phi_k + \delta u_k$$ *corrected argument of latitude (rad)*   (a21)

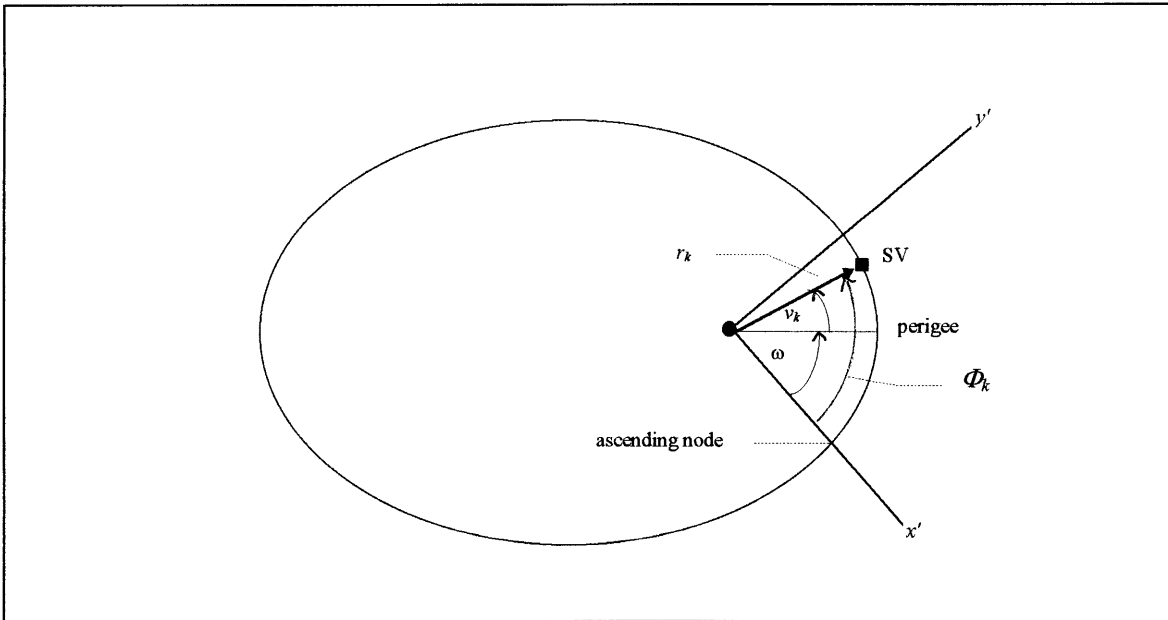$$r_k = A(1 - e\cos(E_k)) + \delta r_k$$ *corrected SV radius (m)*   (a22)

Figure A3. SV Position in Orbital Plane.

The position of the SV in the orbital plane is now given by:

$$x'_k = r_k \cos(u_k) \quad \text{and} \quad y'_k = r_k \sin(u_k) \qquad (m)$$

(a23)

The final step required is to express the SV's position, given in orbital plane coordinates, in the ECEF frame. Since both systems have their origin at the earth's center, all we need to do this is two rotations. Referring to Figure A4, we first rotate the orbital plane about the x' axis, so that the orbit now lays on the x-y plane in the ECEF frame. This rotation requires knowing the *inclination angle* at time T_k, denoted i_k. This angle is essentially the amount that the orbital plane is tilted relative to the equatorial plane.

The *inclination angle* is calculated by:

$$i_k = i_0 + \delta i_k + i T_k \qquad \text{corrected inclination angle (rad)}$$

(a24)

where i_0 and i are provided in the broadcast ephemeris.

The second rotation is about the ECEF frame z axis. Here we rotate the x'-y' axis so they coincide with x-y axis of the ECEF frame. This requires knowing the angle between them. This angle, which is between the Greenwich (zero) Meridian and the *ascending node* at time T_k, is denoted the *longitude of the ascending node* at time T_k, Ω_k, and is calculated by:

$$\Omega_k = \Omega_0 + (\dot{\Omega} + \dot{\Omega}_e)T_k - \dot{\Omega}_e t_{oe} \qquad \text{longitude of ascending node (rad)}$$

(a25)

where Ω_o, Ω, and t_{oe} are provided in the broadcast ephemeris and Ω_e is defined above.

Combining these two rotations, the SV's ECEF coordinates are given by:

$$x_k = x'_k \cos(\Omega_k) - y'_k \cos(i_k)\sin(\Omega_k) \qquad (m)$$

(a26)

$$y_k = x'_k \sin(\Omega_k) + y'_k \cos(i_k)\cos(\Omega_k) \qquad (m)$$

(a27)

$$z_k = y'_k \sin(i_k) \qquad (m)$$

(a28)

The relativistic correction term, Δt_r, required in equation (a6) is calculated by:

$$\Delta t_r = \frac{-2\sqrt{\mu}}{c^2} e\sqrt{A} \sin(E_k) \qquad \text{relativistic correction (s)}$$
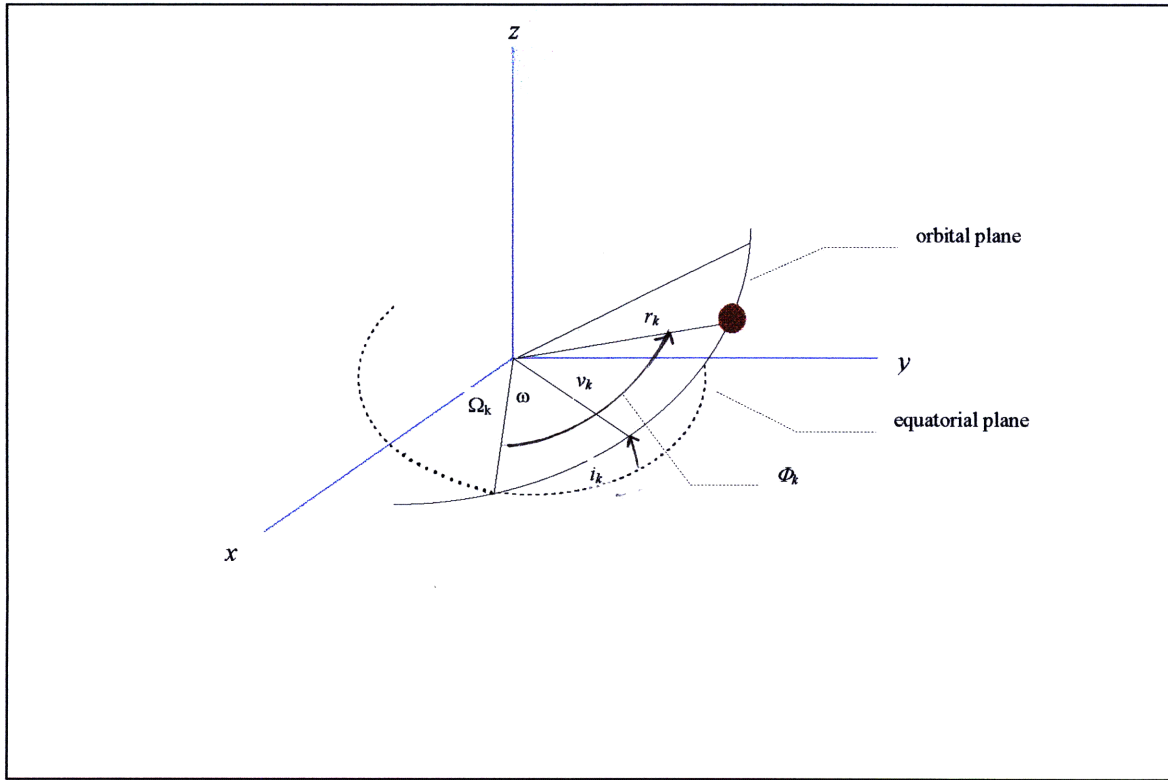
(a29)

85

Figure A4. Relationship of orbital plane to *ECEF* frame.

Appendix B. Conversion of ECEF Coordinates to WGS-84 Latitude, Longitude, and Altitude.

As described in Section 3, radar measurements are typically given in a locally level coordinate frame with the origin at the radar antenna phase center. The local level is considered a plane tangent to the reference ellipsoid at the frame origin. This reference ellipsoid is part of the universal coordinate system called the World Geodetic System - 1984 (WGS-84) which fixes positions relative to the earth. Positions are given by a latitude angle, longitude angle, and height above ellipsoid. The reference ellipsoid is actually an imaginary surface that approximately represents the earth's surface, but is precisely defined so that positions may be determined relative to it. Since the radar frame is typically defined relative to the ellipsoid, when rotating coordinates between the radar frame and the Earth Centered Earth Fixed (ECEF) frame used in the filter, we need to determine the geodetic latitude, δ, and the longitude, λ. Although, the longitude of a position in this coordinate frame is simply represented by the inverse tangent of the ECEF coordinates Y/X, the latitude is not so easily obtained. This can be seen in Figure B1, where we see that the normal line to the locally level plane tangent to the reference ellipsoid does not go through the ECEF origin.
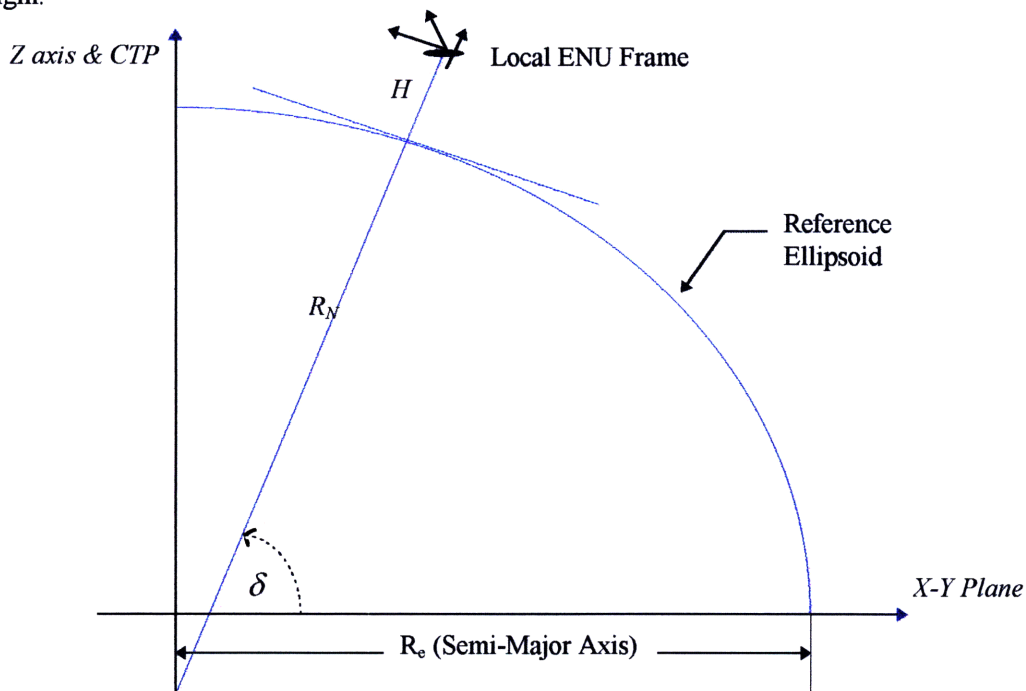

Figure B1. Relationship of *ENU* Frame, Geodetic Latitude, and Reference Ellipsoid.

Given the *ECEF* coordinates (x,y,z) of the radar (*ENU*) frame origin, the following procedure is used to determine the geodetic coordinates. The procedure is iterative.

Define the following constants:

$R_e = 6378137.0$ m (Ellipsoid Semi- Major Axis)

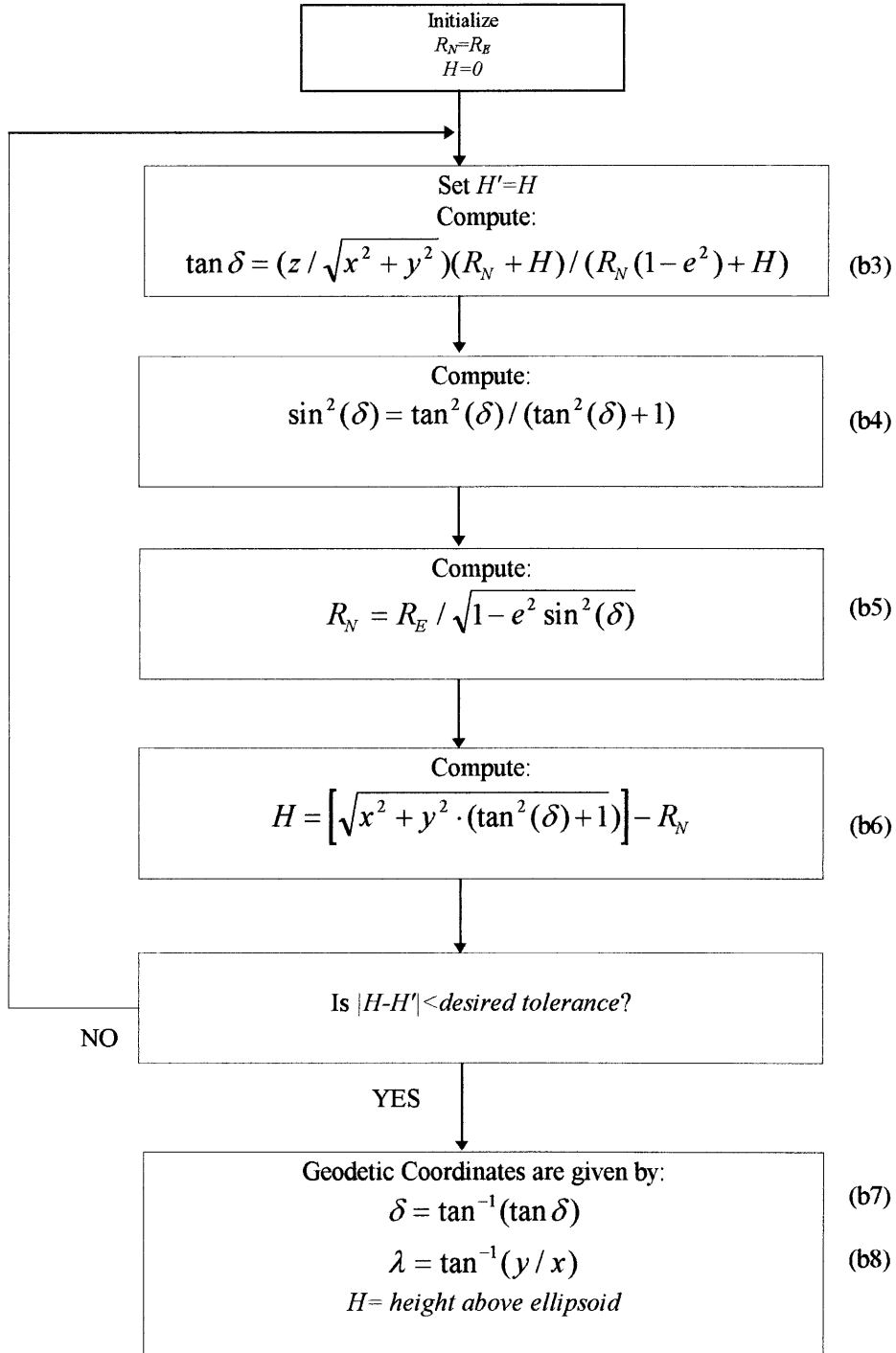$F = 1/298.2572$ (Earth Flattening Factor)

Now let:

$$b = R_e - R_e \cdot F \qquad\qquad\qquad (b1)$$

87

$$e = \frac{\sqrt{R_e^{\,2} - b^2}}{R_e}$$

(b2)

Now proceed with the following iteration:

Initialize
$R_N = R_E$
$H = 0$

Set $H' = H$
Compute:

$$\tan \delta = (z / \sqrt{x^2 + y^2})(R_N + H) / (R_N (1 - e^2) + H)$$

(b3)

Compute:

$$\sin^2(\delta) = \tan^2(\delta) / (\tan^2(\delta) + 1)$$

(b4)

Compute:

$$R_N = R_E / \sqrt{1 - e^2 \sin^2(\delta)}$$

(b5)

Compute:

$$H = \left[\sqrt{x^2 + y^2 \cdot (\tan^2(\delta) + 1)} \right] - R_N$$

(b6)

Is $|H - H'| < $ *desired tolerance?*

NO

YES

Geodetic Coordinates are given by:

$$\delta = \tan^{-1}(\tan \delta)$$

(b7)

$$\lambda = \tan^{-1}(y / x)$$

(b8)

H = height above ellipsoid

References:

1. Singer, R.A., "Estimating Optimal Tracking Filter Performance for Manned Maneuvering Targets", *IEEE Transactions on Aerospace and Electronic Systems*, Vol. AES-6 No.4, July 1970

2. Bar-Shalom,Y., Li, X., *Estimation and Tracking: Principles, Techniques, and Software*, Artech House, 1993.

3. Axelrad,P., Brown,R.G., "GPS Navigation Algorithms", *Global Positioning System: Theory and Applications*, Vol.I, American Institute of Aeronautics and Astronautics, 1994.

4. Dahleh, M., Verghese, G., Notes from a dynamic systems and control course (6.241) taught in the Department of Electrical Engineering and Computer Science at MIT. 1996.

5. Brown, R.G., Hwang, P., *Introduction to Random Signals and Applied Kalman Filtering*, John Wiley and Sons, 1997.

6. Parkinson, B.W., Spilker, J.J., Editors, Axelrad, P., Enge, P., Associate Editors, *Global Postioning System: Theory and Applications*, Vols. I&II. American Institute of Aeronautics and Astronautics, 1994.

7. Leick, A., *GPS Satellite Surveying*, John Wiley and Sons, 1990.

8. Parkinson, B.W., "GPS Error Analysis", *Global Positioning System: Theory and Applications.* Vol.I, American Institute of Aeronautics and Astronautics, 1994.

9. Van Graas, F., Braasch, M.S., "Selective Availability", *Global Positioning System: Theory and Applications*, Vol.I, American Institute of Aeronautics and Astronautics, 1994.

10. Parkinson, B.W., Enge, P.K., "Differential GPS", *Global Positioning System: Theory and Applications*, Vol.II, American Institute of Aeronautics and Astronautics, 1994.

11. Jordan, E.C., Editor, *Reference Data for Engineers: Radio, Electronics, Computer, and Communications*, Seventh Edition, Howard W. Sams & Co. 1986.

12. Skolnik, M.I., *Introduction to Radar Systems*, Second Edition, McGraw-Hill, 1980.

13. Grewal, M. S., Angus, P. A., *Kalman Filtering, Theory and Practice*, Prentice Hall, 1993.

14. Spilker, J.J., "Satellite Constellation and Geometric Dilution of Precision, *Global Positioning System: Theory and Applications*, Vol.I, American Institute of Aeronautics and Astronautics, 1994.

15. Nardone, S. C., Aidala, V.J., "Observability Criteria for Bearings-Only Target Motion Analysis",*IEEE Transactions on Aerospace and Electronic Systems*, Vol. AES-17 No. 2, March 1981.

16. Willner,D., Chang, C. B., Dunn, K.P., "Kalman Filter Configurations for Multiple Radar Systems", MIT Lincoln Lab, TN1976-21, April 1976.

17. Hassan, M.F., Salut, G., Singh, M.G., Title, A., "*A* Decentralized Computational Algorithm for the Global Kalman Filter", *IEEE Transactions on Automatic Control*, Vol AC-23, No. 2, 1978, pp. 262-267.

18. Carlson, N. A., "Federated Filter for Fault Tolerant Integrated Navigation Systems", Presented at Position Location and Navigation Symposium, Nov 1988.

19. Loomis, P.V.W., Carlson , N. A., Bararducci, M.P., "Common Kalman Filter, Fault Tolerant Navigation for Next Generation Aircraft", *Proceedings of the Institute of Navigation*, Santa Barbara CA, Jan 1988.

20. Hackett, J.K., Mubarak,S., "Multi-Sensor Fusion: A Perspective"., *IEEE Transactions*, 1990.

21. Carpenter, J.R., Bishop,R.H., "Navigation Filter Estimate Fusion for Enhanced Spacecraft Rendezvous", *Journal of Guidance, Control, and Dynamics*, Vol 20 No.2 ,March 1997.

22. Milliken, R.J., Zoller, C.J., "Principle of Operation of Navstar and System Charactaristics", *Journal of Navigation*, Institute of Navigation, Reprinted 1980.

23. Minkler, G., Minkler, J., *Aerospace Coordinate Systems and Transformations*, Magellan Book Co., 1990.

24. *Navstar GPS Interface Control Document: ICD-GPS-200.* Rockwell-Collins Corp. Satellite Systems Division November 1987.

25. Farrell, J.L., *Integrated Aircraft Navigation*, Academic Press, Inc., 1976.

26. Willsky, A.S., Notes from a recursive estimation course (6.433) taught in the Department of Electrical Engineering and Computer Science at MIT. 1994.

27. *Matlab Version 5.0*, Numeric computation and visualization software produced by The Mathworks, Inc. Natick, MA, 1997.